AEROBIC AQUEOUS REDOX CATALYSIS BY A RUTHENIUM–HYDRIDE SPECIES AND EVIDENCE FOR THE REDUCING/HYDRIDE TRANSFER ABILITY OF BIOLOGICAL OXIDANTS

A Dissertation
Presented to
the Graduate School of
Clemson University

In Partial Fulfillment
of the Requirements for the Degree
Doctor of Philosophy
Chemistry

---

by
Yamin Htet
May 2017

Accepted by:
Dr. Andrew G. Tennyson, Committee Chair
Dr. Shiou–Jyh Hwu
Dr. Ya–Ping Sun
Dr. Rhett C. Smit

ProQuest Number: 10275040

All rights reserved

INFORMATION TO ALL USERS
The quality of this reproduction is dependent upon the quality of the copy submitted.

In the unlikely event that the author did not send a complete manuscript
and there are missing pages, these will be noted. Also, if material had to be removed,
a note will indicate the deletion.

ProQuest 10275040

Published by ProQuest LLC (2017). Copyright of the Dissertation is held by the Author.

All rights reserved.
This work is protected against unauthorized copying under Title 17, United States Code
Microform Edition © ProQuest LLC.

ProQuest LLC.
789 East Eisenhower Parkway
P.O. Box 1346
Ann Arbor, MI 48106 – 1346

ABSTRACT

Reactive oxygen species (ROS), such as superoxide and hydrogen peroxide, have been classically viewed as being monolithically harmful to biological systems, only leading to disease and dysfunction. This understanding has evolved recently in light of new findings; 1) ROS are essential in fighting infections and 2) antioxidant enzyme, catalase that removes ROS (antioxidant activity) can also generate ROS (pro-oxidant activity) depending on the identity of the corresponding oxidized products.

We hypothesize that a complex that catalyzes oxidization of alcohols will be able to catalyze the reduction of radicals. We chose an organoruthenium catalyst (**Ru1**), air-stable and soluble in water-miscible solvents, as a catalyst for aerobic aqueous redox reaction and 2,2'-azino-bis(3-ethylbenzo-thiazoline-6-sulfonate) radical monoanion ($ABTS^{\bullet-}$) as a model for radical species due to its comparable oxidizing potential to ROS. Because radicals can be reduced using alcohols as terminal reductants, we chose biologically-relevant alcohols that can be recycled to their reduced states by our body.

We have shown that **Ru1** catalyzed the reduction of $ABTS^{\bullet-}$ to its precursor $ABTS^{2-}$ in phosphate buffered saline (pH 7.4). In doing so, **Ru1** used biologically-relevant alcohols containing CH–OH groups such as NAD^+, amino acids, sugars, citric acid cycle metabolites as terminal reductants. Mechanistic evidence reveals that the catalytic radical reduction is achieved by a Ru-hydride intermediate formed by a β-hydride elimination from a ribose subunit in NAD^+ and from a Ru-alkoxide species in citric acid cycles metabolites. These findings demonstrate the undiscovered reducing ability of biological oxidants. We have also revealed a new potential therapeutic strategy

by Ru catalysts that use the same type of Ru-hydride intermediate by demonstrating the catalytic antioxidant effects.

Collectively, these findings illustrate a central principle of redox therapeutics: it is not the identity of the redox catalyst itself that determines whether it produces pro- or antioxidant effects, but rather the identities and concentrations of the species being reduced (the terminal oxidant) and the species being oxidized (the terminal reductant).

DEDICATION

Never despair, keep smiling

Better than wealth with its carriage and pair

Better than rank or a face wondrous fair

Is a heart that life burdens can cheerfully bare

Just a brave loving heart that never despairs

B Wallis April 23rd, 1916

ACKNOWLEDGMENTS

First and foremost, I would like to thank my advisor, Professor Andy Tennyson. This work has been as much as mine as yours. I am deeply appreciated for your generous time and effort devoted to my research projects. You have shaped my career by providing rigorous training and great learning opportunities, with the patience that withstands my blunt ends. I have benefitted immensely as your first graduate student. Your willingness to solve harder scientific problems, your scientific objectivity, your methodological approach in troubleshooting are the skills that I admire and plan to keep your legacy in the future, though not the hairstyle. Without your mentorship, and a sense of sacrifice, I will not have such a productive career as a graduate student.

Secondly, I am fortunate to have very supportive individuals as my committee members. I thank Professor Shiou–Jyh Hwu for our productive research collaborations and for your wisdom and kindness as I try to achieve my goals; Professor Rhett Smith for giving me a chance to collaborate on the projects which has led to two publications; Last but not least, Professor Ya–Ping Sun for graciously providing your guidance while I was trying to navigate through different research groups.

I also thank the Department of Chemistry at Clemson for financial support. I had a chance to work and learn from experienced individuals, Barbara, Will and Robin, at various stages of my graduate school.

Dorothy, your relentless energy is and will always be my inspiration.

I am extra-grateful for those who have shown me love, kindness and forgiveness during my short supply of sanity. I gave up cooking and my private life to do a series of

experiments for several years. Soe and Longyu for being the dearest and earnest friends whom I can always count on, especially during the dark days inside and outside of lab. Soe, for your life-long devoted unconditional friendship since 2003 (and counting). The gang - Craig, Dino, Amir - for helping me keep my cool and take my mind off the PhD and life when needed. Longyu and Lin R.T.C for support, countless delicious meals, midnight sanity chats and introducing me to the fun times when I am not working. Huongzian, Maki, Liem, Van, Sarah H. and Sarah R. for friendship, wine and Korean dramas. Anshuman, Alfredo and Amoah, who know better than anyone what it takes to get through graduate school, for the late night karaoke in lab.

Amy and Florin, for the incredible kindness you have shown me all these years. I am also grateful of my sisters, Ni and Thet, for their care and support. Last but not least, I am indebted to my parents for their love, sacrifices, and unwavering support. All that I am, I owe to my parents.

TABLE OF CONTENTS

Page

TABLE OF CONTENTS (Continued)

CHAPTER

Page

LIST OF TABLES

Table Page

LIST OF SPECTRA

Spectra Page

LIST OF SCHEMES

LIST OF FIGURES

LIST OF FIGURES (Continued)

Figure Page

LIST OF FIGURES (Continued)

Figure Page

CHAPTER ONE

CELLULAR REDOX SYSTEM: THE DUAL ROLES OF OXIDANTS AND REDUCTANTS

"Life is nothing but an electron looking for a place to rest".

"~Albert Szent-Gyrgyi"

1.1 HISTORICAL BACKGROUND AND SIGNIFICANCE

Life is a constant battle to overcome entropy. Living cells simultaneously synthesize thousands of molecules ranging from small inorganics to protein, carbohydrate, fat, and enzymes in the right proportions, only at the right time, in a very precise manner.[1] Energy is required to keep and maintain this well–regulated system in order. This required energy is retained from the flow of electrons during cellular redox reactions.[1] Redox reactions are generally linked to one another and altogether they form the basis of highly complex, interconnected and dynamic cellular network.[1]

Cells proliferate in reducing environment[2] than in oxidizing state. In order to maintain this original state, cells use various redox couples.[2,3] The most abundant cellular redox couple is glutathione (GSH) and its oxidized form, glutathione disulfide (GSSG). The endogenously synthesized tripeptide, GSH, is composed of glycine, cysteine and glutamine, and present at 1–11 mM concentrations in cells, far higher than other cellular redox active couples.[2,4] Higher concentration of GSSG indicates oxidative shift at which biomolecules get oxidized and may be damaged if its original state is not re–established over time. Cells balance the redox state by producing more GSH. This is also true when cells are in more reducing state than its original balance; more GSSG is produced.

Enzymes catalyze the regeneration of GSH or GSSG: glutathione reductase, catalyzes the reduction of GSH from GSSG, and glutathione peroxidase catalyze the oxidation of GSSG from GSH. In cellular environment, NADPH is the major reducing agent and thus, provides necessary electrons for reduction of glutathione whereas $NADP^+$ is the major oxidizing agent for regeneration of GSSG.[4]

$$GSSG + NADPH + H^+ \rightleftharpoons 2GSH + NADP^+ \qquad (1)$$

Temporary perturbation of redox balance in cell, reductive shift or oxidative shift, is a necessary part of normal physiological processes. [3,5] Regulated production of oxidants serves as a signal to produce more endogenous reductants and vice versa. [3,6] Oxidants when present at high concentrations cause detrimental damages to important biomolecules by oxidizing them. This overproduction, also known as oxidative stress, is involved in over a hundred diseases.[7] Yet, ironically, one of the main physiological roles of ROS is to act as a signal molecule to protect cells against oxidative stress.[3] Therefore, the classical view of bad oxidants are destroyed by good antioxidants needs to be used with caution because redox active species can act as both oxidant and reductant (i.e. antioxidants) as will be illustrated in the following sections.

1.2. Endogenously produced redox active inorganic small molecules

1.2.1 Pathological and physiological roles of redox active oxygen species

Oxygen, being essential for our metabolism, is a radical itself and is the main producer of all reactive oxygen species.[5,8] The dual nature of these metabolic species are apparent even in the case with oxygen. Oxygen when it is above its allowed concentration (>21%) becomes a poison to aerobic organisms.[8]

One electron reduction of oxygen produces superoxide (O_2^-). Superoxide itself in aqueous solution is not highly reactive and do not cause direct damage to cells. Most damage is usually caused by it reacting with other radicals (nitric oxide) or free metal ions, producing highly reactive hydroxyl radicals ($HO^\bullet$). Hydroxyl radical is the most

reactive radical that can react readily with anything, change the structure and functions of any important biomolecules (DNA, protein, lipids).[2]

$$O_2 + e \rightarrow O_2^- \quad (2)$$

Exposure to reactive oxygen species (ROS) at low concentrations are normal and essential for our health as shown in **Table 1**. For example, cells use superoxide to kill environmental pathogens.[3] When the level of superoxide exceeds the normal level, cells initiate the defense mechanism to reestablish the redox status. [2] The process signals is called "oxidative burst", in which a large quantity of superoxide is produced. This superoxide production signals the defense system to produce more antioxidants.

Any oxidant given the appropriate conditions can also act as reductant. Standard reduction potential of O_2/ O_2^- is –0.33 V [5] and thus, theoretically *in vitro*, it will reduce any redox couple whose potential is less negative, zero, or positive. Similarly, it can oxidize the redox couples whose potential is more negative. Superoxide in aqueous solution can act as a reducing agent [5] when it reduces the iron complexes such as cytochrome c (Cyt. C) and ferri-EDTA.

$$Cyt.\ C + (Fe^{3+}) + O_2^- \rightarrow O_2 + Cyt.\ C\ (Fe^{2+}) \quad (3)$$

Consequent reduction of O_2^- produces H_2O_2 that can exert intracellular damage. Being neutral in charge, H_2O_2 can diffuse into cells easily whereas negatively charged O_2^- cannot. Once inside the cell, hydrogen peroxide gets reduced to damaging hydroxyl radicals. [5] All reactive oxygen species eventually form $HO^\bullet$ and this chain reaction to form $HO^\bullet$ is responsible for the detrimental effect of reactive oxygen species.

$$O_2^- + 2H^+ + e \rightarrow H_2O_2 \quad (4)$$

$$H_2O_2 + e \rightarrow HO^{\bullet} + {}^{-}OH \quad (5)$$

Similar to superoxide, when at physiological concentrations, H_2O_2 (0.001 to 0.7 μM) serves as cell signaling molecules for a number of important biochemical pathways as shown in **Table 1**.[9] Hydrogen peroxide, when higher than 100 μM can be damaging to cells.

1.2.2 Pathological and physiological roles of redox active nitrogen species

Nitric oxide, another important endogenously produced radical, is known for its pro–oxidant role of generating other nitrogen–containing radicals as well as protecting oxidative damage of cell membranes[10-12] Nitric oxide ($NO^{\bullet}$), though can be toxic in excess, has many physiologically–important functions as shown in **Table 1**. Nitric oxide, though not very reactive, can produce a strong oxidant, peroxynitrite ($ONOO^{-}$), that can damage protein, DNA, lipids, and carbohydrate.[12] Nitric oxide inhibits lipid peroxidation as well as induces the peroxidation process. Lipid peroxidation is considered to be the major pathway leading toward free radical induced cellular damage. The facilitation or inhibition of the lipid peroxidation by $NO^{\bullet}$ depends on the relative concentrations of nitric oxide and superoxide.[11]

1.3 Enzymes as catalyst for redox active species

1.3.1 NADPH oxidase

Since radicals are part of our mechanism, they are produced by pro-oxidant enzymes in our body. Enzymes are designed to produce these ROS when needed to defend against environmental pathogens.[7] This shows that pro–oxidant enzymes take the role of antioxidants. Oxidant enzymes such as NADPH oxidase and nitric oxide synthase,

produces much needed superoxide and nitric oxide respectively, in a strictly controlled manner so that the concentration of ROS would not exceed the required amount.[7] Mice with the knockout of NADH oxidase are found to be more susceptible to infection, implying the essential role of the oxidant enzyme in killing foreign organisms.[2]

1.3.2 Metalloenzymes

Superoxide dismutase (SOD) and catalase are antioxidant metalloenzymes that catalyze the disproportionation of superoxide (Eqn. 6) and hydrogen peroxide (Eqn. 7) respectively. SOD is the prime example of cellular antioxidants because SOD reduces radicals at the diffusion–controlled rate.[2]

$$O_2^- + O_2^- + 2H^+ \rightarrow H_2O_2 + O_2 \qquad (6)$$

$$2\ H_2O_2 \rightarrow 2H_2O + O_2 \qquad (7)$$

However, these antioxidant enzymes can also exhibit pro-oxidant behavior.[13] Catalase catalyzes the degradation of two molecules of hydrogen peroxides to water and oxygen. This reaction occurs by two steps in which H_2O_2 acts as oxidizing agent in the first step (8) and a reducing agent in the second step (9).[14,15]

$$\text{Enz}\,(Fe^{III}) + H_2O_2 \rightarrow \text{Enz}\,(Fe^{IV}{=}O^{\bullet+}) + H_2O \qquad (8)$$

$$H_2O_2 + \text{Enz}\,(Fe^{IV}{=}O^{\bullet+}) \rightarrow \text{Enz} + H_2O + O_2 \qquad (9)$$

Sum of Eqn 8 and 9: $2\ H_2O_2 \rightarrow 2H_2O + O_2$ (7)

When the concentration of hydrogen peroxide is low, the enzyme deviates from the above two–step reactions (Eqn. 7, 8), and generate ROS in the presence of an electron donor.

$$2AH_2 + \text{Enz}\,(Fe^{IV}{=}O^{\bullet+}) \rightarrow H_2O + \text{Enz}\,(Fe^{IV}{=}O^{\bullet+}) + 2AH^{\bullet} \qquad (10)$$

1.4 Therapeutic candidates

1.4.1 SOD Mimics

Superoxide dismutase can (SOD) scavenge superoxide radicals at the diffusion-controlled rate and thus, synthetic mimics of SOD that have comparable radical-scavenging activity are increasingly sought after.[16] Even though the radical scavenging activity of most SOD mimics *in vitro* are as outstanding as the enzyme itself, some SOD mimics have shown pro-oxidant activity *in vivo*.[17] This pro–oxidant behavior of SOD mimics is due to the formation of oxidizing intermediate similar to the dual action of catalase as discussed above.

1.4.2 Vitamin C

Chemically, powerful antioxidants are strong reducing agents and are marketed as "radical scavengers" in part due to their fast reaction rate to deplete oxidants. One such example is vitamin C or ascorbic acid. Vitamin C is the essential antioxidant in humans and deficiency of vitamin C causes scurvy.[18] *In vitro,* at physiological pH, ascorbic acid (pK_{a1} 4.25) becomes ascorbate, its mono-anionic form, which is a very effective antioxidant that readily reduces all types of free radicals with the typical rate constants of 10^5 M^{-1} s^{-1} (pH 7.4).[5,19] Despite the superiority of ascorbic acid as antioxidant *in vitro*, increasing number of human trials and some *in vivo* studies showed that vitamin C has no effect on oxidative stress.[6,19,20] In fact, some *in vivo* studies suggest that administering ascorbic acid to smokers increases the cause of cancer: the evidence of vitamin C acting as a pro-oxidant.[19-21]

Radical scavengers can generate radicals. Ascorbate (AH^-) becomes a pro–oxidant in the presence of free metal ions, producing highly reactive hydroxyl radicals and hydrogen peroxide.[18,20]

$$AH^- + Fe^{3+} \rightarrow A^{\bullet -} + Fe^{2+} + H^+ \quad (11)$$

$$H_2O_2 + Fe^{2+} \rightarrow HO^{\bullet} + Fe^{3+} + {}^-OH \quad (12)$$

However, the possibility of the above reaction (i.e. Fenton reaction) occurring in physiological conditions has been questioned due to the lack of free metal ions *in vivo*. These metal ions are effectively sequestered by enzymes that are specifically designed to do so in extracellular fluids to prevent them catalyzing any free radical–producing reactions. Therefore, the concentration of free iron ions in blood plasma and body fluids is zero in normal healthy cells.[5,22]

Even though vitamin C can act as a pro oxidant, it will more likely to act as an antioxidant rather than a proxidant *in vivo*. [6,19,20] Yet, *in vivo* studies have also shown that the deficiency of vitamin C, as well as the high dose (>500 mg per day) is associated with increased free radical induced damage to DNA, indicating how tightly the redox system is regulated. It is evident in the case of vitamin C that an antioxidant can also be a pro–oxidant and *vice versa*.

1.4.3 Vitamin E

Diet containing fruits and vegetables are known to have vitamins and minerals since Hippocrates (460–377 BC).[20] Since these diet–derived vitamins and minerals are essential for the normal growth of the body, their synthetic analogues are marketed as dietary supplements.[20] For example, Vitamin E is the major lipid-soluble antioxidant that

inhibits oxidation of lipoprotein, the process which leads to the hardening and blockage of blood vessels.[23] As a classical antioxidant, the biologically active form of Vitamin E, α-tocopherol, inhibits the lipid oxidation by scavenging lipid peroxyl radicals ($LOO^{\bullet}$). The resulting radical can trap the second peroxyl radical as in the reaction described below.

$$\alpha\text{–TocH} + LOO^{\bullet} \rightarrow \alpha\text{–Toc}^{\bullet} + LOOH \qquad (13)$$

As in the case of catalase, when the concentration of $LOO^{\bullet}$ is low, the resulting radical abstracts hydrogen from other lipids, deviating from its normal route.

$$\alpha\text{–Toc}^{\bullet} + LH \rightarrow \alpha\text{–TocH} + L^{\bullet} \qquad (14)$$

In this case, vitamin E induces lipid oxidation, rather than inhibiting it. In addition, similar to ascorbate, tocopherol can reduce free metal ions (Fe^{3+} and Cu^{2+}) and exert pro-oxidant effect. However, the lack of free metal ions in human plasma and the very low amount in body fluids (< μM)[5] disregards the possibility of this reaction happening *in vivo*. As expected, the pro-oxidant activity has been observed *in vitro* for other dietary supplements (vitamin A, vitamin C, and β–carotene).[5,20]

CONCLUSIONS

Molecular oxygen that we breath in is the main source of reactive oxygen species and can be both beneficial when it is at a normal concentration (21%) and detrimental for us when it exceeds that level. Reactive species such as superoxide and nitric oxide are as essential to our health as therapeutic antioxidants when they are present at appropriate concentrations and when there are no other species (i.e. transition metal ions) that can perturb their normal route of reaction pathway. Superoxide and nitric oxide serve as cellular messengers in protecting cells against oxidative stress, participate in killing foreign organisms and fighting infections. Production of reactive species, is not only associated with the adverse health effects (cancer, neurodegenerative diseases) but this process is normal and beneficial when it generates the required reactive species (superoxide and nitric oxide) in a strictly-controlled manner. On the other hand, exogenously acquired therapeutics may act as antioxidants as well as pro-oxidants. Similarly, vitamins and metal-based enzyme mimics exhibit dual properties. The resulting biochemical process (i.e. either physiological or pathological) that these reactive species *in vivo* generate depends on the concentration of reactive species, and the nature (oxidizing vs. reducing) of intermediate involved.

OVERALL GOALS AND THESIS STRUCTURE

A well–functioned cell, thus a healthy life, inevitably requires both oxidants and reductants to maintain the dynamic cellular redox system. Cells use extremely complex, and interconnected meshwork of redox signaling system to control the biochemical processes involving redox active species. It is generally accepted that oxidants or

"reactive oxygen species (ROS)" are disease-causing and antioxidants or reductants are the answer to the diseased conditions. However, this oversimplified interpretation of the roles played by redox-active species, both ROS and antioxidant led to many pitfalls especially in the field of antioxidants.

Evidence that excessively high concentrations of ROS are found in diseased conditions is undeniable. However, scientific data has yet to confirm that ROS are the cause of diseases; ROS are implicated in pathogenesis but may or may not participate in pathological pathways. On the other hand, evidence that radical scavengers can also generate radicals have recently been discovered. Excessively increasing exogenous antioxidants will flood the cellular redox system with reductants and will lead to overexpression of antioxidative enzymes. The resulting reductive shift is as detrimental as oxidative shift caused by ROS. The complexity involved in performing thorough mechanistic studies of these redox–active and highly–reactive species in a dynamic system limit our understanding as evident in the clinical trials of Vitamin C. To this end, we study how an organoruthenium complex can act as a catalytic antioxidant in the radical reduction.

Chapter 2 reports a system in which an organoruthenium complex serves as a catalytic reductant, employing the chemically synthesized radical. The ruthenium complex catalyzes the radical degradation and inhibition under biologically-relevant condition via oxidation of biologically relevant alcohols. Amino acids, sugars and citric acid cycle metabolites are found to act as excellent terminal reductants that are essential for the radical reduction because replacing the O–H and C–H groups of alcohols

significantly slows down the reduction. **Chapter 3** describes the detailed mechanism of catalytic radical reduction by the N-heterocyclic carbene ruthenium complex in aqueous buffered solution. Here we describe the catalytic antioxidant mechanism that involves a reducing intermediate, rather than an oxidizing intermediate, in the catalytic reduction. The N-heterocyclic carbene ruthenium complex prevents the pro-oxidant effects that have been observed for current catalytic antioxidants. **Chapter 4** describes the use of nature's oxidizing agent, NAD^+ (Nicotinamide Adenine Dinucleotide) as reductant, providing the evidence that biological oxidants have the ability to transfer hydride.

Table 1.1. Physiological and Pathological processes mediated by classical pro-oxidants

Type of reactive species	**Source of Radical**	**Physiological process**	**Pathological process**
Reactive Oxygen Species (ROS) 1.Superoxide (O_2^-) 2.H_2O_2 3.$HO^\bullet$	Oxygen NAD(P)H oxidase	Oxidative burst Superoxide: 10 pM[11] H2O2: 0.001-0.7 μM[11]	Diseases Superoxide: 0.01-0.1 μM [11] H2O2: 10-100 μM[11]
Reactive Nitrogen Species (RNS) 1.Nitric oxide ($NO^\bullet$) 2. $ONOO^-$	Nitric oxide synthase (NOS)	*Nervous system* Plays a role in long-term memory *Vascular system* Control blood pressure Signaling molecule in the cardiovascular system[10]	*Nervous system* Stroke, epilepsy *Vascular system* Chronic inflammation, transplant rejection, septic shock
Enzyme 1.NAD(P)H oxidase 2.Nitric oxide synthase		Produce oxidants that act as cellular messengers	Excessive production of oxidants

Table 1.2. Physiological and Pathological processes mediated by classical reductants/antioxidants

Type of antioxidant	Physiological process	Pathological process
Enzymes Superoxide dismutase (SOD) Catalase Glutathione Peroxidase (GPx)	Catalyze in the reaction that depletes excess reactive species	Produce oxidants
Dietary supplements Vitamin C (Ascorbate) Vitamin E (α –tocopherol) *Inorganic/Organometallic* SOD mimics	Deplete reactive species	Produce oxidants

RFERENCES

(1) Nelson, D. L.; Cox, M. M. *Principles of Biochemistry*; Lehninger, 2005.

(2) Valko, M.; Leibfritz, D.; Moncol, J.; Cronin, M. T.; Mazur, M.; Telser, J. "Free radicals and antioxidants in normal physiological functions and human disease." *Int J Biochem Cell Biol* **2007**, *39*, 44-84.

(3) Droge, W. "Free radicals in the physiological control of cell function." *Physiol Rev* **2002**, *82*, 47-95.

(4) Schafer, F. Q.; Buettner, G. R. "Redox environment of the cell as viewed through the redox state of the glutathione disulfide/glutathione couple." *Free Radic Biol Med* **2001**, *30*, 1191-212.

(5) Gutteridge, J. M.; Halliwell, B. "Comments on review of Free Radicals in Biology and Medicine, second edition, by Barry Halliwell and John M. C. Gutteridge." *Free Radic Biol Med* **1992**, *12*, 93-5.

(6) Halliwell, B. "The antioxidant paradox." *Lancet* **2000**, *355*, 1179-80.

(7) Sies, H. "Strategies of antioxidant defense." *Eur J Biochem* **1993**, *215*, 213-9.

(8) Abele, D. "Toxic oxygen: the radical life-giver." *Nature* **2002**, *420*, 27.

(9) Stone, J. R.; Yang, S. "Hydrogen peroxide: a signaling messenger." *Antioxid Redox Signal* **2006**, *8*, 243-70.

(10) Tennyson, A. G.; Lippard, S. J. "Generation, translocation, and action of nitric oxide in living systems." *Chem Biol* **2011**, *18*, 1211-20.

(11) Rubbo, H.; Radi, R.; Trujillo, M.; Telleri, R.; Kalyanaraman, B.; Barnes, S.; Kirk, M.; Freeman, B. A. "Nitric oxide regulation of superoxide and peroxynitrite-dependent lipid peroxidation. Formation of novel nitrogen-containing oxidized lipid derivatives." *J Biol Chem* **1994**, *269*, 26066-75.

(12) Beckman, J. S.; Koppenol, W. H. "Nitric oxide, superoxide, and peroxynitrite: the good, the bad, and ugly." *Am J Physiol* **1996**, *271*, C1424-37.

(13) Doctrow, S. R.; Huffman, K.; Marcus, C. B.; Tocco, G.; Malfroy, E.; Adinolfi, C. A.; Kruk, H.; Baker, K.; Lazarowych, N.; Mascarenhas, J.; Malfroy, B. "Salen-manganese complexes as catalytic scavengers of hydrogen peroxide and cytoprotective agents: structure-activity relationship studies." *J Med Chem* **2002**, *45*, 4549-58.

(14) Kirkman, H. N.; Gaetani, G. F. "Mammalian catalase: a venerable enzyme with new mysteries." *Trends Biochem Sci* **2007**, *32*, 44-50.

(15) Chelikani, P.; Fita, I.; Loewen, P. C. "Diversity of structures and properties among catalases." *Cell Mol Life Sci* **2004**, *61*, 192-208.

(16) Doctrow, S. R.; Huffman, K.; Marcus, C. B.; Musleh, W.; Bruce, A.; Baudry, M.; Malfroy, B. "Salen-manganese complexes: combined superoxide dismutase/catalase mimics with broad pharmacological efficacy." *Adv Pharmacol* **1997**, *38*, 247-69.

(17) Doctrow, S. R.; Abelleira, S. M.; Curry, L. A.; Heller-Harrison, R.; Kozarich, J. W.; Malfroy, B.; McCarroll, L. A.; Morgan, K. G.; Morrow, A. R.; Musso, G. F.; et al. "The bradykinin analog RMP-7 increases intracellular free calcium levels in rat brain microvascular endothelial cells." *J Pharmacol Exp Ther* **1994**, *271*, 229-37.

(18) Halliwell, B. "Free radicals, antioxidants, and human disease: curiosity, cause, or consequence?" *Lancet* **1994**, *344*, 721-4.

(19) Carr, A.; Frei, B. "Does vitamin C act as a pro-oxidant under physiological conditions?" *FASEB J* **1999**, *13*, 1007-24.

(20) Soni, M. G.; Thurmond, T. S.; Miller, E. R., 3rd; Spriggs, T.; Bendich, A.; Omaye, S. T. "Safety of vitamins and minerals: controversies and perspective." *Toxicol Sci* **2010**, *118*, 348-55.

(21) Podmore, I. D.; Griffiths, H. R.; Herbert, K. E.; Mistry, N.; Mistry, P.; Lunec, J. "Vitamin C exhibits pro-oxidant properties." *Nature* **1998**, *392*, 559.

(22) Halliwell, B.; Gutteridge, J. M. "Oxygen free radicals and iron in relation to biology and medicine: some problems and concepts." *Arch Biochem Biophys* **1986**, *246*, 501-14.

(23) Bowry, V. W.; Ingold, K. U.; Stocker, R. "Vitamin E in human low-density lipoprotein. When and how this antioxidant becomes a pro-oxidant." *Biochem J* **1992**, *288 (Pt 2)*, 341-4.

CHAPTER TWO

CATALYTIC RADICAL REDUCTION IN AQUEOUS SOLUTION VIA OXIDATION OF BIOLOGICALLY–RELEVANT ALCOHOLS

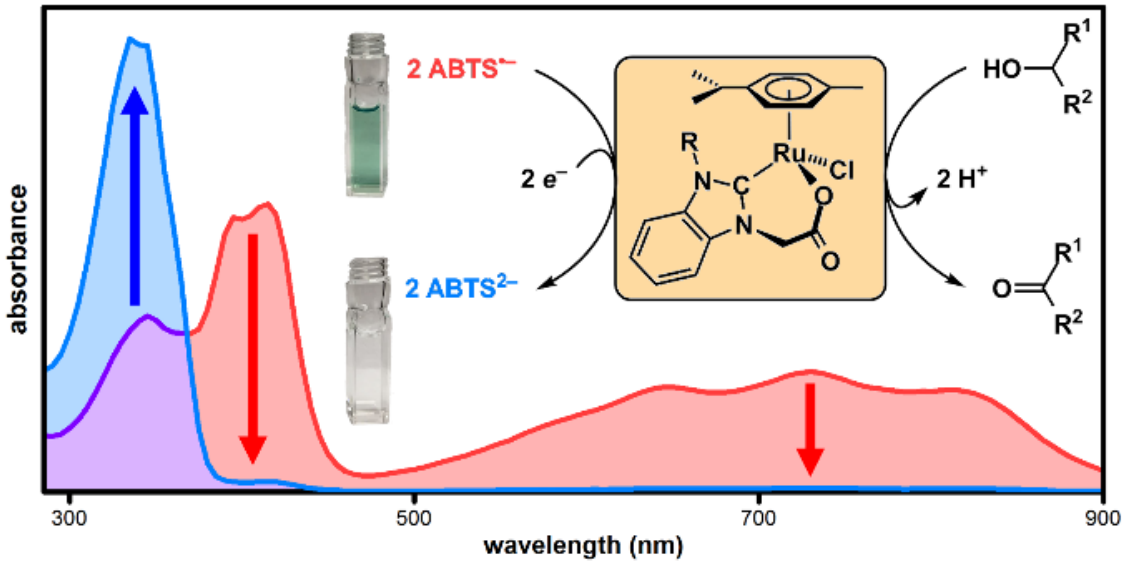

Figure 2. An organoruthenium complex catalyzed radical reduction in buffered aqueous solution using amino acids, sugars, or citric acid cycle metabolites as terminal reductants. These compounds are found abundant in our body and our cellular machinery exits to recycle them after being oxidized.

Reproduced from *Chem. Sci.*, 2016**, DOI:** 10.1039/C6SC00651E**.**with permission from the Royal Society of Chemistry

ABSTRACT

Metalloenzymes that normally perform catalytic antioxidant or radical-degrading functions, as well as small-molecule complexes that mimic them, can also exert pro-oxidant or radical-forming effects depending on the identity of the terminal reductant. Because nitroxyl radicals function as redox active cocatalysts in the aerobic oxidation of alcohols, we hypothesized that catalytic radical reduction could be achieved via the oxidation of biologically-relevant alcohols. Herein we report an organoruthenium complex (**Ru1**) that catalyzed reduction of 2,2'-azino-bis(3-ethylbenzo-thiazoline-6-sulfonate) radical monoanion ($ABTS^{\bullet-}$) to $ABTS^{2-}$ in phosphate buffered saline (pH 7.4) using MeOH, EtOH, *i*-PrOH, serine, threonine, glucose, arabinose, methyl lactate or dimethyl malate as the terminal reductant. Replacing either the C–H and O–H groups of a –CHOH– moiety resulted in the loss of $ABTS^{\bullet-}$ reducing ability. Moreover, **Ru1** was able to inhibit the oxidation of $ABTS^{2-}$ by H_2O_2 and horseradish peroxidase, even after multiple successive challenges with excess H_2O_2 or $ABTS^{\bullet-}$. Collectively, these results demonstrate that **Ru1** inhibits the oxidative formation of and catalyzes the reduction of radicals in aqueous solution via oxidation of biologically-relevant alcohols.

INTRODUCTION

Reactive oxygen species (ROS) such as superoxide (O_2^-) and hydrogen peroxide (H_2O_2) can alter the structures and functions of biomolecules[1,2] via DNA base lesion formation,[3] transition metal ion release from proteins,[4] and membrane phospholipid chain degradation.[5] Antioxidants can prevent or attenuate this damage by reacting with ROS to yield less oxidizing, more stable radical or non-radical products. Superoxide dismutase (SOD) and catalase, for example, are metalloenzymes that protect cells by catalyzing the disproportionation of O_2^- and H_2O_2, respectively.[6] Synthetic Mn–salen and Mn–porphyrin complexes have demonstrated both SOD and catalase activity,[7] and some have entered Phase 1 clinical trials as therapeutics for neurodegenerative and pulmonary diseases.[8]

Recent studies have shown that these classes of synthetic Mn complexes can also exert pro-oxidant effects at low ROS concentrations, [9,10] dichotomous behavior that is consistent with the enzymes they mimic. Catalase converts 2 H_2O_2 into O_2 + 2 H_2O (Scheme 1.1, *i*),[11] wherein the first equivalent of H_2O_2 is reduced to H_2O and generates an Fe(IV)=O$^{\bullet+}$ intermediate, which then oxidizes the second equivalent of H_2O_2 to O_2 and releases H_2O.[12] At low H_2O_2 concentrations, this Fe(IV)=O$^{\bullet+}$ intermediate can abstract H$^\bullet$ from other molecules (i.e., A–H) and thus exhibit peroxidase-like reactivity (Scheme 1.1, *ii*).[13] Conversely, peroxidase can exhibit catalase-like reactivity at low A–H / high H_2O_2 concentrations.[14] Because the Mn–salen and Mn–porphyrin complexes proceed through high-valent Mn oxo/hydroxo intermediates[15-18] with oxidizing power comparable to Fe(IV)=O$^{\bullet+}$, their reactivity will mimic catalase or peroxidase based on the availability

of H_2O_2. Therefore, the function of catalase and its biomimetic Mn complexes as either antioxidants or pro-oxidants will be determined by the nature of the terminal reductant.

A catalytic oxidation reaction important in synthetic chemistry is the aerobic oxidation of R^1–CHOH–R^2 to R^1–C(=O)–R^2 that does not cause any (1) over-oxidation to R–COOH or (2) undesired reactions at other functional groups.[19-23] One strategy employs a copper or ruthenium catalyst in conjunction with a nitroxyl radical, such as 2,2,6,6-tetramethylpiperidinyl-*N*-oxyl (TEMPO), to oxidize R^1–CHOH–R^2 to R^1–C(=O)–R^2 with concomitant formation of TEMPO–H (Scheme 1.1, *iii*). Subsequent regeneration of the TEMPO radical occurs with the oxidation of TEMPO–H by O_2, which functions as the terminal oxidant for this reaction (Scheme 1.1, *iv*). Because the TEMPO radical is reduced by R^1–CHOH–R^2 in the aerobic alcohol oxidation catalytic cycle, we hypothesized that the catalytic reduction of other radicals could also be achieved via the oxidation (i.e., dehydrogenation) of non-tertiary alcohols (Scheme 1.1, *v*). Herein we report the validation of this hypothesis with an organoruthenium complex that catalyzes the reduction and inhibits the formation of radicals in buffered aqueous solutions via the oxidation of biologically-relevant non-tertiary alcohols. Given the successes of Group 8 transfer hydrogenation catalysts as chemotherapeutics[24,25] in particular and the burgeoning scope of medicinal applications for transition metal-based catalytic systems[26-28] in general, we anticipate that the reduction of radicals via the Ru-catalyzed oxidation of alcohols will lead to new strategies for protecting against ROS *in vivo*.

RESULTS AND DISCUSSION

Approach and rationale

We recently reported a Ru complex supported by a chelating N-heterocyclic carbene–carboxylate ligand (**Ru1**, Scheme 1.2A) that catalyzed the hydrogenation of C=O, C=N and C=C bonds, in which the H_2 transferred was obtained from the oxidation of *i*-PrOH to acetone.[32] Based on this catalytic chemical reactivity observed with **Ru1** and previous reports of other Ru complexes with chelating carboxylate ligands exerting antioxidant effects in cells, which derived from irreversible stoichiometric reactions with nitric oxide,[33,34] we hypothesized that **Ru1** would function as a catalytic antioxidant, reducing radicals using non-tertiary alcohols as terminal reductants. Using methods previously reported by our group,[32,35] the N-heterocyclic carbene (NHC) ligand precursor [**1**H_2][Br] was treated with Ag_2O to afford the Ag–NHC complex [Ag(**1**)]$_n$ (**2**). The NHC ligand was subsequently transferred to Ru via the reaction of **2** with [{RuCl(η^6-cymene)}$_2$(μ-Cl)$_2$], which yielded the Ru–NHC complex [RuCl(**1**)(η^6-cymene)] (**Ru1**).

As a radical substrate to probe antioxidant activity, 2,2'-azino-bis(3-ethylbenzothiazoline-6-sulfonate) radical monoanion ($ABTS^{\bullet-}$, Scheme 1.2B) was selected on the basis of its large extinction coefficient (ε) at long wavelengths (ε_{750} = 1.6 × 10^4 M^{-1} cm^{-1} in EtOH and ε_{734} = 1.5 × 10^4 M^{-1} cm^{-1} in aqueous buffer),[30] its reversible one-electron reduction to $ABTS^{2-}$ ($E_{1/2}$ = 0.68 V vs. NHE) falling within the range of potentials accessible in biological systems (–0.4 to +0.8 V vs. NHE),[36] and its stability in aerobic, protic media. The longer absorption wavelength and greater extinction coefficient for $ABTS^{\bullet-}$ enables spectroscopic analysis of radical-degrading and -forming

reactions (1) with less interference from other optically absorbing species present in biological systems and (2) at lower concentrations‡ more relevant to oxidative stress than would be possible with direct measurements of $O_2^{\bullet-}$ ($\varepsilon_{250} = 1.9 \times 10^3$ M^{-1} cm^{-1}) or H_2O_2 ($\varepsilon_{240} = 43.6$ M^{-1} cm^{-1}).[37,38] Furthermore, the $1e^-$ reduction potential for $ABTS^{\bullet-}$ is lower than or comparable to the standard reduction potentials for several of the oxidizing species associated with oxidative stress in biological systems (e.g., $E° = 1.78$ V for H_2O_2, 1.6 V for $RO^{\bullet}$, 1.0 V for $ROO^{\bullet}$, 0.92 V for $Cys–S^{\bullet}$, 0.70 for O_2, etc.), [36] therefore $ABTS^{\bullet-}$ is a reasonable substrate for approximating biologically-relevant oxidants.

As a non-catalytic antioxidant control, Trolox (Scheme 1.2C) was employed given its use as a benchmark in a variety of radical degradation and antioxidant studies.[39] Trolox can serve as a $1e^-$ or $2e^-$ reductant, whereby the first $1e^-$ oxidation is accompanied by rapid H^+ loss to form a phenoxyl radical ($TrO^{\bullet}$), which can then undergo a second $1e^-$ oxidation to form a phenoxonium cation (TrO^+). However, in methanol (MeOH) or ethanol (EtOH) solutions, these processes converge into a single $2e^-$ oxidation.[40] Subsequent hydrolysis of TrO^+ can then cleave the tertiary carbon–oxonium bond, which renders the $2e^-$ oxidation of Trolox irreversible.

Because ROS and other oxidants can cause damage to critical biomolecules, inhibiting the formation of these oxidizing species in biological systems can potentially prevent the onset of harmful pathologies.[2] As a model system, we selected the oxidation of $ABTS^{2-}$ to $ABTS^{\bullet-}$ by horseradish peroxidase (HRP) and H_2O_2 (i.e., Scheme 1.1, *ii*).[31] However, before studying the ability of **Ru1** to inhibit $ABTS^{\bullet-}$ formation, it was first necessary to explore the fundamental reactivity of **Ru1** with $ABTS^{\bullet-}$ under controlled

conditions and achieve the catalytic reduction of $ABTS^{\bullet-}$ to $ABTS^{2-}$ in buffered aqueous solution.

Catalytic radical reduction in EtOH

Addition of 5 μM **Ru1** (CH_3CN stock) to 50 μM $ABTS^{\bullet-}$ in EtOH caused a 100% decay in $ABTS^{\bullet-}$ concentration within 15 min (Fig. 2.1, red line), accompanied by the formation of 50 μM $ABTS^{2-}$ (Fig. 2.2), indicating the 1:1 conversion of $ABTS^{\bullet-}$ to $ABTS^{2-}$ by **Ru1**. No $ABTS^{\bullet-}$ degradation occurred when CH_3CN alone was added (Fig. 2.1, dotted green line), indicating that **Ru1** was essential for the reduction of $ABTS^{\bullet-}$ to $ABTS^{2-}$ and that CH_3CN did not impact $ABTS^{\bullet-}$ stability. No $ABTS^{\bullet-}$ formation was observed in an aerobic solution containing 5 μM **Ru1** and 50 μM $ABTS^{2-}$, indicating that **Ru1** does not oxidize $ABTS^{2-}$ to $ABTS^{\bullet-}$ under these conditions. In contrast to **Ru1**, the addition of 5 μM Trolox caused a rapid (within mixing time) 22% decrease in $ABTS^{\bullet-}$ concentration (Fig. 2.1, blue line), which corresponded to the reduction of 10 μM $ABTS^{\bullet-}$ (2 equiv. vs Trolox) and was consistent with the ability of Trolox to serve as a non-catalytic $2e^-$ reductant in EtOH solution.[40]

To assess its catalytic potential and corresponding regeneration, the reactivity of **Ru1** with multiple sequential aliquots of excess $ABTS^{\bullet-}$ was examined. After the reduction of 50 μM $ABTS^{\bullet-}$ by 5 μM **Ru1** was complete (Fig. 2.3, red line), 2 additional 50 μM $ABTS^{\bullet-}$ aliquots were introduced[§] and complete $ABTS^{\bullet-}$ reduction was observed in each instance, indicating that **Ru1** remained catalytically competent for the complete reduction of 150 μM $ABTS^{\bullet-}$ (30 turnovers). Unlike **Ru1**, the addition of successive 10 μM aliquots[§] of $ABTS^{\bullet-}$ following the initial reduction by 5 μM Trolox (Fig. 2.3, blue

line) only caused the radical absorbance to increase by amounts equivalent to the concentration of $ABTS^{\bullet-}$ added, indicating that the antioxidant capacity of Trolox had been exhausted after the reduction of only 2 equiv. of $ABTS^{\bullet-}$. However, subsequent addition of 5 μM **Ru1** to the exhausted Trolox solution containing 70 μM $ABTS^{\bullet-}$ resulted in 100% radical reduction within 30 min.

Addition of 5 μM ascorbate ($AscH^-$) or 5 μM glutathione (GSH) to a solution of 50 μM $ABTS^{\bullet-}$ in EtOH caused the $ABTS^{\bullet-}$ concentration to decrease by 5% or 60% (Figs. 2.4–2.5), values that were consistent with their ability to function as $1e^-$ or $6e^-$ reductants, respectively, under these experimental conditions.[41-43] Similar to the experiments with Trolox, subsequent addition of $ABTS^{\bullet-}$ only afforded increases in radical absorbance equal to the concentration of $ABTS^{\bullet-}$ added, which likewise indicated that the antioxidant capacity of $AscH^-$ and GSH had been exhausted. Quantitative radical reduction could nonetheless be achieved via addition of 5 μM **Ru1** to the exhausted $AscH^-$ or GSH solutions that contained excess $ABTS^{\bullet-}$. Collectively, these data demonstrate that **Ru1** can catalytically reduce $ABTS^{\bullet-}$ and, because it is regenerated after each reaction cycle, that a catalytic antioxidant can offer significantly greater protection than traditional stoichiometric antioxidants, such as Trolox, $AscH^-$ and GSH.

Although $ABTS^{\bullet-}$ degradation has been previously observed with other Ru complexes,[44-46] **Ru1** is the first to demonstrate catalytic $ABTS^{\bullet-}$ reduction. It is important to note that the previous studies measured percentage of $ABTS^{\bullet-}$ degradation with respect to Ru complex concentration, for the purpose of determining dose dependence. However, the reported absorbance vs. time plots displayed significantly slower $ABTS^{\bullet-}$

degradation for the Ru complexes compared to Trolox (much like **Ru1** vs. Trolox, Fig. 2.1) and 100% $ABTS^{\bullet-}$ degradation at multiple Ru concentrations (demonstrating dose *independence*). Thus, it is possible that a previously reported Ru complex may have degraded $ABTS^{\bullet-}$ catalytically, but its significantly slower reactivity compared to Trolox created the appearance that the percent of $ABTS^{\bullet-}$ degraded was dependent on Ru complex concentration and led to the conclusion that the observed radical degradation was non-catalytic.

Catalytic radical reduction in aqueous buffer

As a catalyst for the $1e^-$ reduction of $ABTS^{\bullet-}$ to $ABTS^{2-}$, **Ru1** itself cannot serve as the terminal reductant for this reaction, a role most likely played by the EtOH solvent for the experiments displayed in Fig. 2.1. To test this hypothesis and identify the chemical features required for terminal reductant function, it was first necessary to determine experimental conditions under which no $ABTS^{\bullet-}$ degradation occurred in the presence of **Ru1** alone. Phosphate-buffered saline (PBS, pH 7.4) was selected as a suitable reaction medium because neither the solvent (H_2O) nor the buffer components (Na_2HPO_4, KH_2PO_4, NaCl, KCl) would undergo oxidation to supply the electrons necessary for the reduction of $ABTS^{\bullet-}$ (i.e., Fig. 2.6, *i*). No degradation of $ABTS^{\bullet-}$ in PBS was observed after treatment with 5 μM **Ru1** (Fig. 2.6, *ii*), indicating this solution lacked a suitable terminal reductant. Subsequent addition of 50 mM EtOH to this PBS solution containing 5 μM **Ru1** and 50 μM $ABTS^{\bullet-}$ caused the $ABTS^{\bullet-}$ concentration to decrease (Fig. 2.6, *iii*), evidence that the electrons needed for the $ABTS^{\bullet-}$ reduction observed in Fig. 1 were ultimately supplied by the EtOH solvent.

If the hypothesis that the oxidation of R_1–CHOH–R_2 to R_1–C(=O)–R_2 provides the electrons necessary for the reduction of $ABTS^{\bullet-}$ to $ABTS^{2-}$ is correct (i.e., Scheme 2.1, *v*), then both the O–H and C–H groups in a –CHOH– moiety will be essential for terminal reductant function. To test this hypothesis, PBS solutions containing 5 μM **Ru1** and 50 μM $ABTS^{\bullet-}$ were treated with 50 mM MeOH, *i*-PrOH, *t*-BuOH, ethylene glycol (EG) or 1,2-dimethoxyethane (DME) and the $ABTS^{\bullet-}$ concentration was measured. With MeOH, *i*-PrOH and EG, the $ABTS^{\bullet-}$ concentration began to decrease immediately following addition of the alcohol, indicating that these alcohols could serve as terminal reductants (Figs. 2.7–2.9). In contrast, no $ABTS^{\bullet-}$ reduction was observed with DME or *t*-BuOH (e.g., Fig. 2.10, *ii*). However, when the addition of 50 mM *t*-BuOH was followed by 50 mM EtOH, $ABTS^{\bullet-}$ reduction did occur (Fig. 2.10, *iii*), revealing that the lack of reactivity with *t*-BuOH was not due to catalyst deactivation but rather the inability of *t*-BuOH to serve as a terminal reductant. Collectively, these results show that the C–H and O–H groups of a –CHOH– moiety are both essential for terminal reductant function, which is consistent with the hypothesis that oxidation of R_1–CHOH–R_2 to R_1–C(=O)–R_2 provides the reducing equivalents necessary to convert $ABTS^{\bullet-}$ to $ABTS^{2-}$. Replacing either the C–H group with C–Me or the O–H group with O–Me precludes this oxidation and thus the ability to function as a terminal reductant, which is supported by the lack of $ABTS^{\bullet-}$ reduction observed with *t*-BuOH and DME.

Biologically–relevant terminal reductants

A wide variety of biomolecules comprise –CHOH– groups, therefore we hypothesized that sugars, amino acids and citric acid cycle metabolites could serve as

suitable terminal reductants in **Ru1**-catalyzed $ABTS^{\bullet-}$ reduction. To test this hypothesis, PBS solutions containing 5 μM **Ru1** and 50 μM $ABTS^{\bullet-}$ were treated with 50 mM serine, threonine, glucose, arabinose, malic acid or lactic acid. Reduction of $ABTS^{\bullet-}$ was markedly slower following the addition of the amino acids compared to the sugars, consistent with the greater number of CH–OH groups per molecule in the latter (Fig. 2.11). No significant differences in reactivity were observed between serine and threonine or between glucose and arabinose.

Malic acid and lactic acid are metabolites of the citric acid cycle and each comprises a –CHOH– group. However, no $ABTS^{\bullet-}$ reduction occurred following the addition of 50 mM malic acid or lactic acid to 5 μM **Ru1** and 50 μM $ABTS^{\bullet-}$ in PBS (Fig. 2.12). Malate and lactate will be the predominant species in pH 7.4 PBS, and these carboxylate anions can function as chelating bidentate ligands, which could potentially disrupt the catalytic activity of **Ru1**. To prevent catalyst deactivation, the methyl esters of these substrates were used. Addition of 50 mM methyl lactate (Me-lactate) or dimethyl malate (Me_2-malate) to PBS solutions containing 5 μM **Ru1** and 50 μM $ABTS^{\bullet-}$ caused the $ABTS^{\bullet-}$ concentration to decrease rapidly. None of the biologically-relevant alcohols afforded $ABTS^{\bullet-}$ reduction in the absence of **Ru1**, and no oxidation of $ABTS^{2-}$ to $ABTS^{\bullet-}$ by **Ru1** was observed under any experimental conditions in PBS.

Inhibition of oxidative radical formation

Having obtained unambiguous evidence that **Ru1** catalyzes $ABTS^{\bullet-}$ reduction using biologically-relevant alcohols as terminal reductants, we next sought to demonstrate that **Ru1** could also inhibit radical formation. As the model system, we

utilized the *in situ* oxidation of $ABTS^{2-}$ to $ABTS^{\bullet-}$ by horseradish peroxidase (HRP) and H_2O_2 (i.e., Scheme 2.1, *ii*).[31] Addition of 10 μM H_2O_2 to a PBS solution of 10 nM HRP, 20 μM $ABTS^{2-}$, 5 μM **Ru1**, and 50 mM EtOH caused the $ABTS^{\bullet-}$ concentration to increase immediately. The $ABTS^{\bullet-}$ concentration peaked at 1.0 μM after 2.3 min, which then gradually declined and complete $ABTS^{\bullet-}$ reduction was observed 13 min after the peak (Fig. 2.13A, red line). No $ABTS^{\bullet-}$ formation occurred when 10 μM H_2O_2 was added to 5 μM **Ru1** and 20 μM $ABTS^{2-}$ in PBS, indicating that **Ru1** did not cause any pro-oxidant reactions. Because **Ru1** and Trolox were added as 30 μL aliquots from 5.0 mM stock solutions in CH_3CN, 10 μM H_2O_2 was added to a PBS solution containing 10 nM HRP, 20 μM $ABTS^{2-}$ and 0.19 M CH_3CN to control for the influence of this solvent. The radical absorbance immediately began to increase and reached a maximum of 17.9 μM after 50 min (Fig. 2.13A, dotted green line and Fig. 2.14). In contrast, the addition of 10 μM H_2O_2 to a PBS solution of 5 μM Trolox, 10 nM HRP and 20 μM $ABTS^{2-}$ resulted in no change in $ABTS^{\bullet-}$ concentration for the first 7.6 min, demonstrating that Trolox completely halted $ABTS^{\bullet-}$ formation (Fig. 2.13A, blue line). After 7.6 min, however, the $ABTS^{\bullet-}$ concentration began to increase and reached a maximum of 9.3 μM at 12 min after the onset of $ABTS^{\bullet-}$ formation. Notably, the maximum [$ABTS^{\bullet-}$] observed in the presence of Trolox was 8.6 μM lower than the control, which was consistent with the ability of Trolox to function as a $2e^-$ reductant (cf., Fig. 2 or Scheme 2.2). For the control and Trolox experiments, the decline in $ABTS^{\bullet-}$ concentration after peaking was consistent with normal $ABTS^{\bullet-}$ thermal decay.

To determine if **Ru1** remained catalytically competent after the complete reduction of $ABTS^{\bullet-}$ formed by 10 nM HRP and 10 μM H_2O_2, two additional 10 μM aliquots of H_2O_2 were introduced (Fig. 2.13B, red line). Impressively, the concentration of $ABTS^{\bullet-}$ never exceeded 0.4 μM and decreased back to zero in less than 16 min after the introduction of the second and third H_2O_2 aliquots. In contrast, addition of the second 10 μM H_2O_2 aliquot to the Trolox experiment caused the $ABTS^{\bullet-}$ concentration to gradually increase by 7.9 μM over the course of 38 min (Fig. 2.13B, blue line), effectively resulting in complete oxidation of $ABTS^{2-}$ to $ABTS^{\bullet-}$ (96% of the 17.9 μM observed for control). It was therefore unsurprising that the third 10 μM H_2O_2 aliquot produced no change in radical absorbance. Subsequent addition of 50 mM EtOH and 5 μM **Ru1** caused the $ABTS^{\bullet-}$ concentration to decrease rapidly, affording quantitative $ABTS^{\bullet-}$ reduction in less than 30 min.

To confirm that the results obtained with **Ru1** arose from its ability to catalyze $ABTS^{\bullet-}$ reduction, rather than inhibiting HRP or another chemical reaction, two 10 μM aliquots of chemically synthesized $ABTS^{\bullet-}$ were introduced after the $ABTS^{\bullet-}$ concentration had decreased to zero following the initial addition of 10 μM H_2O_2 (Fig. 2.13C, red line). The first and second $ABTS^{\bullet-}$ aliquots produced immediate increases in $ABTS^{\bullet-}$ concentration corresponding to 6.3 and 6.7 μM, respectively, followed by rapid decreases in radical absorbance that resulted in quantitative radical reduction within 75 s of aliquot addition. With the Trolox experiment, however, the first and second $ABTS^{\bullet-}$ aliquots caused [$ABTS^{\bullet-}$] to increase by 9.9 and 9.7 μM, respectively, with no observable changes in radical absorbance other than thermal decay (Fig. 2.13C, blue line). Addition

of 50 mM EtOH and 5 μM **Ru1** after the second $ABTS^{\bullet-}$ aliquot afforded complete $ABTS^{\bullet-}$ reduction within 30 min, similar to the experiment with multiple H_2O_2 aliquots. Both $AscH^-$ and GSH inhibited the HRP-induced oxidation of $ABTS^{2-}$, albeit for shorter periods of time and less effectively than Trolox. The introduction of additional H_2O_2 (Figs. 2.14–2.15) or $ABTS^{\bullet-}$ aliquots (Figs. 2.16–2.17) only afforded increases in $ABTS^{\bullet-}$ concentration that mirrored the behaviors observed for Trolox (i.e., Figs. 2.13B–C). Subsequent addition of 50 mM EtOH and 5 μM **Ru1** to the $AscH^-$ and GSH solutions containing excess $ABTS^{\bullet-}$ produced quantitative radical reduction, consistent with the Trolox experiments.

Synthetic Procedures

General synthetic considerations. N-(*p*-tolyl)benzimidazole and $ABTS^{\bullet-}$ were prepared as previously described.[29,30] All other materials were of reagent quality and used as received. All solvents used were HPLC grade. ^1H and $^{13}C\{^1H\}$ NMR spectra were recorded using a Bruker 500 MHz spectrometer. Chemical shifts δ (in ppm) for ^1H and ^{13}C NMR are referenced to $SiMe_4$ using the residual protio-solvent as an internal standard. For ^1H NMR: $CDCl_3$, 7.26 ppm; DMSO-d_6, 2.50 ppm. For ^{13}C NMR: $CDCl_3$, 77.16 ppm; DMSO-d_6, 39.52 ppm. Coupling constants (*J*) are expressed in hertz (Hz). Infrared spectra were recorded with 4 cm^{-1} resolution on a Shimadzu IRAffinity-1S spectrometer equipped with a Pike Technologies MIRacle ATR (diamond) sampling accessory. Elemental analyses were performed at Atlantic Microlab, Inc. (Norcross, GA). All reactions were performed under an inert atmosphere under an N_2 atmosphere using standard Schlenk or glovebox techniques with the exclusion of light. All subsequent

manipulations were performed under ambient conditions using standard benchtop techniques without the exclusion of light. When required, solvents were dried and deoxygenated using an Innovative Technologies solvent purification system, and then stored over molecular sieves (3 Å) in a drybox.

Synthesis of 2-(3-{*p*-tolyl}-benzimidazol-1-ium-1-yl)-acetate hydrobromide [1H$_2$][Br]. Bromoacetic acid (503 mg, 3.62 mmol) and N-(*p*-tolyl)benzimidazole (500 mg, 2.41 mmol) were dissolved with 20 mL of toluene in a vial equipped with a stir bar. The vial was then sealed with a Teflon-lined cap and the clear, dark orange-brown solution was heated to 120 °C. After 16 h, a white precipitate had formed, at which point the reaction mixture was allowed to cool to room temperature and the precipitate was collected by filtration. The resulting solid was washed with minimum toluene followed by CH_2Cl_2 and was then dried *in vacuo* to afford 514 mg (1.48 mmol, 80% yield) of the desired product as a white powder. ^{1}H NMR (500 MHz, DMSO-d_6): δ = 13.95 (s, 1H), 10.18 (s, 1H), 8.18 (d, J = 8.0, 1H), 7.85 (d, J = 8.0, 1H), 7.78–7.73 (m, 4H), 7.57 (d, J = 8.0, 2H), 5.58 (s, 2H), 2.47 (s, 3H). ^{13}C NMR (125 MHz, DMSO-d_6): δ 167.5, 143.3, 140.5, 131.5, 130.8, 130.6, 130.4, 127.4, 127.1, 124.8, 114.3, 113.4, 47.8, 20.7. FT-IR (KBr): 3421 (vw), 2953 (m), 2372 (m), 1718 (m), 1560, 1508 (m), 1381 (m), 1300 (m), 1225 (m), 822, 754, 742, 482 (vw) cm^{-1}. Anal. Calcd. for $C_{16}H_{16}BrN_2O_{2.5}$ ([**1**H$_2$][Br]•0.5H$_2$O): C, 53.95; H, 4.53; N, 7.86. Found: C, 54.01; H, 4.35; N, 7.79.

Synthesis of [Ag(1)]$_n$ (2). To a solution of [**1**H$_2$][Br] (500 mg, 144 μmol) in anhydrous CH_2Cl_2 (50 mL) under nitrogen was added Ag_2O (502 mg, 217 μmol), and the resulting white suspension was allowed to stir at room temperature in the absence of

light. After 24 h, the reaction mixture was filtered and the resulting grey solid was washed with $CHCl_3$ (10 mL). The filtrate solvent was removed under reduced pressure and the resulting solids were then dried *in vacuo* to afford 452 mg (121 μmol, 84% yield) of the desired product as an off-white powder. ^{1}H NMR (500 MHz, DMSO-d_6): δ 7.71 (d, J = 8.5, 1H), 7.58 (d, J = 8.0, 2H), 7.44–7.38 (m, 5H), 5.09 (s, 2H), 2.39 (s, 3H). ^{13}C NMR (125 MHz, DMSO-d_6): δ 138.6, 135.2, 134.1, 133.4, 130.3, 125.6, 124.1, 112.7, 111.6, 99.5, 79.1, 52.1, 20.6. FT-IR (KBr): 3416 (w), 1608, 1516, 1475, 1439, 1385, 1308, 1250, 1207 (m), 1109 (m), 1094 (m), 1018 (m), 835, 814, 746, 715, 482 (w) cm^{-1}. Anal. Calcd. for $C_{16}H_{14}N_2O_{2.5}Ag$ (**2**•0.5H_2O): C, 50.36; H, 3.77; N, 7.49. Found: C, 50.23; H, 4.09; N, 7.05.

Synthesis of [RuCl(1)(η^6-cymene)] (Ru1). To a stirred solution of **2** (100 mg, 134 μmol) in anhydrous CH_2Cl_2 (10 mL) under nitrogen was added [RuCl(η^6-cymene)(μ-Cl)]$_2$ (82 mg, 134 μmol) dissolved in 10 mL of CH_2Cl_2. During the course of the addition, the mixture changed first to a clear red and then to a clear orange solution with concomitant formation of a white precipitate, and the reaction was allowed to stir at room temperature. After 24 h, the reaction mixture was filtered through a 0.2 μm PTFE filter (to remove AgCl) with the aid of CH_2Cl_2 (4 mL). The filtrate solvent was removed under reduced pressure and the resulting solids were then dried *in vacuo* to afford 71.7 mg (134 μmol, 98%) of the desired product as a light red-orange powder. ^{1}H NMR (500 MHz, $CDCl_3$): δ 7.95 (d, J = 8.0, 1H), 7.49–7.44 (m, 2H), 7.41 (d, J = 10.0, 1H), 7.37–7.32 (m, 2H), 7.25–7.23 (m, 1H), 7.04 (d, J = 8.5, 1H), 5.43 (d, J = 6.0, 1H), 5.18 (d, J = 6.0, 1H), 5.16 (d, J = 6.5, 1H), 5.04 (d, J = 5.5, 1H), 4.91 (d, J = 17.0, 1H), 4.71 (d, J = 18.5, 1H),

3.95 (d, J = 5.5, 1H), 2.60 (sep, 1H), 2.52 (s, 3H), 2.03 (s, 3H), 1.08 (d, J = 7.5, 3H). ^{13}C NMR (125 MHz, $CDCl_3$): δ 186.6, 169.2, 140.3, 136.8, 136.0, 134.0, 131.1, 131.0, 129.7, 127.4, 124.2, 124.1, 111.3, 110.2, 104.7, 103.2, 90.0, 89.4, 83.6, 80.3, 49.9, 30.9, 23.3, 22.0, 21.5, 19.0. FT-IR (KBr): 3429 (vw), 3055 (w), 2959 (m), 2872 (w), 2230 (w), 2100 (w), 1628 (vs), 1514, 1475, 1443, 1373 (w), 1356, 1300, 1244, 1207 (m), 1190 (m), 1014, 930, 862, 843 (m), 827 (m), 804, 748, 663 (m), 615, 555, 476 (m), 470, 424, 405 cm^{-1}. Anal. Calcd. for $C_{26}H_{23}ClN_2O_2Ru$: C, 58.26; H, 5.08; N, 5.23. Found: C, 57.98; H, 4.95; N, 5.17.

Spectroscopic and Kinetic Analysis Procedures

General spectroscopic considerations. UV–visible absorption spectra were acquired on a Varian Cary 50 Bio spectrometer equipped with a water-cooled Quantum Northwest TC-125 peltier temperature controller. All solution measurements were performed at 25.0 ± 0.1 °C in matched gas-tight quartz cuvettes (Precision Scientific) with 1 cm path lengths and 3.0 mL analyte solution volumes. Absorption spectra were acquired from 900 to 200 nm with a scanning speed of 300 nm min^{-1} and a resolution of 0.5 nm. Each kinetic analysis experiment (5 second intervals) was performed in quadruplicate on four different days. Stock solutions were prepared fresh daily and filtered (0.2 μm PTFE) immediately prior to use.

Kinetic analysis of ABTS$^{\bullet-}$ degradation in EtOH. An aliquot of ABTS$^{\bullet-}$ (40 μL from a 3.75 mM stock solution in H_2O) was added to EtOH to afford the ABTS$^{\bullet-}$ working solution in EtOH. The absorbance spectrum of this working solution was acquired to confirm ABTS$^{\bullet-}$ concentration and the single wavelength kinetics program

was initiated. After 20 s, the cuvette was removed from the spectrometer without stopping the kinetics program, an aliquot of **Ru1**, Trolox, ascorbate or glutathione was added, the cuvette was covered and mixed via repeated inversion for 3 s, placed back in the spectrometer, and the kinetics program was allowed to continue. After the kinetics program had completed, the absorbance spectrum was acquired to confirm formation of $ABTS^{2-}$ from the peak at 340 nm.

Representative procedure for kinetic analysis of $ABTS^{\bullet-}$ degradation by Ru1 in PBS. An aliquot of $ABTS^{\bullet-}$ (40 μL from a 3.75 mM stock solution in H_2O) was added to PBS to afford the $ABTS^{\bullet-}$ working solution in PBS. The absorbance spectrum of this working solution was acquired to confirm $ABTS^{\bullet-}$ concentration and the single wavelength kinetics program was initiated. After 20 s, the cuvette was removed from the spectrometer without stopping the kinetics program, an aliquot of **Ru1** (30 μL from 0.5 mM stock solution in CH_3CN) was added, the cuvette was covered and mixed via repeated inversion for 3 s, placed back in the spectrometer, and the kinetics program was allowed to continue. After 5 min, an aliquot of EtOH (30 μL from 5.0 M stock solution in H_2O) was added, the cuvette was covered and mixed via repeated inversion for 3 s, placed back in the spectrometer, and the kinetics program was allowed to continue. After the kinetics program had completed, the absorbance spectrum was acquired to confirm formation of $ABTS^{2-}$ from the peak at 340 nm.

Kinetic analysis of $ABTS^{\bullet-}$ formation by HRP in PBS. Derived from a literature procedure.[31] Aliquots of $ABTS^{2-}$ (30 μL from a 2.0 mM stock solution in H_2O), HRP (30 μL from a 1.0 μM stock solution in H_2O), and **Ru1**, Trolox, ascorbate or

glutathione were added to PBS (pH 7.4) to afford the $ABTS^{2-}$/**Ru1** (or Trolox or ascorbate or glutathione)/HRP working solution in PBS. The absorbance spectrum of this working solution was acquired to confirm no $ABTS^{\bullet-}$ - had formed. An aliquot of H_2O_2 (30 μL from 1.0 mM stock solution in H_2O) was added, the cuvette was covered and mixed via repeated inversion for 3 s, placed back in the spectrometer, and the single wavelength kinetics program was initiated. For the control enzyme experiments, the aliquot of H_2O_2 was added directly after HRP, and the analysis was performed with no other additives.

CONCLUSIONS

An organoruthenium complex (**Ru1**) that was previously reported to catalyze the hydrogenation of unsaturated organic substrates, using the oxidation of *i*-PrOH to acetone to supply the needed H_2, can also catalyze the reduction of $ABTS^{\bullet-}$ to $ABTS^{2-}$ in buffered aqueous solution. By itself, **Ru1** was unreactive towards $ABTS^{\bullet-}$ and the presence of a non-tertiary alcohol was essential for $ABTS^{\bullet-}$ reduction to occur. Replacing either the C–H or O–H group in a –CHOH– moiety with C–Me or O–Me, respectively, resulted in the loss of $ABTS^{\bullet-}$ reducing ability. Given the previously reported transfer hydrogenation activity of **Ru1** and the fact that **Ru1**-catalyzed $ABTS^{\bullet-}$ reduction required a reactant comprising a –CHOH– moiety, we deduced that the reducing equivalents necessary for the $1e^-$ reduction of $ABTS^{\bullet-}$ to $ABTS^{2-}$ were supplied by the oxidation of R_1–CHOH–R_2 to R_1–C(=O)–R_2. Consistent with this deduction, a diverse array of biologically-relevant non-tertiary alcohols, including amino acids, sugars and citric acid cycle metabolites, were found to be suitable terminal reductants for the reduction of $ABTS^{\bullet-}$ catalyzed by **Ru1**. Furthermore, **Ru1** was able to inhibit the oxidation of $ABTS^{2-}$ to $ABTS^{\bullet-}$ by H_2O_2 and horseradish peroxidase with the help of a non–tertiary alcohol. In contrast, non-catalytic antioxidants (Trolox, ascorbate, glutathione), only offered limited protection that, once exhausted, had no impact on $ABTS^{\bullet-}$ formation or stability. Impressively, no $ABTS^{\bullet-}$ formation or other pro-oxidant effects by **Ru1** were observed under any experimental conditions. The mechanism for the catalytic reduction of $ABTS^{\bullet-}$ by **Ru1** and non-tertiary alcohols, along with the biological applications, will be detailed in subsequent reports.

Acknowledgements

We are grateful to A. Mangalum for preceding work and helpful insight into the synthesis of **2** and **Ru1**.

Notes

‡ In PBS, an $ABTS^{\bullet-}$ concentration of 6.7 μM would give rise to an absorbance value of 0.1. Achieving a similar value with $O_2^{\bullet-}$ or H_2O_2 would require a concentration of 53 μM or 2.29 mM, respectively.

§ The concentration of the successive $ABTS^{\bullet-}$ aliquots was selected based on the concentration of the initial 50 μM $ABTS^{\bullet-}$ that was degraded by the antioxidant. Because **Ru1** degraded all of the initial 50 μM $ABTS^{\bullet-}$ and Trolox only degraded 10 μM, the concentration of the multiple sequential aliquots added was 50 μM with **Ru1** and 10 μM with Trolox.

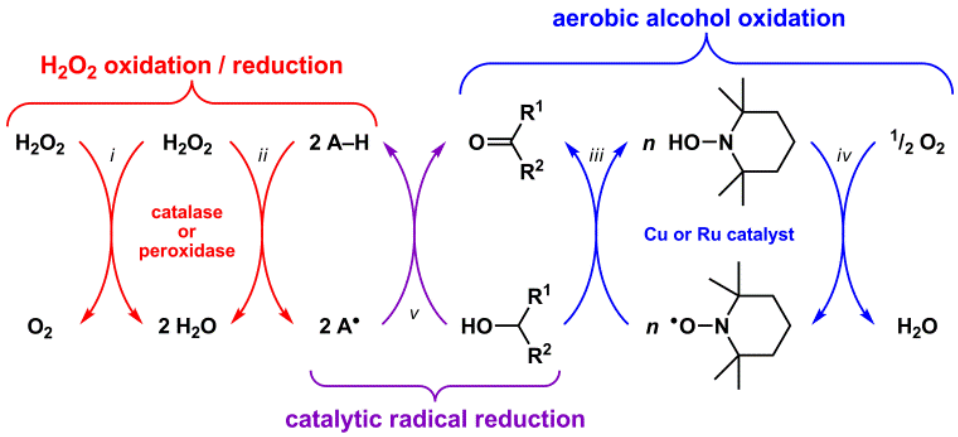

Scheme 2.1. Catalase normally catalyzes the disproportionation of 2 $H_2O_2 \rightarrow O_2 + 2\ H_2O$ (*i*), but at low H_2O_2 concentrations it can abstract $H^{\bullet}$ from other molecules (A–H) and produce radicals ($A^{\bullet}$) in a manner similar to peroxidase (*ii*). Copper or ruthenium complexes can catalyze the oxidation of R^1–CHOH–R^2 to R^1–C(=O)–R^2 using a nitroxyl radical (e.g., TEMPO, $n = 1$ for Cu, $n = 2$ for Ru) as the $H^{\bullet}$ abstracting reagent (*iii*) and O_2 as the terminal oxidant (*iv*). By a similar mechanism, a complex could catalyze radical reduction using a biologically relevant non-tertiary alcohol as the terminal reductant (*v*).

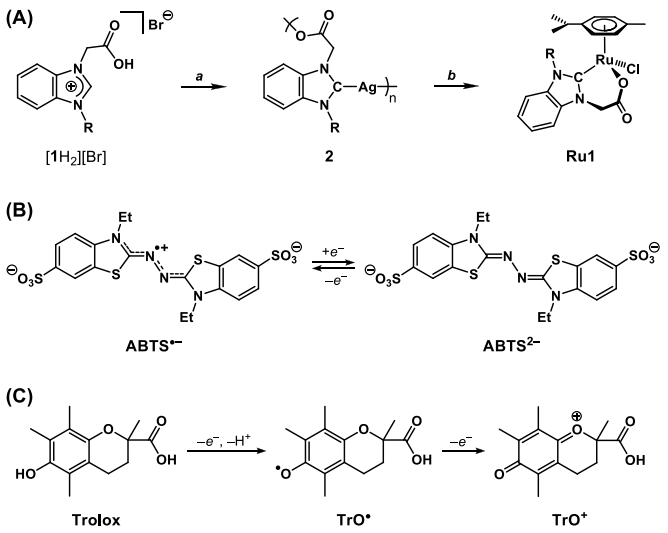

Scheme 2.2. (**A**) Synthesis of [**1**H_2][Br], **2** and **Ru1**. Reagents and conditions: (*a*) Ag_2O (1.5 equiv.) or (*b*) [{RuCl(η^6-cymene)}$_2$(μ-Cl)$_2$] (1:1 Ag/Ru), CH_2Cl_2, room temperature, 24 h. R = *p*-tolyl. (**B**) One-electron redox interconversion between $ABTS^{\bullet-}$ and $ABTS^{2-}$ (NH_4^+ counterions omitted for clarity). (**C**) First and second one-electron oxidations of Trolox.

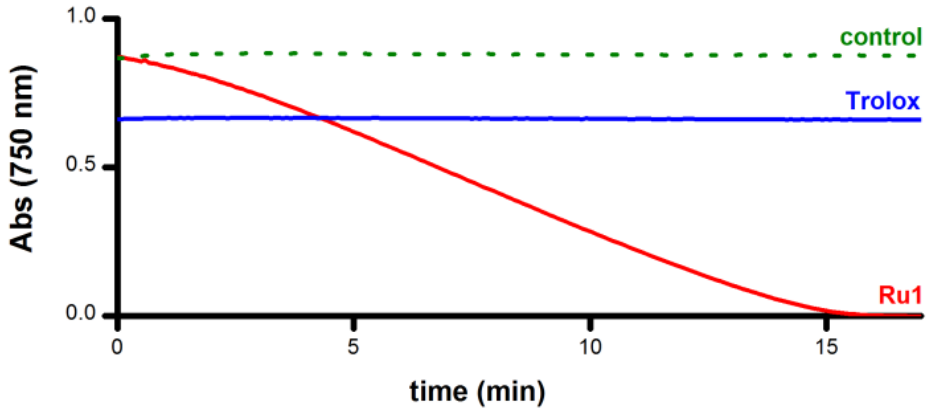

Fig. 2.1. Plot of relative [$ABTS^{\bullet-}$] vs. time in EtOH following the addition of **Ru1** (CH_3CN stock, red line), Trolox (CH_3CN stock, blue line), or CH_3CN alone (dotted green line). Conditions: $[\mathbf{Ru1}]_0$ or [Trolox] = 5 μM, $[ABTS^{\bullet-}]_0$ = 50 μM, EtOH, 25 °C; [$ABTS^{\bullet-}$] determined using absorbance measured at 750 nm and $\varepsilon_{750} = 1.6 \times 10^4\ M^{-1}\ cm^{-1}$ (ref 33)

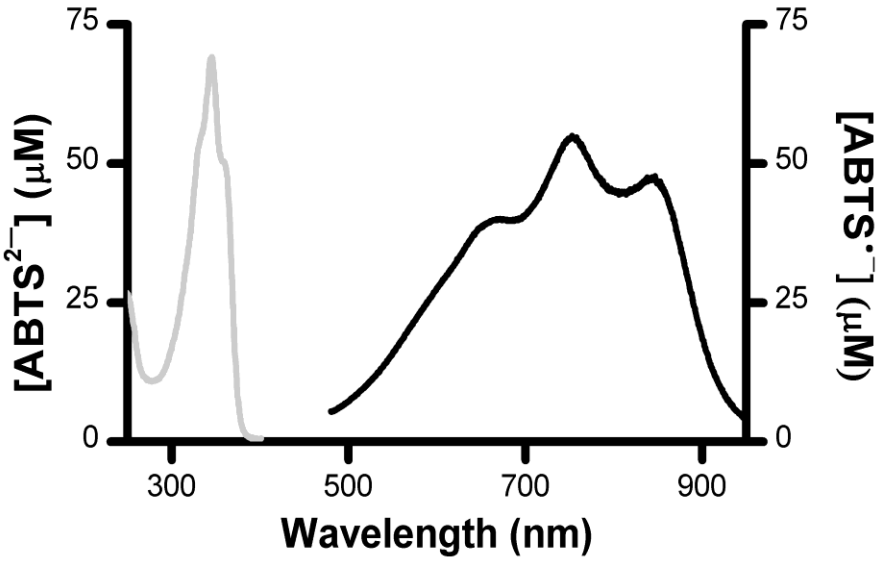

Fig. 2.2. UV/vis of $ABTS^{2-}$ formed from $ABTS^{\bullet-}$ degradation by **Ru1** in EtOH. The absorbance at 340 nm (grey line) represents the total amount of $ABTS^{2-}$ which includes the additional $ABTS^{2-}$ formed and $ABTS^{2-}$ from the original stock solution. Conditions: $[\mathbf{Ru1}]_0$ = 5 μM, $[ABTS^{\bullet-}]_0$ = 50 μM, EtOH, 25 °C, absorbance measured from 200–950 nm.

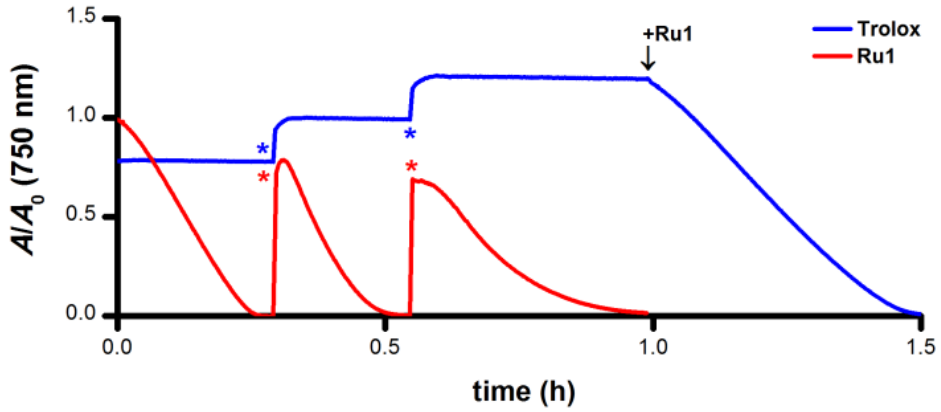

Fig. 2.3. Plot of relative [$ABTS^{\bullet-}$] vs. time which shows the reduction of $ABTS^{\bullet-}$ after adding **Ru1** (red line) followed by 2 additional 50 μM $ABTS^{\bullet-}$ aliquots (*) and Trolox (blue line) followed by 2 additional 10 μM $ABTS^{\bullet-}$ aliquots (*), then 5 μM **Ru1**. Conditions: $[\mathbf{Ru1}]_0$ or $[Trolox]_0$ = 5 μM, $[ABTS^{\bullet-}]_0$ = 50 μM, EtOH, 25 °C; [$ABTS^{\bullet-}$] determined using absorbance measured at 750 nm and $\varepsilon_{750} = 1.6 \times 10^4\ M^{-1}\ cm^{-1}$ (ref 33)

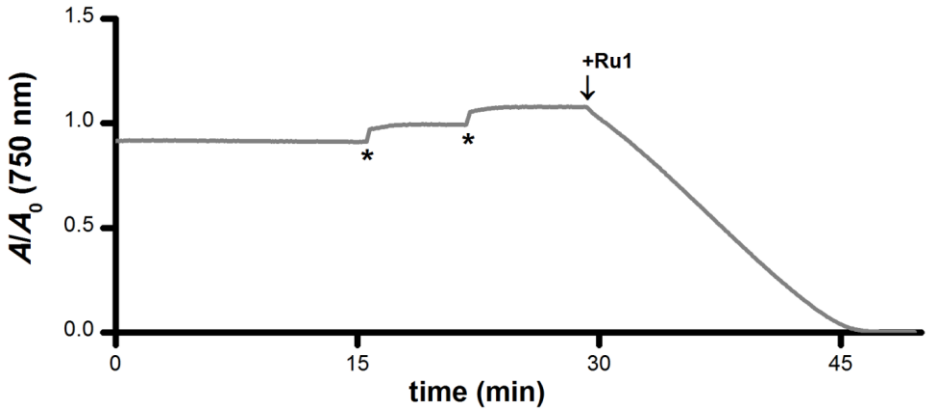

Fig. 2.4. Addition of 5 μM ascorbate ($AscH^-$) to an EtOH solution containing 50 μM $ABTS^{\bullet-}$ caused a rapid (within mixing time) 10% decrease in the absorbance at 750 nm, consistent with ascorbate functioning as a $1e^-$ reductant (i.e., $AscH^- \rightarrow Asc^{\bullet}$). Two additional 5 μM $ABTS^{\bullet-}$ aliquots were then introduced (*), which only caused the absorbance at 750 nm to increase by amounts equivalent to the concentration of $ABTS^{\bullet-}$ added, indicating that the antioxidant capacity of ascorbate had been exhausted after the reduction of only 1 equiv. of $ABTS^{\bullet-}$. Subsequent addition of 5 μM **Ru1** produced a 100% decrease in radical absorbance, indicating that **Ru1** could achieve quantitative $ABTS^{\bullet-}$ reduction under experimental conditions in which ascorbate (a traditional antioxidant) had been exhausted. Conditions: $[AscH^-]_0$ = 5 μM, [**Ru1**] = 5 μM, $[ABTS^{\bullet-}]_0$ = 50 μM, EtOH, 25 °C; absorbance measured at 750 nm.

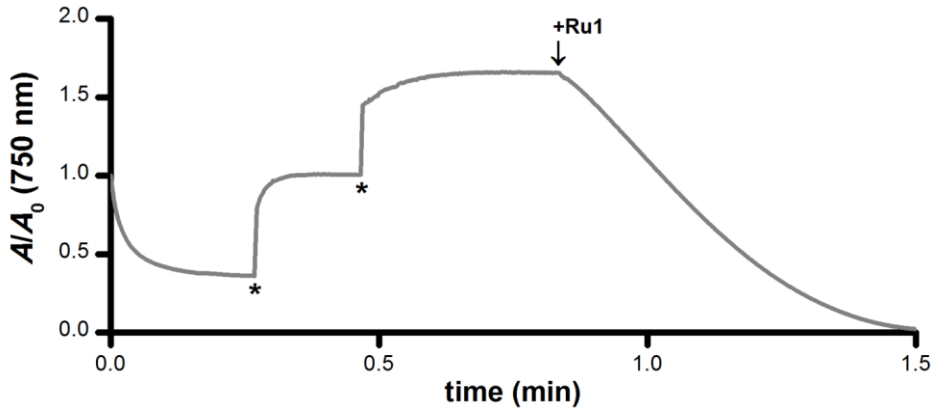

Fig. 2.5. Addition of 5 μM glutathione (G–SH) to an EtOH solution containing 50 μM $ABTS^{\bullet-}$ caused a gradual 60% decrease in the absorbance at 750 nm, consistent with glutathione functioning as a $6e^-$ reductant (i.e., G–SH → $G–SO_3H$). Two additional 30 μM $ABTS^{\bullet-}$ aliquots were then introduced (*), which only caused the absorbance at 750 nm to increase by amounts equivalent to the concentration of $ABTS^{\bullet-}$ added, indicating that the antioxidant capacity of glutathione had been exhausted after the reduction of only 6 equiv. of $ABTS^{\bullet-}$. Subsequent addition of 5 μM **Ru1** produced a 100% decrease in radical absorbance, indicating that **Ru1** could achieve quantitative $ABTS^{\bullet-}$ reduction under experimental conditions in which glutathione (a traditional antioxidant) had been exhausted. Conditions: $[G–SH]_0$ = 5 μM, [**Ru1**] = 5 μM, $[ABTS^{\bullet-}]_0$ = 50 μM, EtOH, 25 °C; absorbance measured at 750 nm.

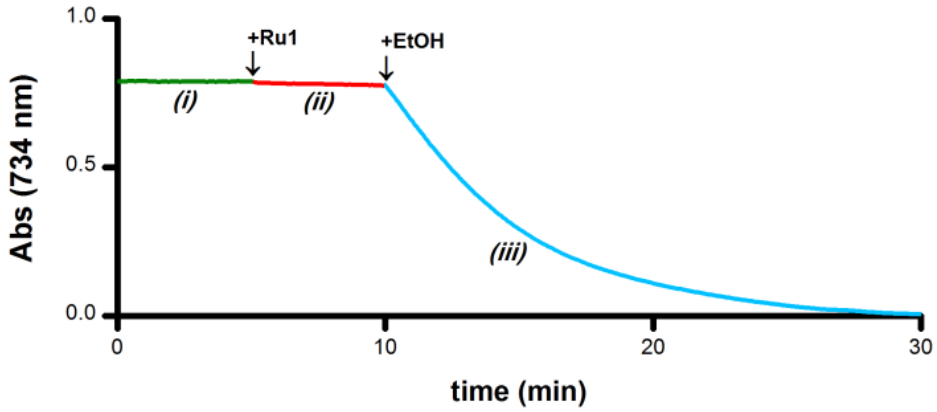

Fig. 2.6. Plot of relative [ABTS$^{\bullet-}$] vs. time which shows the catalytic reduction of ABTS$^{\bullet-}$ by **Ru1** in PBS. By itself, ABTS$^{\bullet-}$ was stable in PBS (*i*, green line). Addition of **Ru1** did not cause ABTS$^{\bullet-}$ reduction (*ii*, red line). Subsequent addition of EtOH caused the absorbance to decrease (*iii*, blue line), which indicated that EtOH functioned as a terminal reductant. Conditions: [**Ru1**]$_0$ = 5 μM, [ABTS$^{\bullet-}$]$_0$ = 50 μM, [EtOH]$_0$ = 50 mM, PBS (pH 7.4), 25 °C; [ABTS$^{\bullet-}$] determined using absorbance measured at 734 nm and $\varepsilon_{734} = 1.5 \times 10^4\ M^{-1}\ cm^{-1}$ (ref 33)

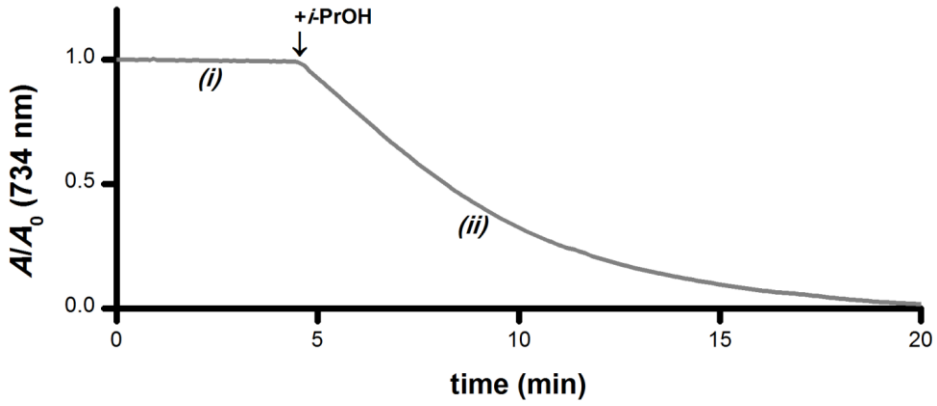

Fig. 2.7. Catalytic $ABTS^{\bullet-}$ reduction in PBS by **Ru1** with *i*-PrOH as the terminal reductant. No $ABTS^{\bullet-}$ degradation was observed in a PBS solution containing only **Ru1** (*i*), but subsequent addition of *i*-PrOH caused the absorbance at 734 nm to decrease (*ii*). Conditions: $[\mathbf{Ru1}]_0$ = 5 μM, $[ABTS^{\bullet-}]_0$ = 50 μM, $[i\text{-PrOH}]_0$ = 50 mM, PBS (pH 7.4), 25 °C, absorbance measured at 734 nm.

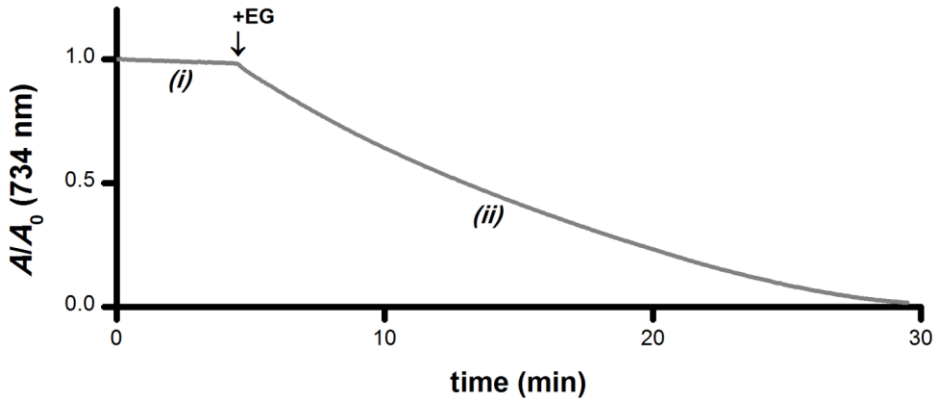

Fig. 2.8. Catalytic $ABTS^{\bullet-}$ reduction in PBS by **Ru1** with ethylene glycol (EG) as the terminal reductant. No $ABTS^{\bullet-}$ degradation was observed in a PBS solution containing only **Ru1** (*i*), but subsequent addition of EG caused the absorbance at 734 nm to decrease (*ii*). Conditions: $[\mathbf{Ru1}]_0$ = 5 μM, $[ABTS^{\bullet-}]_0$ = 50 μM, $[EG]_0$ = 50 mM, PBS (pH 7.4), 25 °C, absorbance measured at 734 nm.

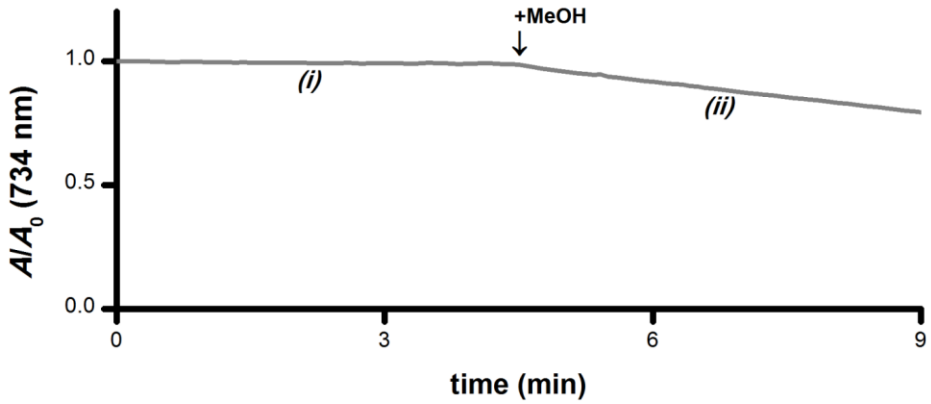

Fig. 2.9. Catalytic $ABTS^{\bullet-}$ reduction in PBS by **Ru1** with MeOH as the terminal reductant. No $ABTS^{\bullet-}$ degradation was observed in a PBS solution containing only **Ru1** (*i*), but subsequent addition of MeOH caused the absorbance at 734 nm to decrease (*ii*). Conditions: $[\mathbf{Ru1}]_0$ = 5 μM, $[ABTS^{\bullet-}]_0$ = 50 μM, $[MeOH]_0$ = 50 mM, PBS (pH 7.4), 25 °C, absorbance measured at 734 nm.

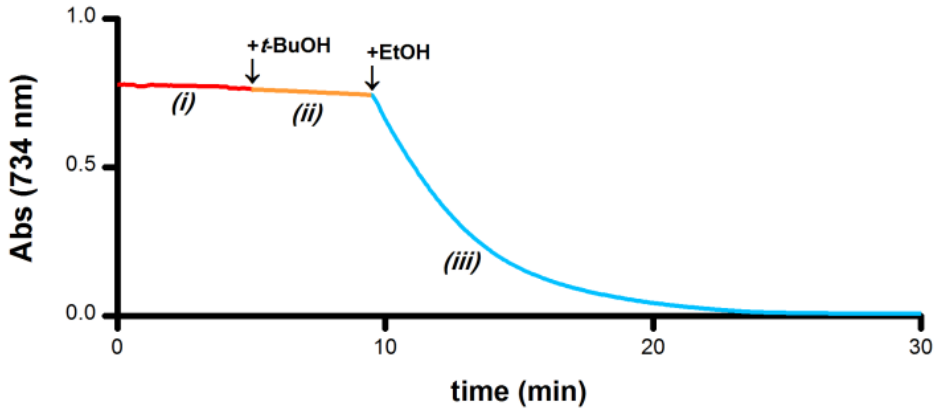

Fig. 2.10. Plot of relative [ABTS$^{\bullet-}$] vs. time which shows the catalyst is not deactivated by *t*-BuOH. In a PBS solution containing only **Ru1**, ABTS$^{\bullet-}$ was stable (*i*, red line). Addition of *t*-BuOH did not cause any ABTS$^{\bullet-}$ reduction (*ii*, orange line). Subsequent addition of EtOH resulted in ABTS$^{\bullet-}$ degradation (*iii*, blue line), indicating that the lack of reactivity with *t*-BuOH was not due to catalyst deactivation. Conditions: [**Ru1**]$_0$ = 5 μM, [ABTS$^{\bullet-}$]$_0$ = 50 μM, [*t*-BuOH]$_0$ = 50 mM, [EtOH]$_0$ = 50 mM, PBS (pH 7.4), 25 °C; [ABTS$^{\bullet-}$] determined using absorbance measured at 734 nm and $\varepsilon_{734} = 1.5 \times 10^4$ M^{-1} cm^{-1} (ref 33).

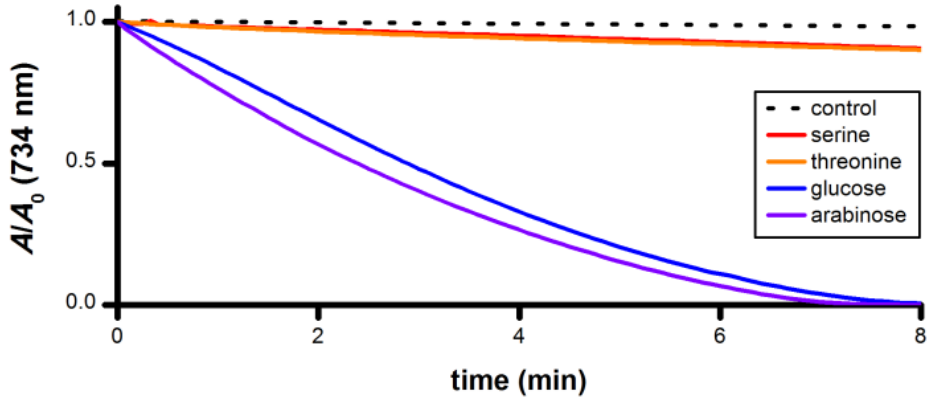

Fig. 2.11. Plot of relative [ABTS$^{\bullet-}$] vs. time following the addition of amino acid or sugar (t = 0) to PBS solutions containing ABTS$^{\bullet-}$ and **Ru1**. Conditions: [**Ru1**]$_0$ = 5 μM, [ABTS$^{\bullet-}$]$_0$ = 50 μM, [ROH]$_0$ = 50 mM, PBS (pH 7.4), 25 °C; [ABTS$^{\bullet-}$] determined using absorbance measured at 734 nm and $\varepsilon_{734} = 1.5 \times 10^4$ M^{-1} cm^{-1} (ref 33).

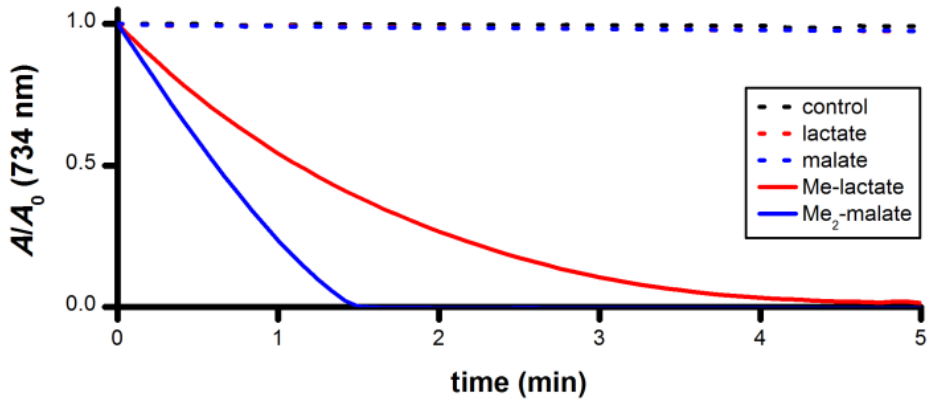

Fig. 2.12. Plot of relative [ABTS$^{\bullet-}$] vs. time following the addition of lactate, malate or their methyl esters (t = 0) to PBS solutions containing ABTS$^{\bullet-}$ and **Ru1**. Conditions: [**Ru1**]$_0$ = 5 μM, [ABTS$^{\bullet-}$]$_0$ = 50 μM, [ROH]$_0$ = 50 mM, PBS (pH 7.4), 25 °C; [ABTS$^{\bullet-}$] determined using absorbance measured at 734 nm and ε_{734} = 1.5 × 10^4 M^{-1} cm^{-1} (ref 33)

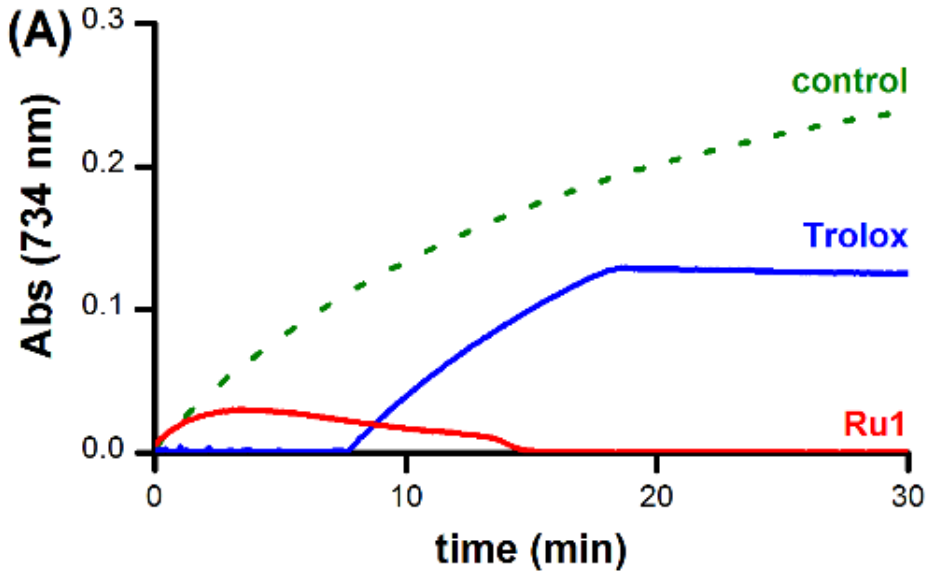

Fig. 2.13 (**A**) Plot of relative [$ABTS^{\bullet-}$] vs. time which shows the *in situ* oxidation of $ABTS^{2-}$ to $ABTS^{\bullet-}$ via HRP and H_2O_2 in the presence of **Ru1** and EtOH (red line), Trolox (blue line) or 0.19 M CH_3CN as a control (dotted green line). Conditions: $[HRP]_0$ = 10 nM, $[\mathbf{Ru1}]_0$ or $[Trolox]_0$ = 5 μM, $[H_2O_2]_0$ = 10 μM, $[ABTS^{2-}]_0$ = 20 μM, $[EtOH]_0$ = 50 mM, PBS (pH 7.4) at 25 °C; [$ABTS^{\bullet-}$] determined using absorbance measured at 734 nm and $\varepsilon_{734} = 1.5 \times 10^4\ M^{-1}\ cm^{-1}$ (ref 33)

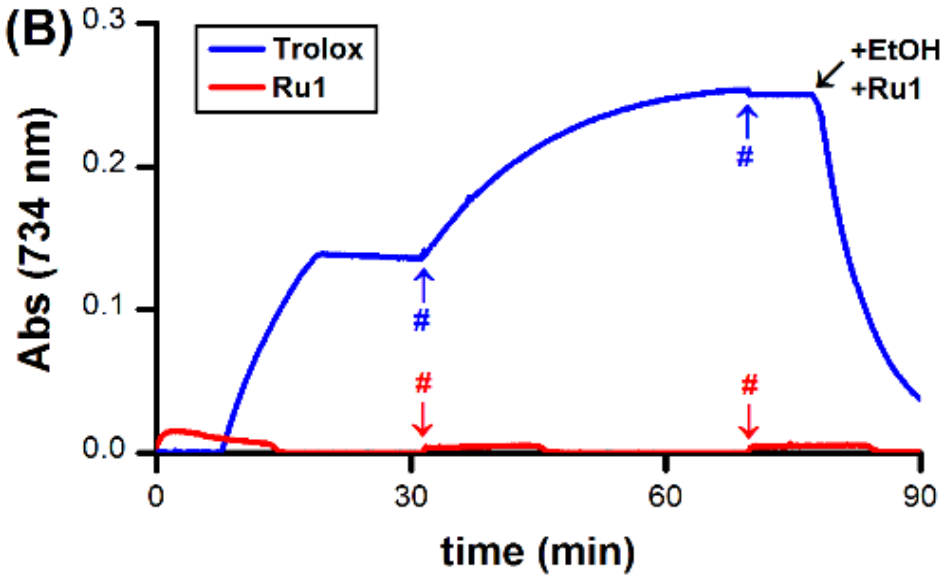

Fig. 2.13.B Plot of relative [$ABTS^{\bullet-}$] vs. time which shows the $ABTS^{\bullet-}$ formation by HRP in the presence of **Ru1** and EtOH (red line) or Trolox (blue line) followed by two additional aliquots of 10 μM H_2O_2 (#). For the Trolox experiments shown, 50 mM EtOH and 5 μM **Ru1** were added after the final aliquot of H_2O_2 or $ABTS^{\bullet-}$, respectively. Conditions: $[HRP]_0$ = 10 nM, $[\mathbf{Ru1}]_0$ or $[Trolox]_0$ = 5 μM, $[H_2O_2]_0$ = 10 μM, $[ABTS^{2-}]_0$ = 20 μM, $[EtOH]_0$ = 50 mM, PBS (pH 7.4) at 25 °C; [$ABTS^{\bullet-}$] determined using absorbance measured at 734 nm and $\varepsilon_{734} = 1.5 \times 10^4\ M^{-1}\ cm^{-1}$ (ref 33)

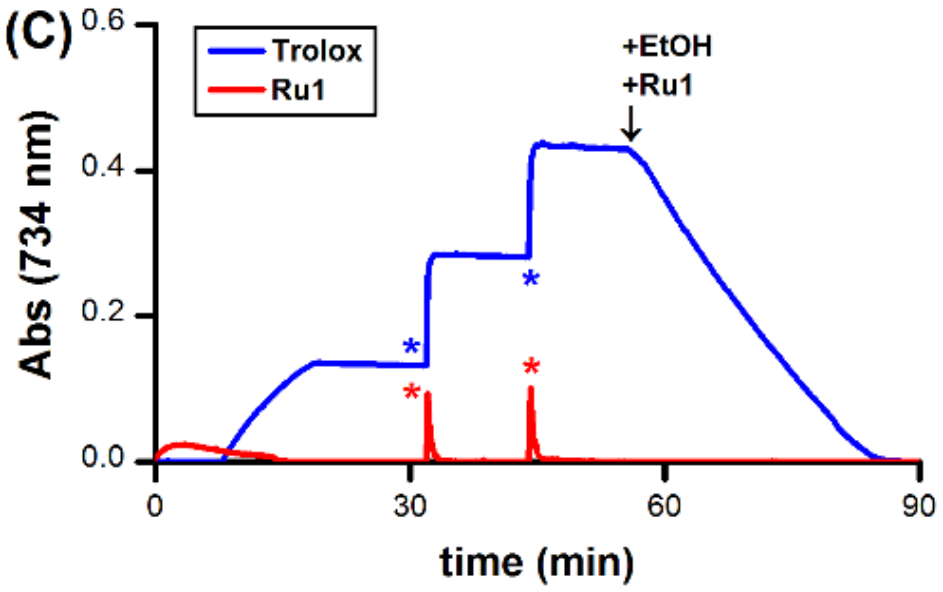

Fig. 2.13 C. Plot of relative [$ABTS^{\bullet-}$] vs. time which shows the two 10 μM aliquots of chemically synthesized $ABTS^{\bullet-}$ (*). For the Trolox experiments shown, 50 mM EtOH and 5 μM **Ru1** were added after the final aliquot of H_2O_2 or $ABTS^{\bullet-}$, respectively. Conditions: $[HRP]_0$ = 10 nM, $[\mathbf{Ru1}]_0$ or $[Trolox]_0$ = 5 μM, $[H_2O_2]_0$ = 10 μM, $[ABTS^{2-}]_0$ = 20 μM, $[EtOH]_0$ = 50 mM, PBS (pH 7.4) at 25 °C; [$ABTS^{\bullet-}$] determined using absorbance measured at 734 nm and $\varepsilon_{734} = 1.5 \times 10^4\ M^{-1}\ cm^{-1}$ (ref 33)

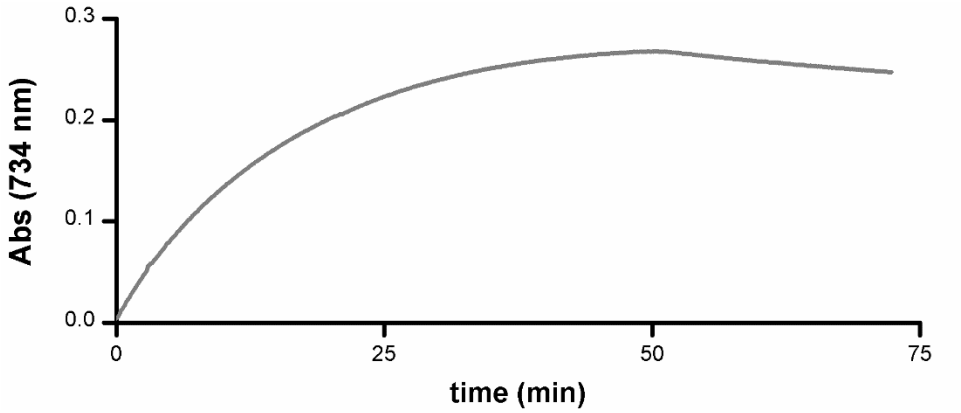

Fig. 2.14. *In situ* oxidation of $ABTS^{2-}$ to $ABTS^{\bullet-}$ via horseradish peroxidase (HRP) and H_2O_2 in the presence of 0.19 M CH_3CN. Formation of $ABTS^{\bullet-}$ began immediately following addition of H_2O_2 (t = 0). After 50 min, [$ABTS^{\bullet-}$] reached a maximum of 17.9 μM. The subsequent gradual decline in A_{734} was due to normal $ABTS^{\bullet-}$ thermal decay. Conditions: $[CH_3CN]_0$ = 0.19 M, $[HRP]_0$ = 10 nM, $[H_2O_2]_0$ = 10 μM, $[ABTS^{2-}]_0$ = 20 μM; PBS (pH 7.4), 25 °C; absorbance measured at 734 nm.

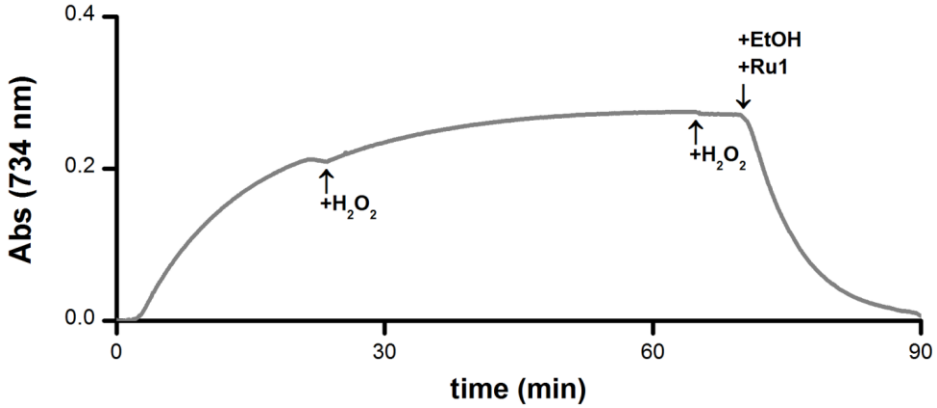

Fig. 2.15. *In situ* oxidation of $ABTS^{2-}$ to $ABTS^{\bullet-}$ via horseradish peroxidase (HRP) and H_2O_2 in the presence of 5 μM glutathione (G–SH) followed by two additional aliquots of 10 μM H_2O_2. No $ABTS^{\bullet-}$ formation was observed for the first 1.4 min after the addition of the first H_2O_2 aliquot. After 1.4 min, $ABTS^{\bullet-}$ began to form and, 20 min after onset, [$ABTS^{\bullet-}$] reached a maximum of 14.1 μM. The subsequent gradual decline in A_{734} was due to normal $ABTS^{\bullet-}$ thermal decay. Addition of the second 10 μM H_2O_2 aliquot resulted in complete oxidation of the remaining $ABTS^{2-}$ over the course of 41 min, and addition of the third 10 μM H_2O_2 aliquot afforded no change in A_{734}. Subsequent addition of 50 mM EtOH and 5 μM **Ru1** caused $ABTS^{\bullet-}$ reduction to occur that was complete within 20 min of the addition of **Ru1**. Conditions: $[G–SH]_0$ = 5 μM, $[HRP]_0$ = 10 nM, $[H_2O_2]_0$ = 10 μM, $[ABTS^{2-}]_0$ = 20 μM; [**Ru1**] = 5 μM, [EtOH] = 50 mM; PBS (pH 7.4), 25 °C; absorbance measured at 734 nm.

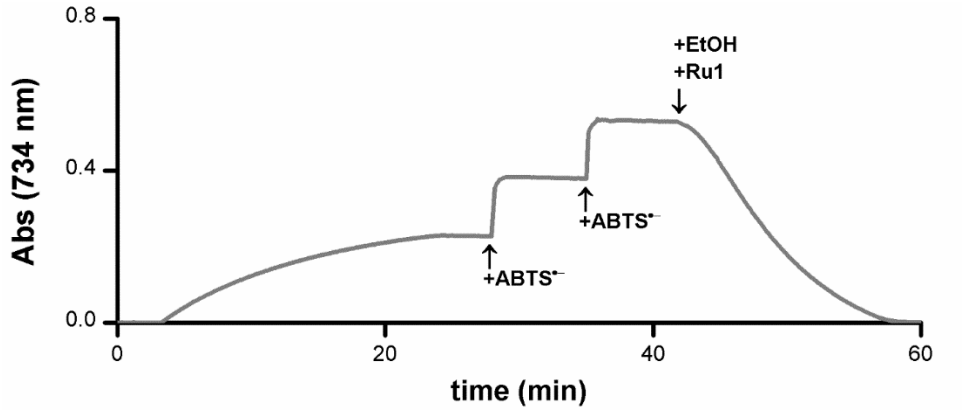

Fig. 2.16. *In situ* oxidation of $ABTS^{2-}$ to $ABTS^{\bullet-}$ via horseradish peroxidase (HRP) and H_2O_2 in the presence of 5 μM ascorbate ($AscH^-$) followed by two aliquots of 10 μM $ABTS^{\bullet-}$. No $ABTS^{\bullet-}$ formation was observed for the first 3.3 min after the addition of the first H_2O_2 aliquot. After 3.3 min, $ABTS^{\bullet-}$ began to form and, 21 min after onset, [$ABTS^{\bullet-}$] reached a maximum of 15.3 μM. The subsequent gradual decline in A_{734} was due to normal $ABTS^{\bullet-}$ thermal decay. Addition of the first and second 10 μM $ABTS^{\bullet-}$ aliquots caused A_{734} to increase by amounts proportional to the $ABTS^{\bullet-}$ added. The gradual decline in A_{734} following each $ABTS^{\bullet-}$ aliquot was due to normal $ABTS^{\bullet-}$ thermal decay. Subsequent addition of 50 mM EtOH and 5 μM **Ru1** caused $ABTS^{\bullet-}$ reduction to occur that was complete within 18 min of the addition of **Ru1**. Conditions: $[AscH^-]_0$ = 5 μM, $[HRP]_0$ = 10 nM, $[H_2O_2]_0$ = 10 μM, $[ABTS^{2-}]_0$ = 20 μM; [**Ru1**] = 5 μM, [EtOH] = 50 mM; PBS (pH 7.4), 25 °C; absorbance measured at 734 nm.

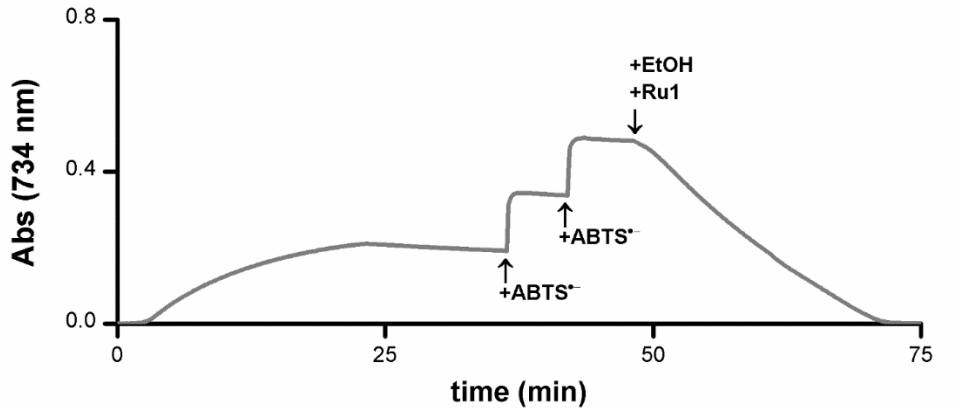

Fig. 2.17. *In situ* oxidation of $ABTS^{2-}$ to $ABTS^{\bullet-}$ via horseradish peroxidase (HRP) and H_2O_2 in the presence of 5 μM glutathione (G–SH) followed by two aliquots of 10 μM $ABTS^{\bullet-}$. No $ABTS^{\bullet-}$ formation was observed for the first 1.4 min after the addition of the first H_2O_2 aliquot. After 1.4 min, $ABTS^{\bullet-}$ began to form and, 22 min after onset, [$ABTS^{\bullet-}$] reached a maximum of 14.0 μM. The subsequent gradual decline in A_{734} was due to normal $ABTS^{\bullet-}$ thermal decay. Addition of the first and second 10 μM $ABTS^{\bullet-}$ aliquots caused A_{734} to increase by amounts proportional to the $ABTS^{\bullet-}$ added. The gradual decline in A_{734} following each $ABTS^{\bullet-}$ aliquot was due to normal $ABTS^{\bullet-}$ thermal decay. Subsequent addition of 50 mM EtOH and 5 μM **Ru1** caused $ABTS^{\bullet-}$ reduction to occur that was complete within 24 min of the addition of **Ru1**. Conditions: $[G–SH]_0$ = 5 μM, $[HRP]_0$ = 10 nM, $[H_2O_2]_0$ = 10 μM, $[ABTS^{2-}]_0$ = 20 μM; [**Ru1**] = 5 μM, [EtOH] = 50 mM; PBS (pH 7.4), 25 °C; absorbance measured at 734 nm.

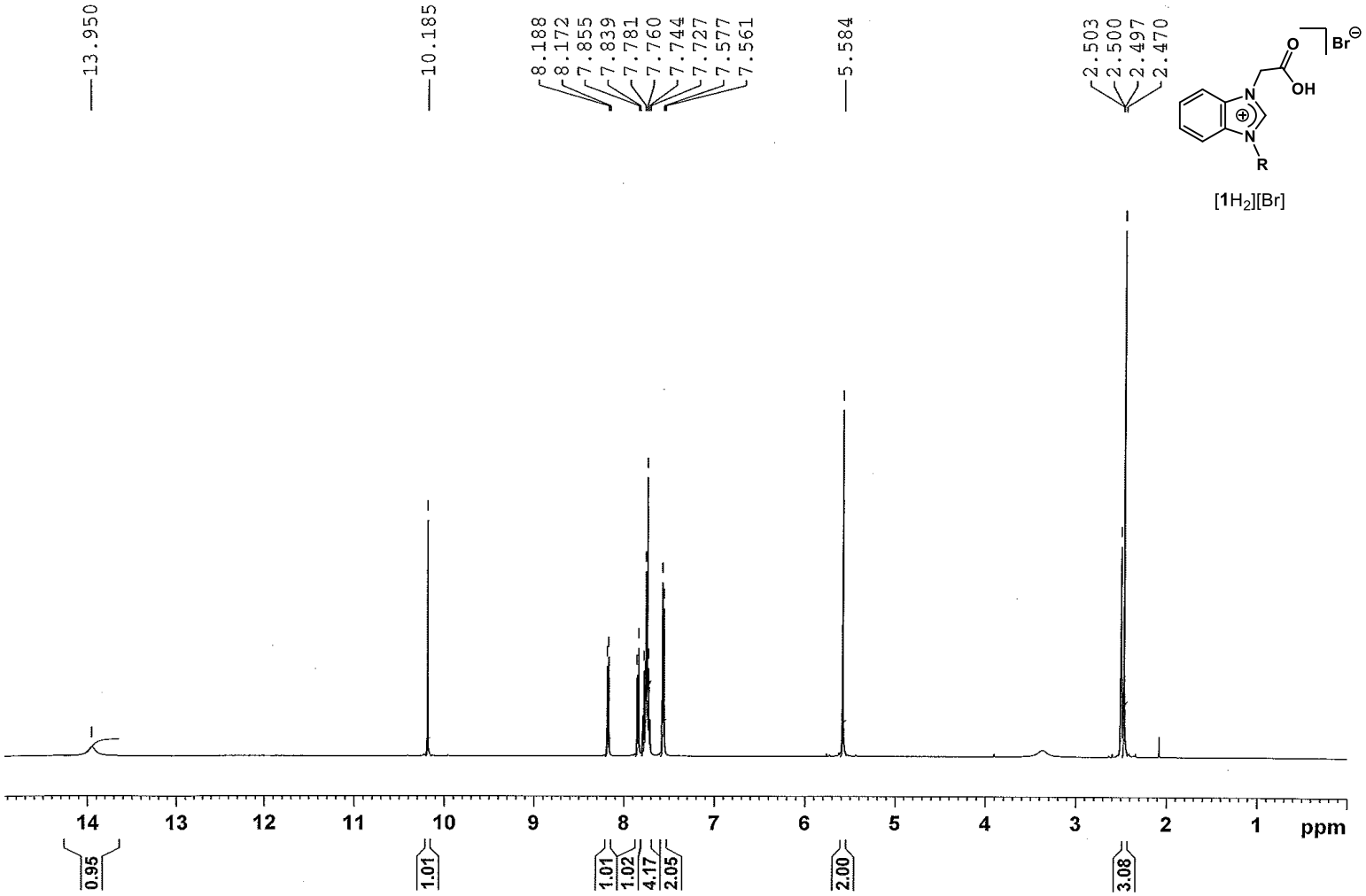
13.950
10.185
8.188
8.172
7.855
7.839
7.781
7.760
7.744
7.727
7.577
7.561
5.584
2.503
2.500
2.497
2.470
Br
O
OH
N
N
R
[1H2][Br]
14
13
12
11
10
9
8
7
6
5
4
3
2
1
ppm
0.95
1.01
1.01
1.02
4.17
2.05
2.00
3.08

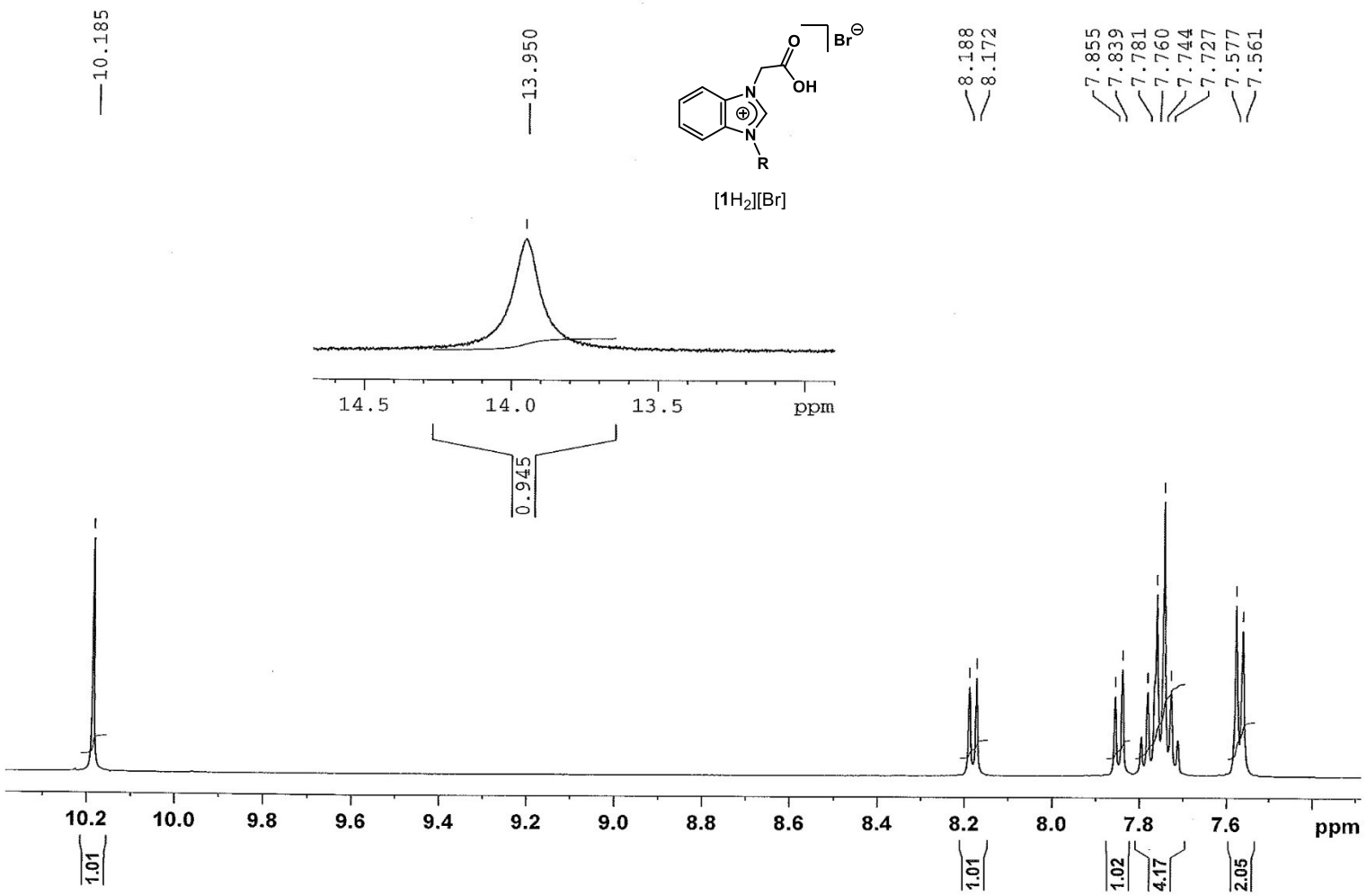
10.185
13.950
8.188
8.172
7.855
7.839
7.781
7.760
7.744
7.727
7.577
7.561
[1H2][Br]
14.5
14.0
13.5
ppm
0.945
10.2
10.0
9.8
9.6
9.4
9.2
9.0
8.8
8.6
8.4
8.2
8.0
7.8
7.6
ppm
1.01
1.01
1.02
4.17
2.05

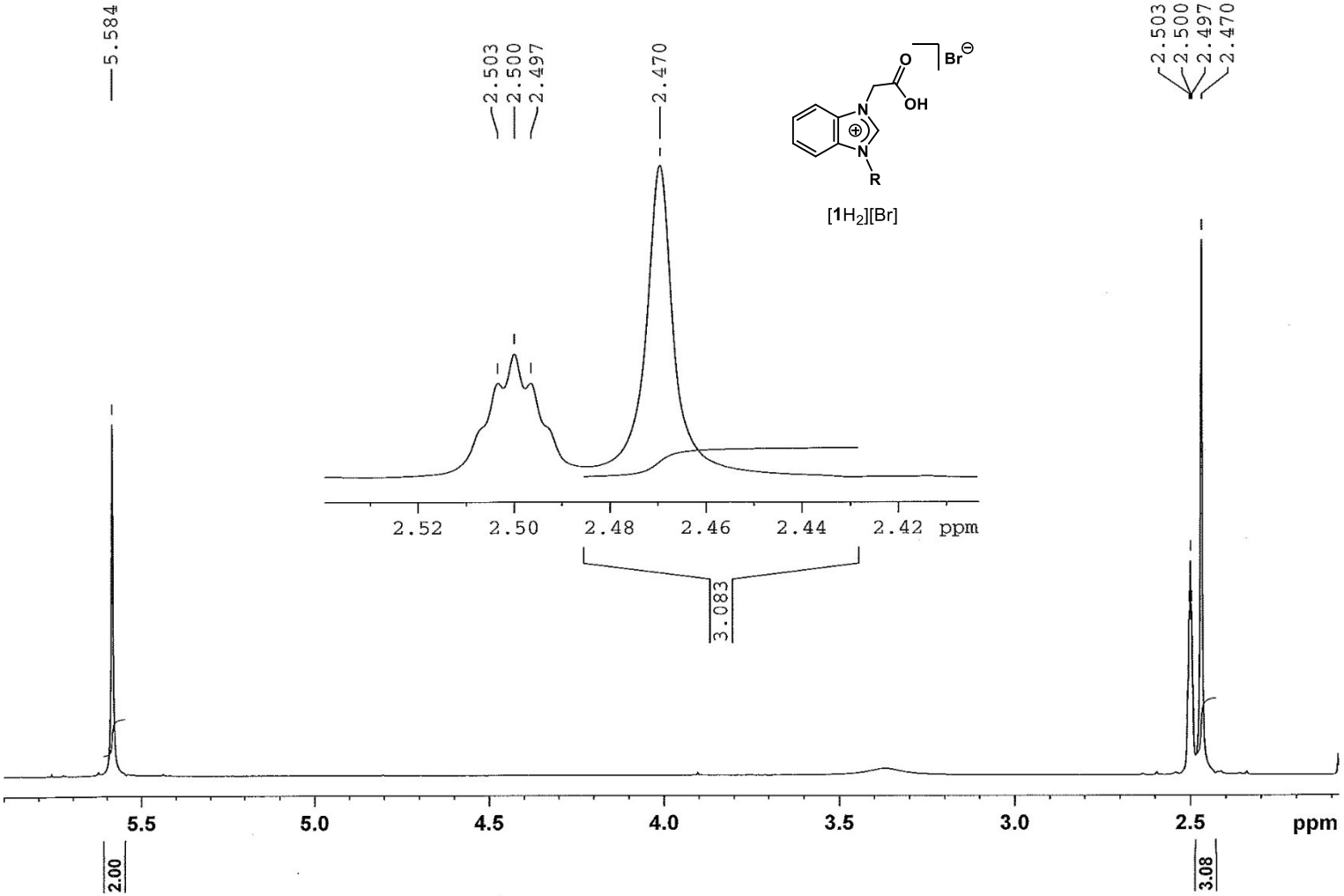
5.584
2.503
2.500
2.497
2.470
2.503
2.500
2.497
2.470
[1H2][Br]
2.52
2.50
2.48
2.46
2.44
2.42 ppm
3.083
5.5
5.0
4.5
4.0
3.5
3.0
2.5
ppm
2.00
3.08

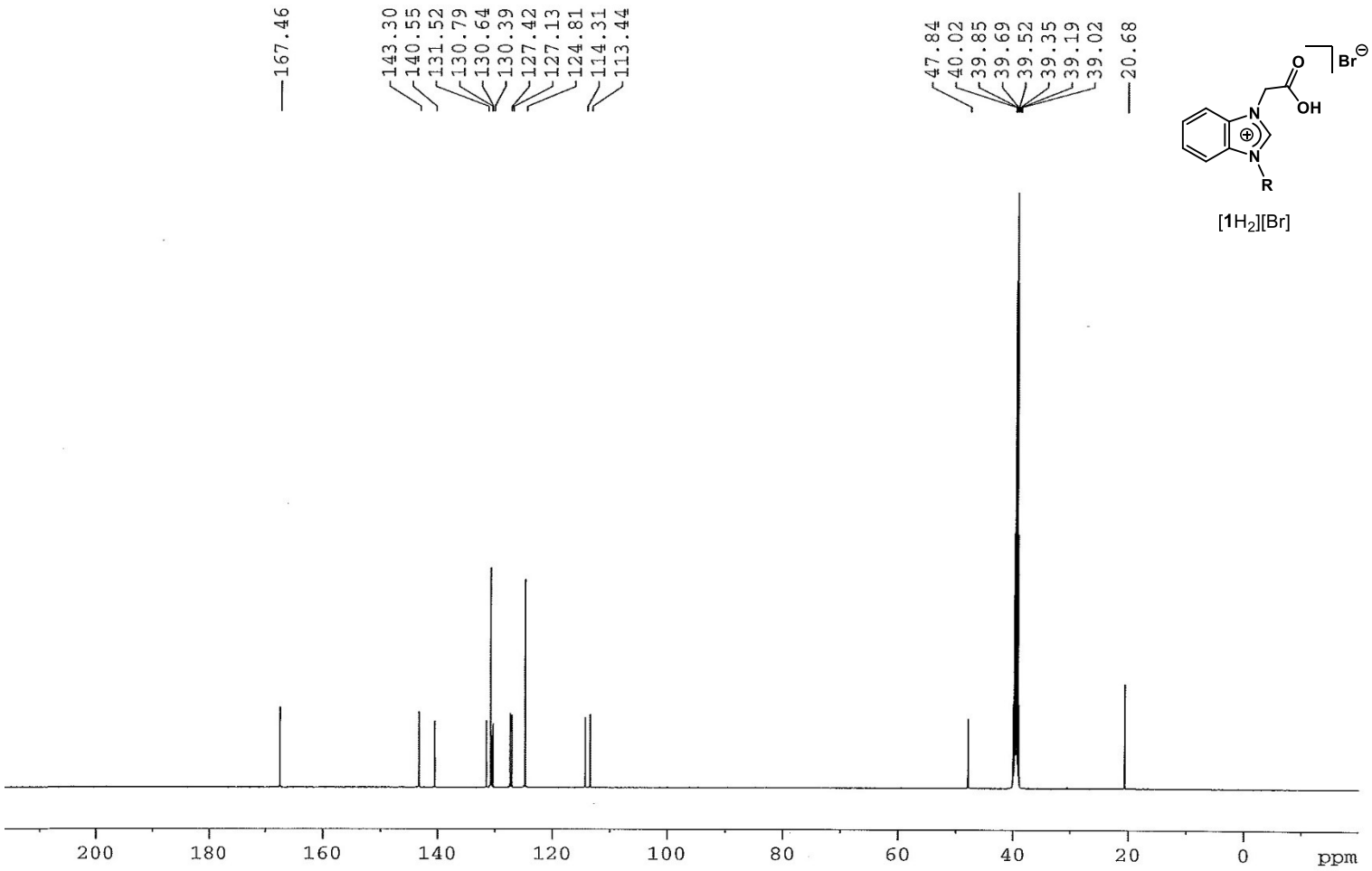
167.46
143.30
140.55
131.52
130.79
130.64
130.39
127.42
127.13
124.81
114.31
113.44
47.84
40.02
39.85
39.69
39.52
39.35
39.19
39.02
20.68
Br
O
OH
N
N
R
[1H2][Br]
200
180
160
140
120
100
80
60
40
20
0
ppm

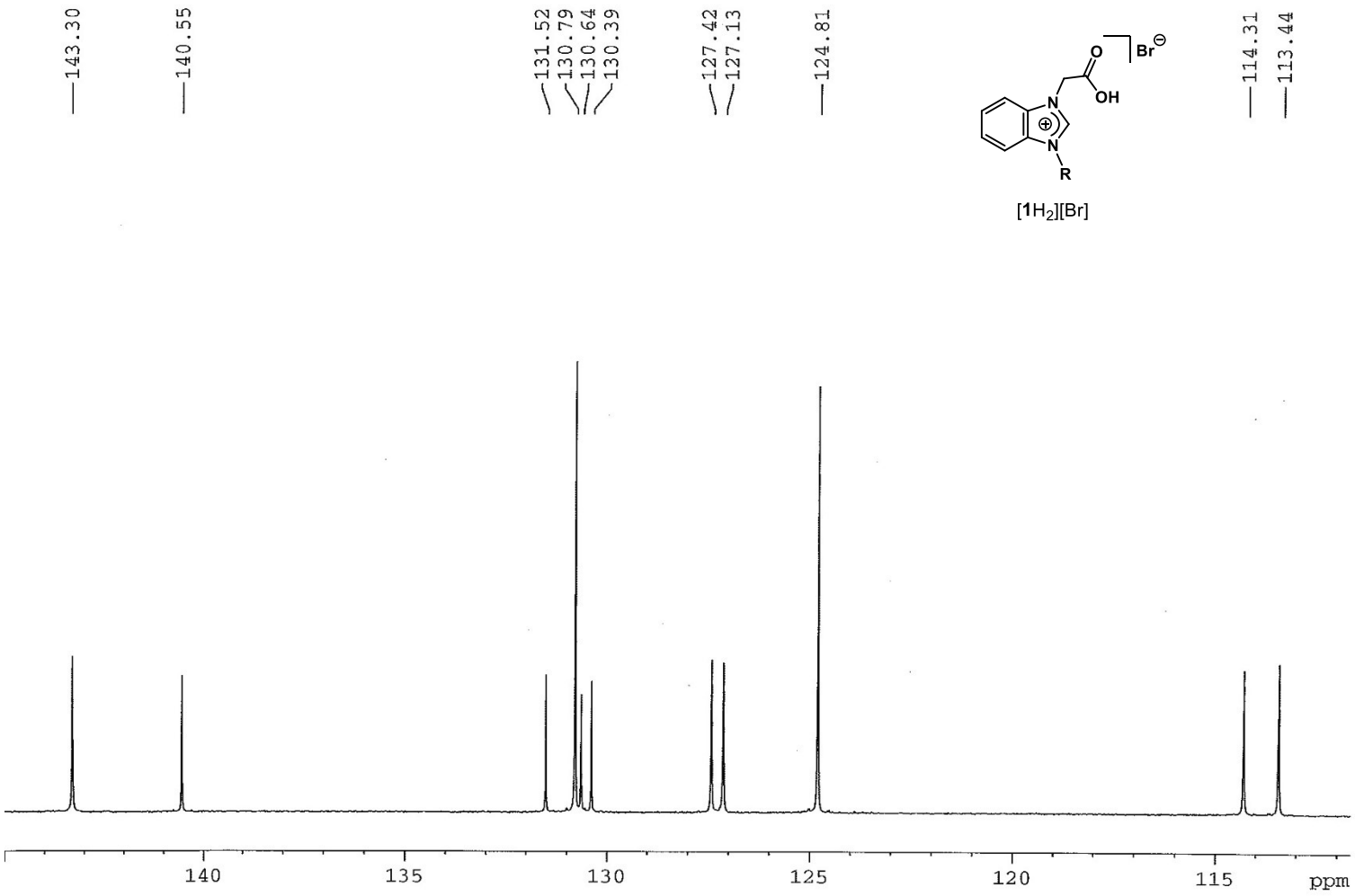
143.30
140.55
131.52
130.79
130.64
130.39
127.42
127.13
124.81
114.31
113.44
Br⊖
O
OH
N
N
R
140
135
130
125
120
115
ppm

[1H$_2$][Br]

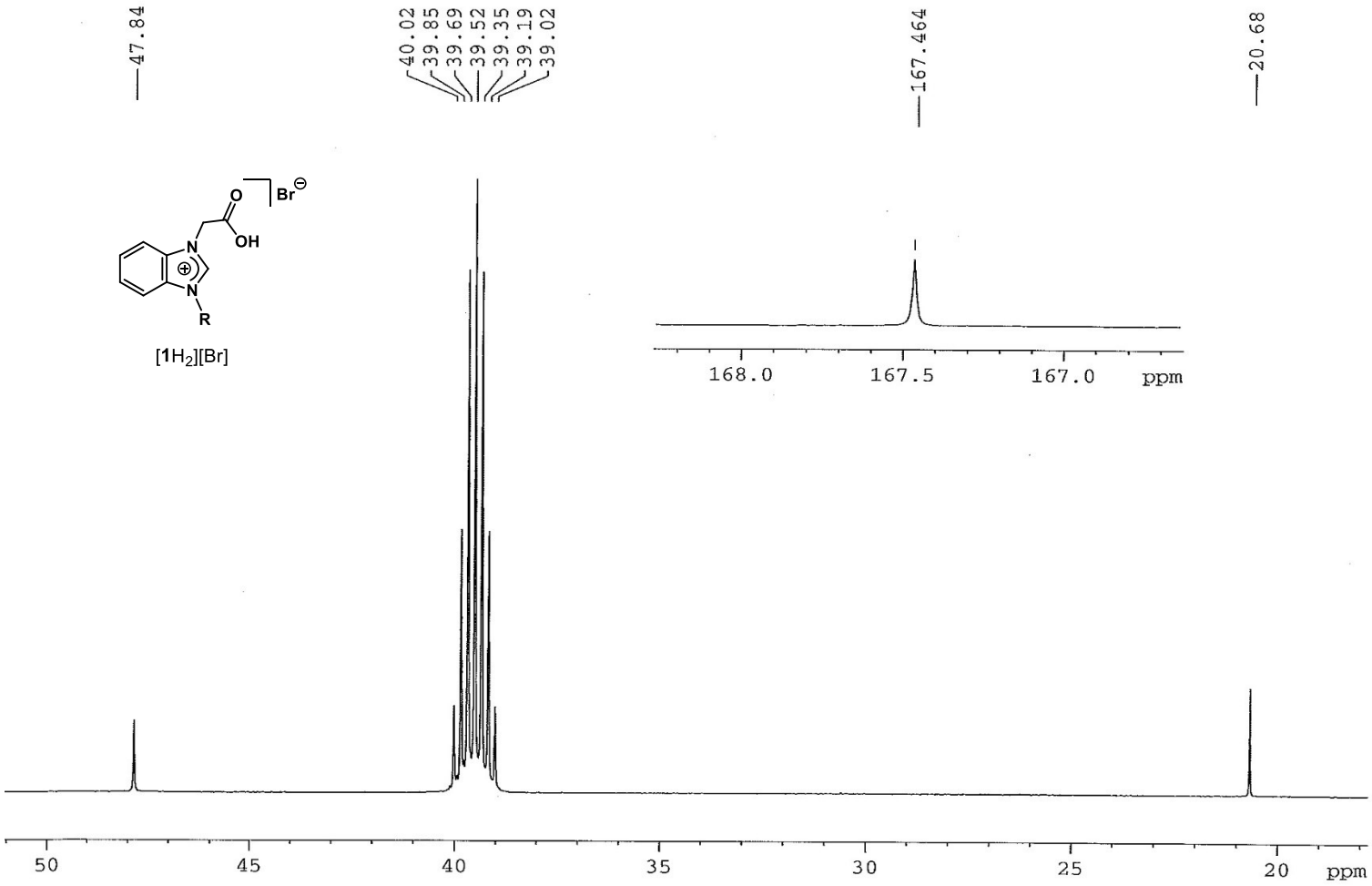
47.84
40.02
39.85
39.69
39.52
39.35
39.19
39.02
167.464
20.68
O
Br⊖
OH
N
N
R
[1H2][Br]
168.0
167.5
167.0
ppm
50
45
40
35
30
25
20
ppm

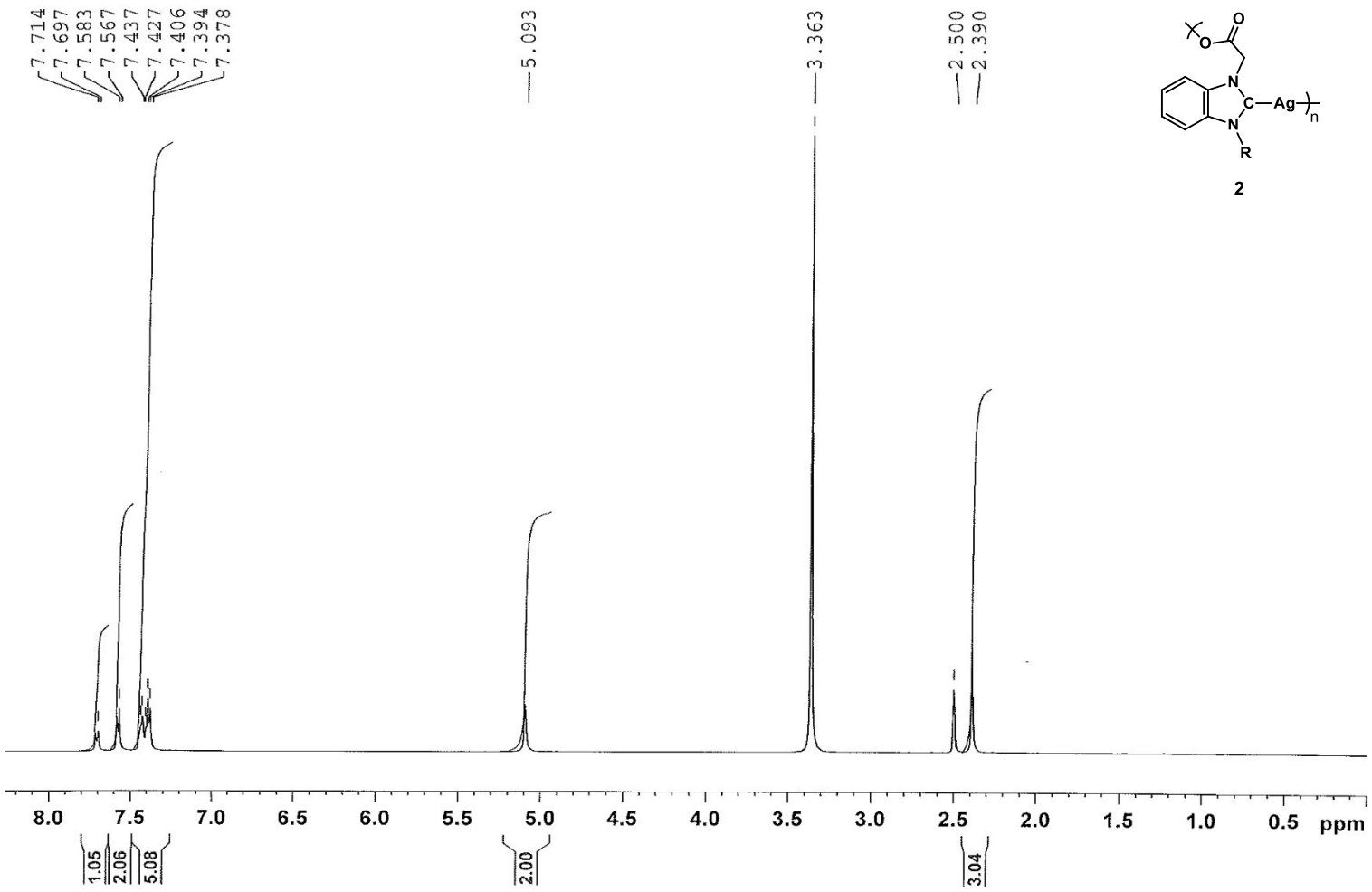
7.714
7.697
7.583
7.567
7.437
7.427
7.406
7.394
7.378
5.093
3.363
2.500
2.390
O
O
N
C—Ag
n
N
R
2
8.0
7.5
7.0
6.5
6.0
5.5
5.0
4.5
4.0
3.5
3.0
2.5
2.0
1.5
1.0
0.5
ppm
1.05
2.06
5.08
2.00
3.04

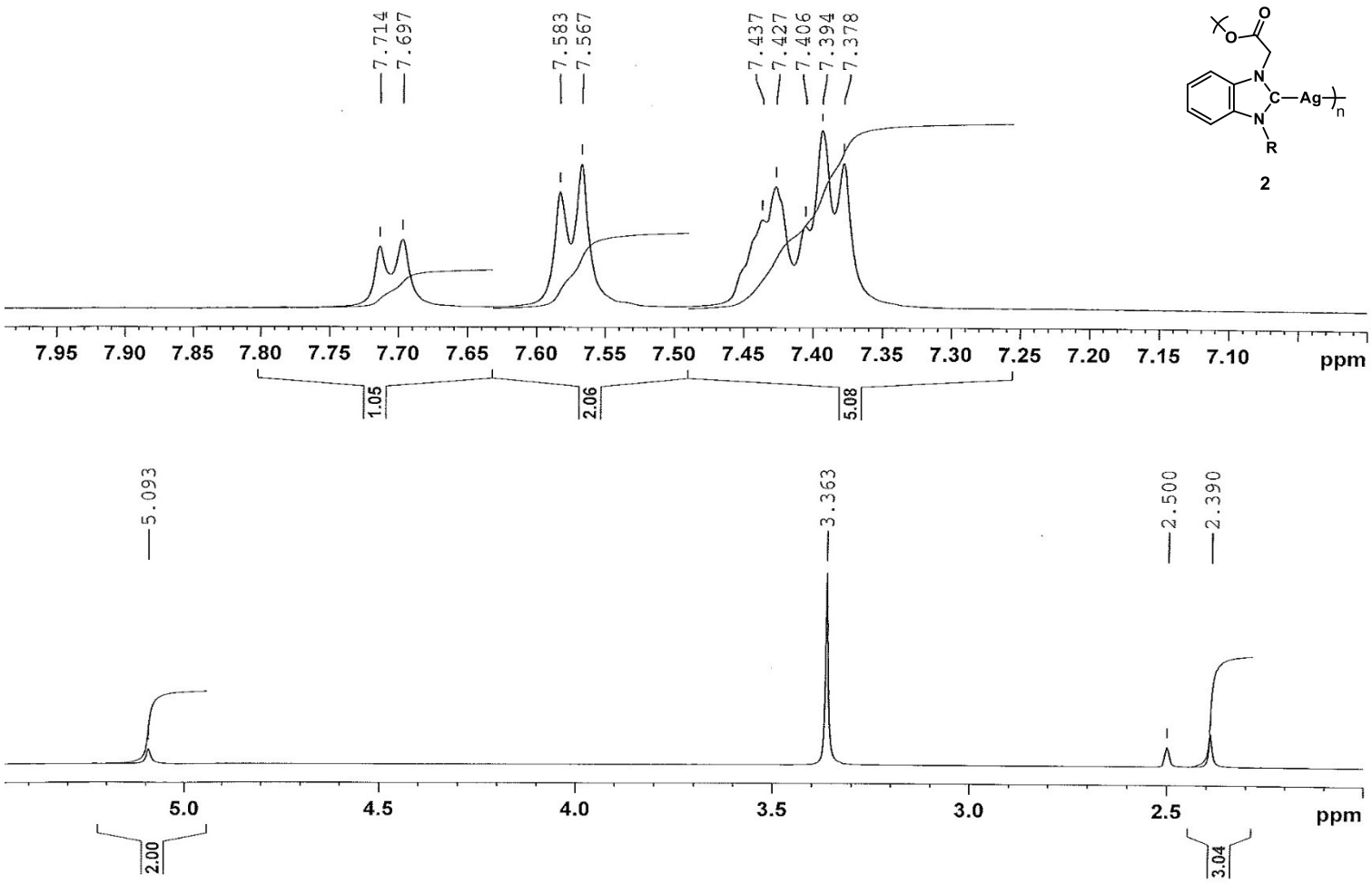
7.714
7.697
7.583
7.567
7.437
7.427
7.406
7.394
7.378
7.95 7.90 7.85 7.80 7.75 7.70 7.65 7.60 7.55 7.50 7.45 7.40 7.35 7.30 7.25 7.20 7.15 7.10
ppm
1.05
2.06
5.08
5.093
3.363
2.500
2.390
5.0 4.5 4.0 3.5 3.0 2.5
ppm
2.00
3.04
O
O
N
C
Ag
n
N
R
2

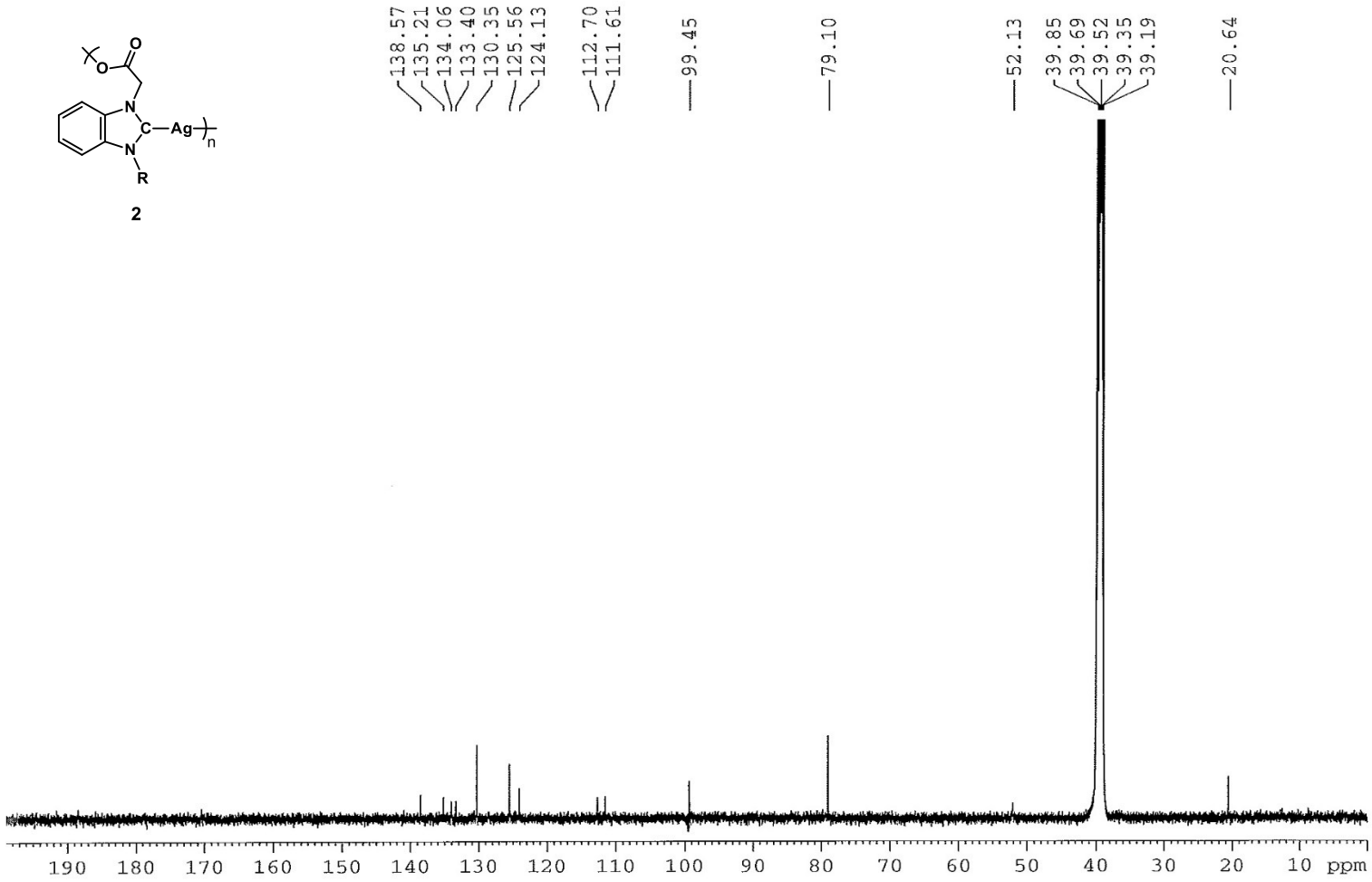
O
O
N
C
Ag
n
N
R
2
138.57
135.21
134.06
133.40
130.35
125.56
124.13
112.70
111.61
99.45
79.10
52.13
39.85
39.69
39.52
39.35
39.19
20.64
190 180 170 160 150 140 130 120 110 100 90 80 70 60 50 40 30 20 10 ppm

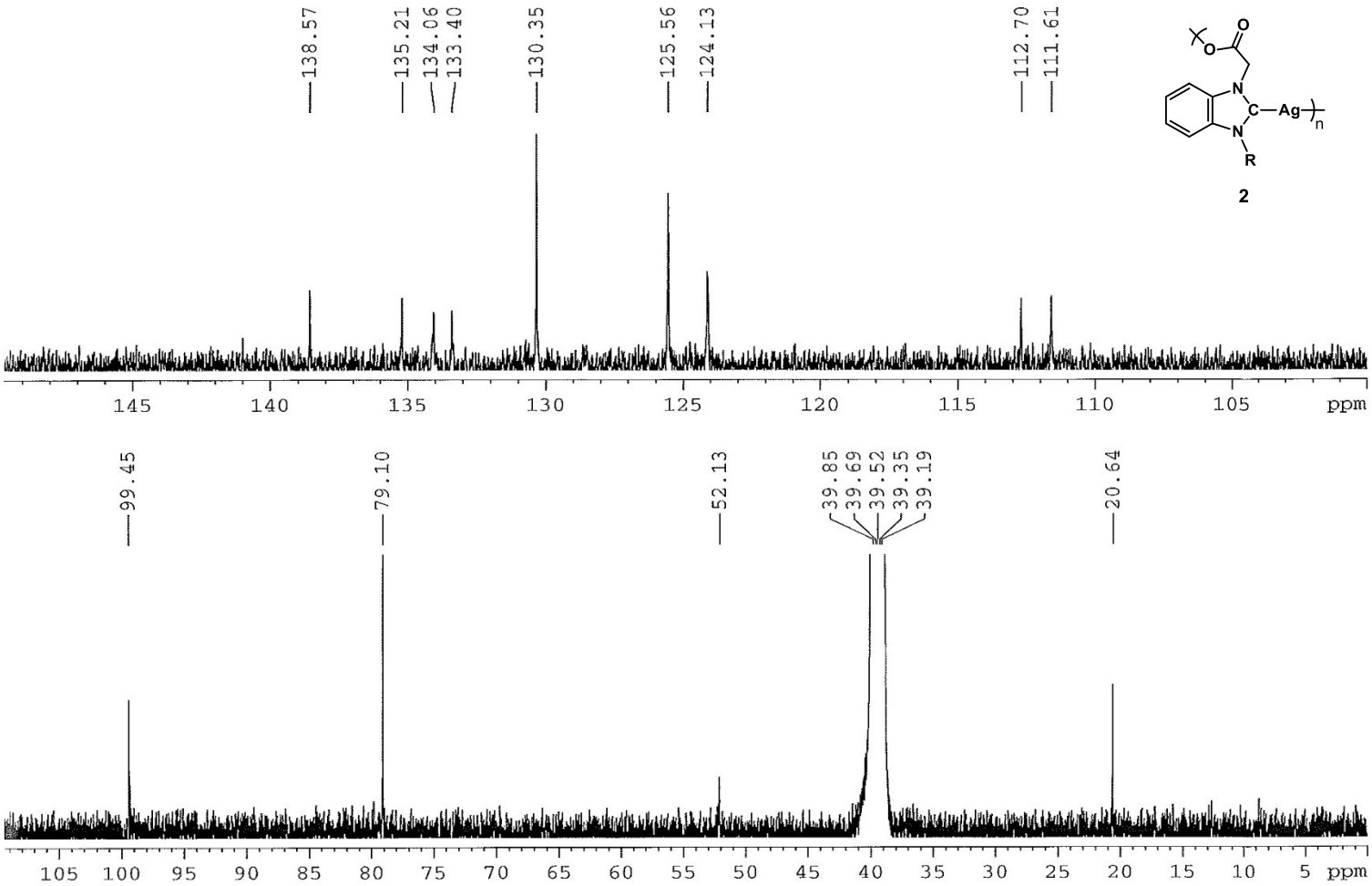
138.57
135.21
134.06
133.40
130.35
125.56
124.13
112.70
111.61
145
140
135
130
125
120
115
110
105
ppm
99.45
79.10
52.13
39.85
39.69
39.52
39.35
39.19
20.64
105
100
95
90
85
80
75
70
65
60
55
50
45
40
35
30
25
20
15
10
5
ppm

2

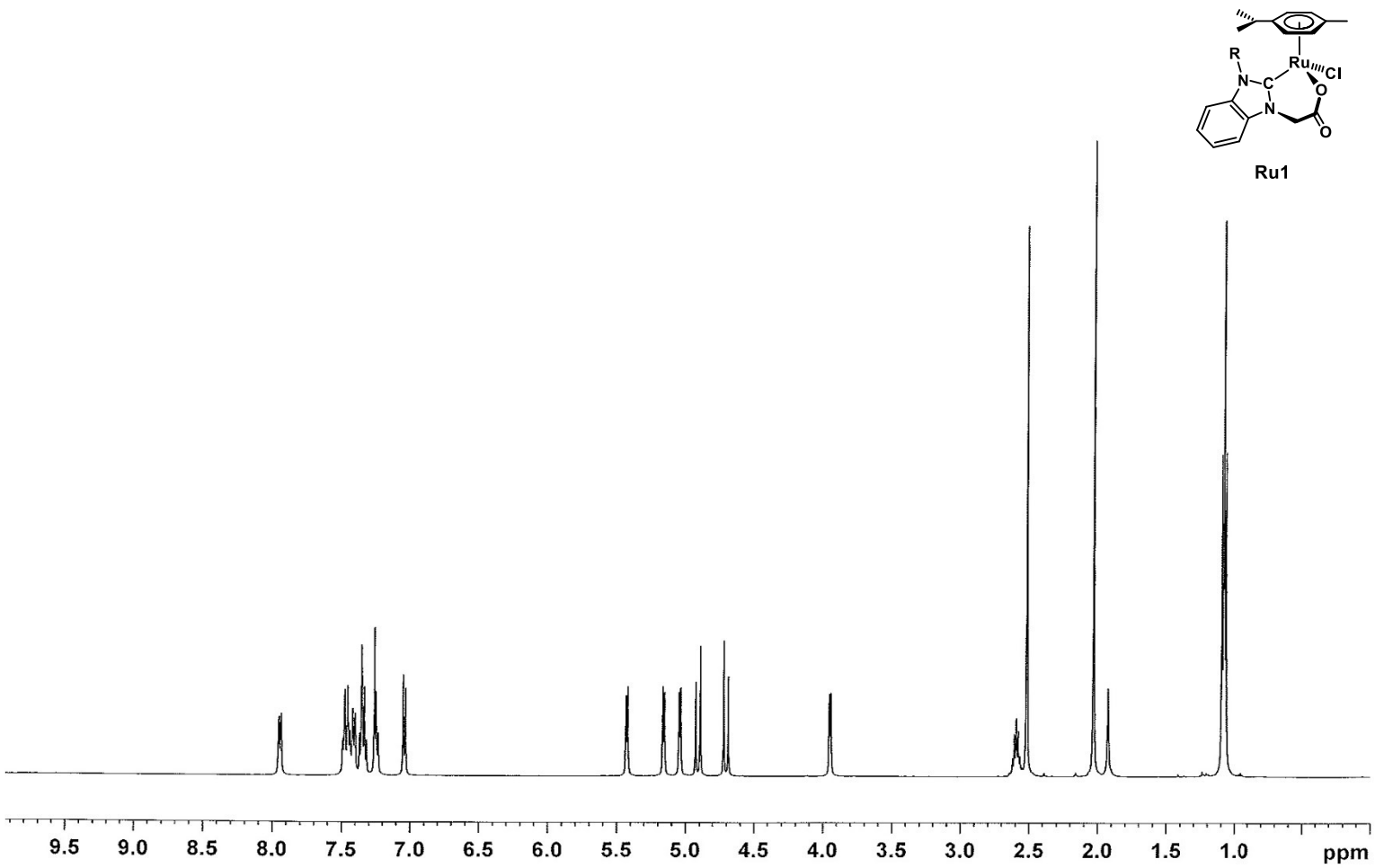
R
Ru
Cl
N
C
N
O
O
Ru1
9.5
9.0
8.5
8.0
7.5
7.0
6.5
6.0
5.5
5.0
4.5
4.0
3.5
3.0
2.5
2.0
1.5
1.0
ppm

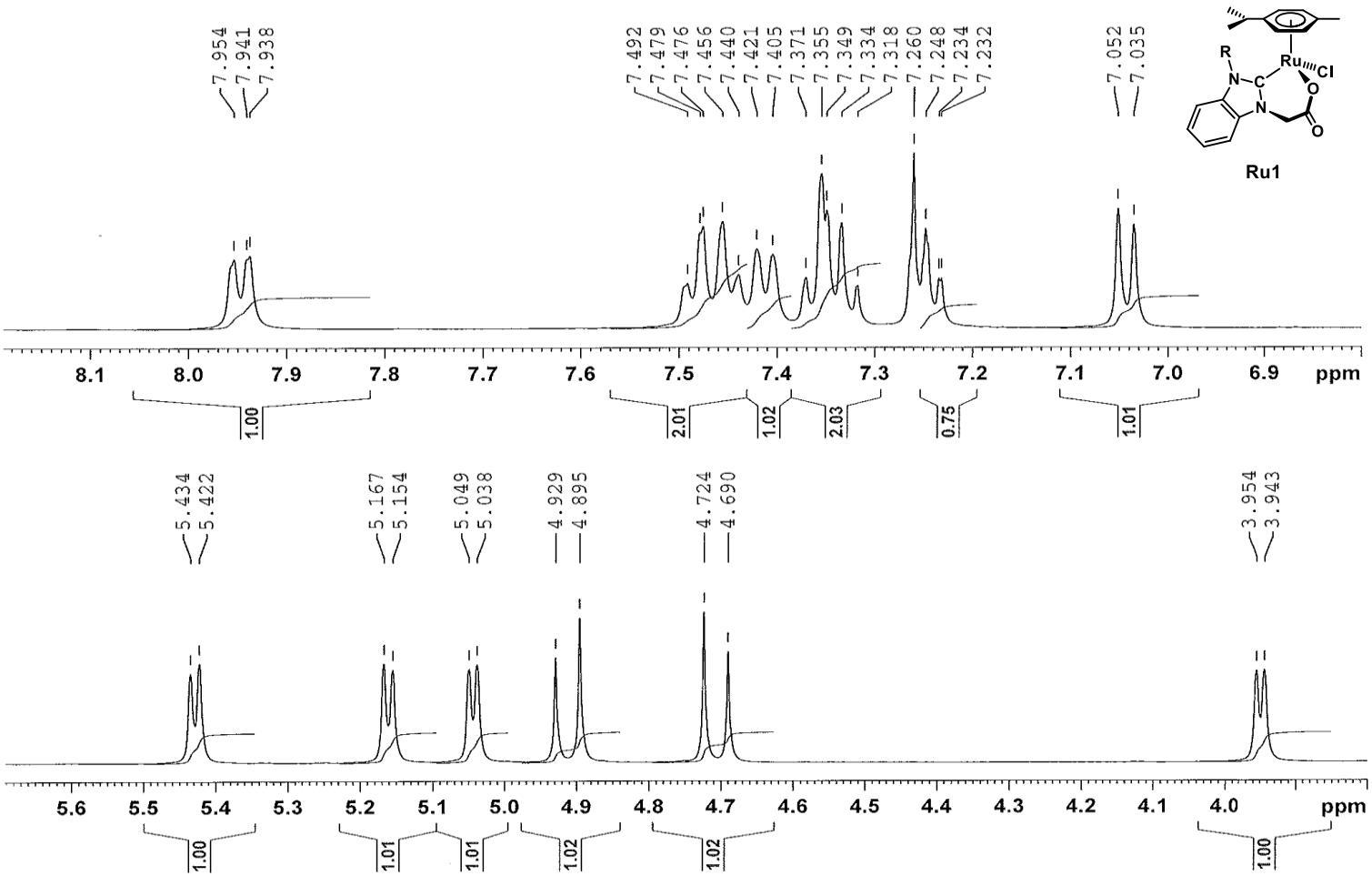
7.954
7.941
7.938
7.492
7.479
7.476
7.456
7.440
7.421
7.405
7.371
7.355
7.349
7.334
7.318
7.260
7.248
7.234
7.232
7.052
7.035
Ru1
8.1
8.0
7.9
7.8
7.7
7.6
7.5
7.4
7.3
7.2
7.1
7.0
6.9
ppm
1.00
2.01
1.02
2.03
0.75
1.01
5.434
5.422
5.167
5.154
5.049
5.038
4.929
4.895
4.724
4.690
3.954
3.943
5.6
5.5
5.4
5.3
5.2
5.1
5.0
4.9
4.8
4.7
4.6
4.5
4.4
4.3
4.2
4.1
4.0
ppm
1.00
1.01
1.01
1.02
1.02
1.00

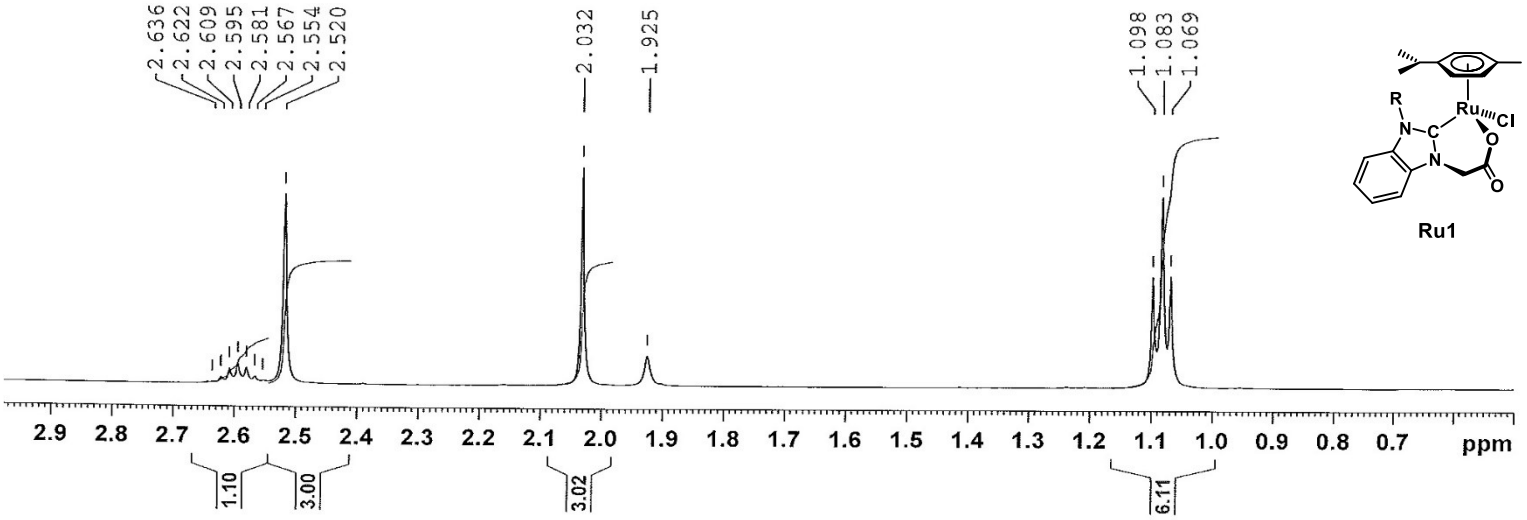
2.636
2.622
2.609
2.595
2.581
2.567
2.554
2.520
2.032
1.925
1.098
1.083
1.069
2.9 2.8 2.7 2.6 2.5 2.4 2.3 2.2 2.1 2.0 1.9 1.8 1.7 1.6 1.5 1.4 1.3 1.2 1.1 1.0 0.9 0.8 0.7 ppm
1.10
3.00
3.02
6.11
R
N
C
N
Ru
Cl
O
O
Ru1

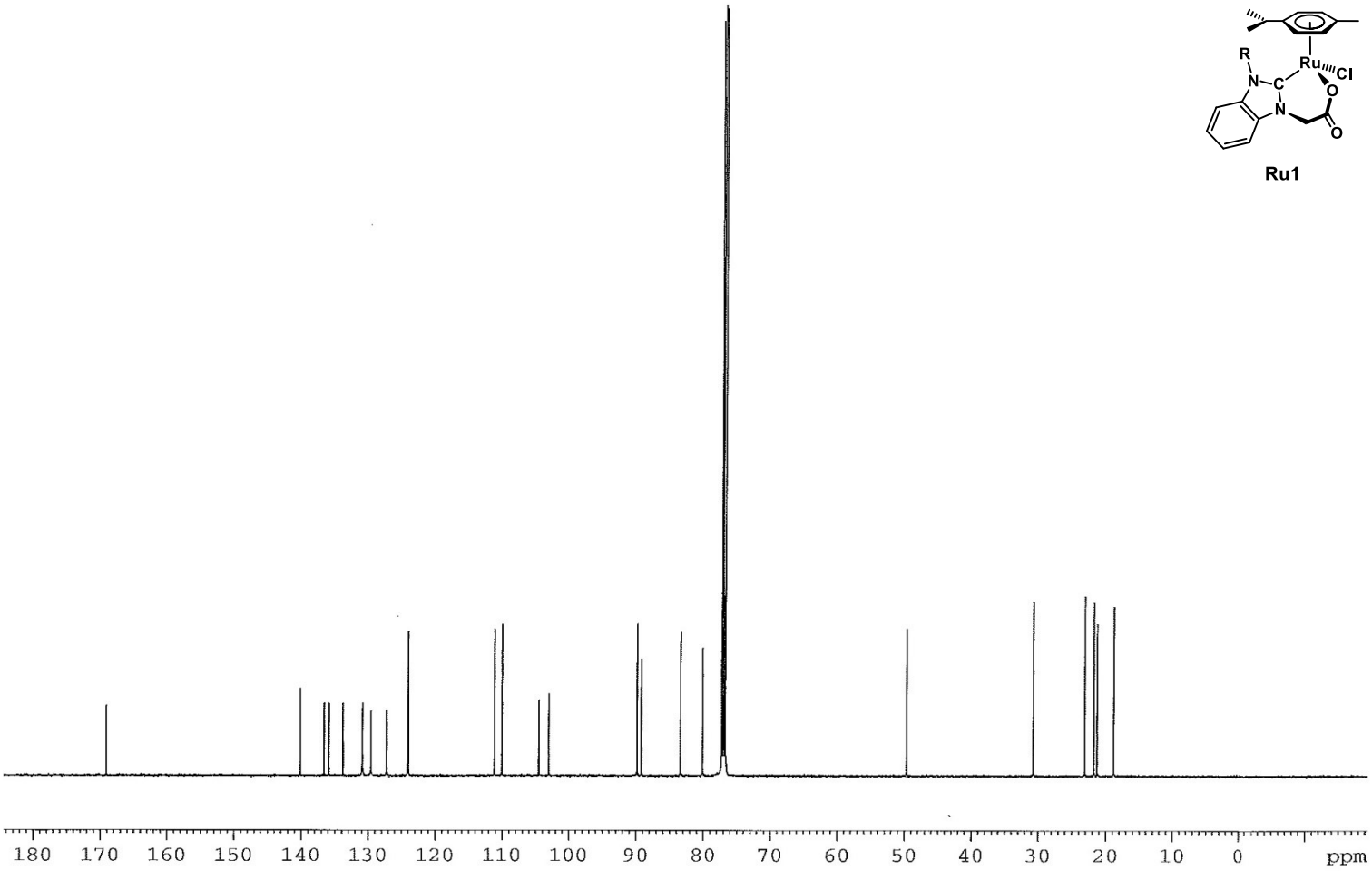
R
Ru
Cl
N
C
N
O
O
Ru1
180 170 160 150 140 130 120 110 100 90 80 70 60 50 40 30 20 10 0 ppm

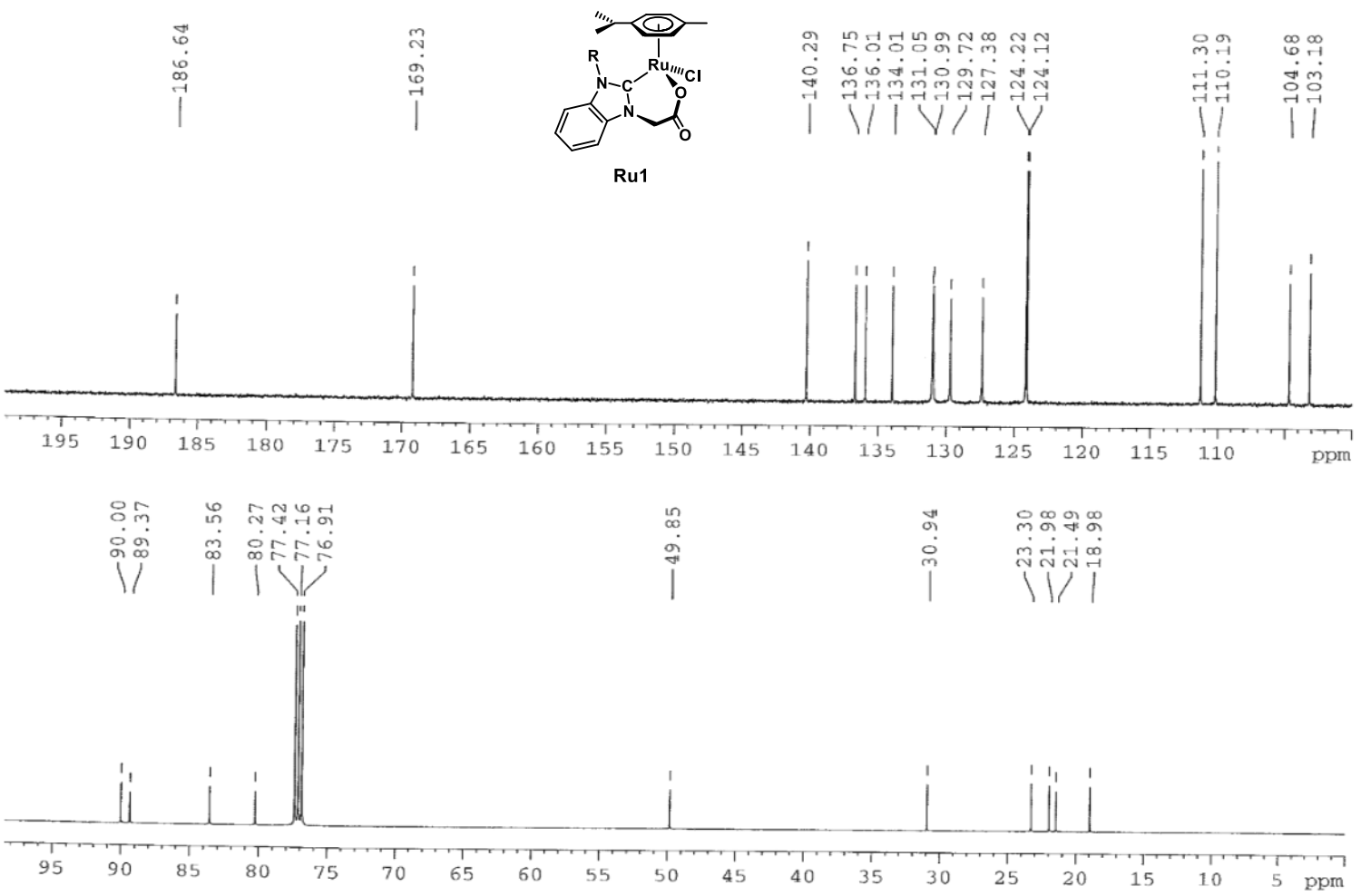
186.64
169.23
140.29
136.75
136.01
134.01
131.05
130.99
129.72
127.38
124.22
124.12
111.30
110.19
104.68
103.18
R
N
C
N
Ru
Cl
O
O
Ru1
195 190 185 180 175 170 165 160 155 150 145 140 135 130 125 120 115 110 ppm
90.00
89.37
83.56
80.27
77.42
77.16
76.91
49.85
30.94
23.30
21.98
21.49
18.98
95 90 85 80 75 70 65 60 55 50 45 40 35 30 25 20 15 10 5 ppm

REFERENCES

(1) Murphy, M. P. "How mitochondria produce reactive oxygen species." *Biochem J* **2009**, *417*, 1-13.

(2) Valko, M.; Leibfritz, D.; Moncol, J.; Cronin, M. T.; Mazur, M.; Telser, J. "Free radicals and antioxidants in normal physiological functions and human disease." *Int J Biochem Cell Biol* **2007**, *39*, 44-84.

(3) Cooke, M. S.; Evans, M. D.; Dizdaroglu, M.; Lunec, J. "Oxidative DNA damage: mechanisms, mutation, and disease." *FASEB J* **2003**, *17*, 1195-214.

(4) Maret, W. "Zinc coordination environments in proteins as redox sensors and signal transducers." *Antioxid Redox Signal* **2006**, *8*, 1419-41.

(5) Stocker, R.; Keaney, J. F., Jr. "Role of oxidative modifications in atherosclerosis." *Physiol Rev* **2004**, *84*, 1381-478.

(6) Fukai, T.; Ushio-Fukai, M. "Superoxide dismutases: role in redox signaling, vascular function, and diseases." *Antioxid Redox Signal* **2011**, *15*, 1583-606.

(7) Miriyala, S.; Spasojevic, I.; Tovmasyan, A.; Salvemini, D.; Vujaskovic, Z.; St Clair, D.; Batinic-Haberle, I. "Manganese superoxide dismutase, MnSOD and its mimics." *Biochim Biophys Acta* **2012**, *1822*, 794-814.

(8) Batinic-Haberle, I.; Tovmasyan, A.; Roberts, E. R.; Vujaskovic, Z.; Leong, K. W.; Spasojevic, I. "SOD therapeutics: latest insights into their structure-activity relationships and impact on the cellular redox-based signaling pathways." *Antioxid Redox Signal* **2014**, *20*, 2372-415.

(9) Do Amaral, S.; Esposito, B. P. "Fluorimetric study of the pro-oxidant activity of EUK8 in the presence of hydrogen peroxide." *Biometals* **2008**, *21*, 425-32.

(10) Evans, M. K.; Tovmasyan, A.; Batinic-Haberle, I.; Devi, G. R. "Mn porphyrin in combination with ascorbate acts as a pro-oxidant and mediates caspase-independent cancer cell death." *Free Radic Biol Med* **2014**, *68*, 302-14.

(11) Chelikani, P.; Fita, I.; Loewen, P. C. "Diversity of structures and properties among catalases." *Cell Mol Life Sci* **2004**, *61*, 192-208.

(12) Hersleth, H. P.; Ryde, U.; Rydberg, P.; Gorbitz, C. H.; Andersson, K. K. "Structures of the high-valent metal-ion haem-oxygen intermediates in peroxidases, oxygenases and catalases." *J Inorg Biochem* **2006**, *100*, 460-76.

(13) Kirkman, H. N.; Gaetani, G. F. "Mammalian catalase: a venerable enzyme with new mysteries." *Trends Biochem Sci* **2007**, *32*, 44-50.

(14) Vlasits, J.; Jakopitsch, C.; Bernroitner, M.; Zamocky, M.; Furtmuller, P. G.; Obinger, C. "Mechanisms of catalase activity of heme peroxidases." *Arch Biochem Biophys* **2010**, *500*, 74-81.

(15) Kubota, R.; Imamura, S.; Shimizu, T.; Asayama, S.; Kawakami, H. "Synthesis of water-soluble dinuclear mn-porphyrin with multiple antioxidative activities." *ACS Med Chem Lett* **2014**, *5*, 639-43.

(16) Sharpe, M. A.; Ollosson, R.; Stewart, V. C.; Clark, J. B. "Oxidation of nitric oxide by oxomanganese-salen complexes: a new mechanism for cellular protection by superoxide dismutase/catalase mimetics." *Biochem J* **2002**, *366*, 97-107.

(17) Itoh, M.; Motoda, K.-i.; Shindo, K.; Kamiusuki, T.; Sakiyama, H.; Matsumoto, N.; Ōkawa, H. "μ-Pyrazolato-μ-carboxylato- and di(μ-pyrazolato)dimanganese(II) complexes: synthesis, characterization and catalase-like function." *J. Chem. Soc., Dalton Trans.* **1995**, 3635-3641.

(18) Naruta, Y.; Maruyama, K. "High Oxygen-Evolving Activity of Rigidly Linked Manganese(Iii) Porphyrin Dimers - a Functional-Model of Manganese Catalase." *Journal of the American Chemical Society* **1991**, *113*, 3595-3596.

(19) Sheldon, R. A. "Recent advances in green catalytic oxidations of alcohols in aqueous media." *Catalysis Today* **2015**, *247*, 4-13.

(20) Ryland, B. L.; Stahl, S. S. "Practical aerobic oxidations of alcohols and amines with homogeneous copper/TEMPO and related catalyst systems." *Angew Chem Int Ed Engl* **2014**, *53*, 8824-38.

(21) Seki, Y.; Oisaki, K.; Kanai, M. "Chemoselective aerobic oxidation catalyzed by a metal/stable organoradical redox conjugate." *Tetrahedron Letters* **2014**, *55*, 3738-3746.

(22) Parmeggiani, C.; Cardona, F. "Transition metal based catalysts in the aerobic oxidation of alcohols." *Green Chemistry* **2012**, *14*, 547-564.

(23) Schultz, M. J.; Sigman, M. S. "Recent advances in homogeneous transition metal-catalyzed aerobic alcohol oxidations." *Tetrahedron* **2006**, *62*, 8227-8241.

(24) Soldevila-Barreda, J. J.; Romero-Canelon, I.; Habtemariam, A.; Sadler, P. J. "Transfer hydrogenation catalysis in cells as a new approach to anticancer drug design." *Nat Commun* **2015**, *6*, 6582.

(25) Fu, Y.; Romero, M. J.; Habtemariam, A.; Snowden, M. E.; Song, L. J.; Clarkson, G. J.; Qamar, B.; Pizarro, A. M.; Unwin, P. R.; Sadler, P. J. "The contrasting chemical reactivity of potent isoelectronic iminopyridine and azopyridine osmium(II) arene anticancer complexes." *Chemical Science* **2012**, *3*, 2485-2494.

(26) Soldevila-Barreda, J. J.; Sadler, P. J. "Approaches to the design of catalytic metallodrugs." *Current Opinion in Chemical Biology* **2015**, *25*, 172-183.

(27) Sasmal, P. K.; Streu, C. N.; Meggers, E. "Metal complex catalysis in living biological systems." *Chemical Communications* **2013**, *49*, 1581-1587.

(28) Gasser, G.; Metzler-Nolte, N. "The potential of organometallic complexes in medicinal chemistry." *Current Opinion in Chemical Biology* **2012**, *16*, 84-91.

(29) Hanan, E. J.; Chan, B. K.; Estrada, A. A.; Shore, D. G.; Lyssikatos, J. P. "Mild and General One-Pot Reduction and Cyclization of Aromatic and Heteroaromatic 2-Nitroamines to Bicyclic 2H-Imidazoles." *Synlett* **2010**, 2759-2764.

(30) Re, R.; Pellegrini, N.; Proteggente, A.; Pannala, A.; Yang, M.; Rice-Evans, C. "Antioxidant activity applying an improved ABTS radical cation decolorization assay." *Free Radical Biology and Medicine* **1999**, *26*, 1231-1237.

(31) Pitulice, L.; Pastor, I.; Vilaseca, E.; Madurga, S.; Isvoran, A.; Cascante, M.; Mas, F. *Biocatal. Biotransform.* **2013**, *2*, 1-5.

(32) Mangalum, A.; McMillen, C. D.; Tennyson, A. G. "Synthesis, coordination chemistry and reactivity of transition metal complexes supported by a chelating benzimidazolylidene carboxylate ligand." *Inorganica Chimica Acta* **2015**, *426*, 29-38.

(33) Fricker, S. P.; Slade, E.; Powell, N. A.; Vaughan, O. J.; Henderson, G. R.; Murrer, B. A.; Megson, I. L.; Bisland, S. K.; Flitney, F. W. "Ruthenium complexes as nitric oxide scavengers: a potential therapeutic approach to nitric oxide-mediated diseases." *British Journal of Pharmacology* **1997**, *122*, 1441-1449.

(34) Cameron, B. R.; Darkes, M. C.; Yee, H.; Olsen, M.; Fricker, S. P.; Skerlj, R. T.; Bridger, G. J.; Davies, N. A.; Wilson, M. T.; Rose, D. J.; Zubieta, J. "Ruthenium(III) polyaminocarboxylate complexes: Efficient and effective nitric oxide scavengers." *Inorganic Chemistry* **2003**, *42*, 1868-1876.

(35) Mangalum, A.; Htet, Y.; Roe, D. A.; McMillen, C. D.; Tennyson, A. G. "Net charge effects in N-heterocyclic carbene-ruthenium complexes with similar oxidation states and coordination geometries." *Inorganica Chimica Acta* **2015**, *435*, 320-326.

(36) Jungwirth, U.; Kowol, C. R.; Keppler, B. K.; Hartinger, C. G.; Berger, W.; Heffeter, P. "Anticancer Activity of Metal Complexes: Involvement of Redox Processes." *Antioxidants & Redox Signaling* **2011**, *15*, 1085-1127.

(37) Bielski, B. H. J.; Allen, A. O. "Mechanism of Disproportionation of Superoxide Radicals." *Journal of Physical Chemistry* **1977**, *81*, 1048-1050.

(38) Yusa, K.; Shikama, K. "Oxidation of Oxymyoglobin to Metmyoglobin with Hydrogen-Peroxide - Involvement of Ferryl Intermediate." *Biochemistry* **1987**, *26*, 6684-6688.

(39) Huang, D. J.; Ou, B. X.; Prior, R. L. "The chemistry behind antioxidant capacity assays." *Journal of Agricultural and Food Chemistry* **2005**, *53*, 1841-1856.

(40) Karbarz, M.; Malyszko, J. "Voltammetric behavior of trolox in methanol and ethanol solutions." *Electroanalysis* **2008**, *20*, 1884-1890.

(41) Creutz, C. "The Complexities of Ascorbate as a Reducing Agent." *Inorganic Chemistry* **1981**, *20*, 4449-4452.

(42) Pullar, J. M.; Vissers, M. C. M.; Winterbourn, C. C. "Glutathione oxidation by hypochlorous acid in endothelial cells produces glutathione sulfonamide as a major product but not glutathione disulfide." *Journal of Biological Chemistry* **2001**, *276*, 22120-22125.

(43) Enami, S.; Hoffmann, M. R.; Colussi, A. J. "Ozone Oxidizes Glutathione to a Sulfonic Acid." *Chemical Research in Toxicology* **2009**, *22*, 35-40.

(44) Sathyadevi, P.; Krishnamoorthy, P.; Bhuvanesh, N. S. P.; Kalaiselvi, P.; Padma, V. V.; Dharmaraj, N. "Organometallic ruthenium(II) complexes: Synthesis, structure and influence of substitution at azomethine carbon towards DNA/BSA binding, radical scavenging and cytotoxicity." *European Journal of Medicinal Chemistry* **2012**, *55*, 420-431.

(45) Liu, Y. A.; Zhang, X. N.; Zhang, R.; Chen, T. F.; Wong, Y. S.; Liu, J.; Zheng, W. J. "Ruthenium-Porphyrin Complexes Induce Apoptosis by Inhibiting the Generation of Intracellular Reactive Oxygen Species in the Human Hepatoma Cell Line (HepG(2))." *European Journal of Inorganic Chemistry* **2011**, 1974-1980.

(46) Alfaro, J. M.; Prades, A.; del Carmen Ramos, M.; Peris, E.; Ripoll-Gomez, J.; Poyatos, M.; Burgos, J. S. "Biomedical properties of a series of ruthenium-N-heterocyclic carbene complexes based on oxidant activity in vitro and assessment in vivo of biosafety in zebrafish embryos." *Zebrafish* **2010**, *7*, 13-21.

CHAPTER THREE

CATALYTIC RADICAL REDUCTION IN AQUEOUS SOLUTION BY A RUTHENIUM HYDRIDE INTERMEDIATE

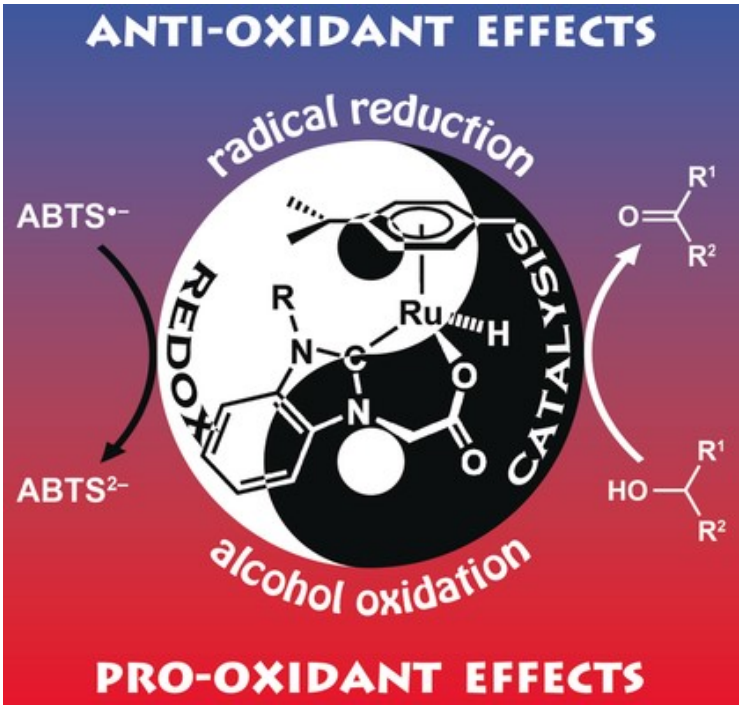

Figure 3. Catalytic radical reduction in buffered aqueous solutions was achieved by a Ru complex with non-tertiary alcohol terminal reductants. Primary kinetic isotope effects were observed with both C−H and O−H bonds. Radical reduction was faster at higher pH, and no reaction occurred in pure H_2O. Mechanistic studies suggest that the catalytically active species is a Ru-hydride intermediate formed by β-hydride elimination from a Ru-alkoxide.

This is the final published version of the following article:
Angew. Chem., Int. Ed., 2016, **DOI:** 10.1002/anie.201601887.which has been published in final form at http://onlinelibrary.wiley.com/doi/10.1002/anie.201601887/full

ABSTRACT

Some manganese complexes can catalyze both antioxidant and pro-oxidant reactions whereby the disparate reactivity modes are determined by the catalyst environment and afford distinct therapeutic effects. We recently reported the reduction of radicals in buffered aqueous solution catalyzed by a ruthenium complex with biologically relevant non–tertiary alcohols as terminal reductants. Mechanistic evidence is presented, indicating that this catalytic radical reduction is achieved by a Ru-hydride intermediate formed by a β–hydride elimination from a Ru–alkoxide species. A similar mechanism and Ru–hydride intermediate was previously reported to kill cancer cells with catalytic pro–oxidant effects. Therefore, our demonstration of catalytic pro–oxidant effects by the same type of intermediate reveals new potential therapeutic strategies and applications for catalytic systems that form Ru–hydride intermediates.

INTRODUCTION

Reactive oxygen species (ROS) and other free radicals can damage critical biomolecules in living systems and are implicated in a wide variety of pathologies.[1,2] Antioxidants can reduce ROS or oxidizing radicals and thus protect against damage, but they typically proceed through stoichiometric reductions that deplete their protective capacity.[3] However, a catalytic reduction could regenerate an antioxidant after each turnover and thus enable it to provide significantly greater protection. Manganese porphyrin-based complexes can catalyze $O_2^{\bullet-}$ and H_2O_2 disproportionation reactions and have shown beneficial antioxidant effects in stroke and diabetes therapy by reducing ROS levels.[4-9] Interestingly, some of these Mn complexes (two of which are in Phase 1 clinical trials) can also produce pro–oxidant effects in cancer cells, which endows them with potent chemotherapeutic activity.[4-11] The ability of a Mn complex to produce antioxidant or pro-oxidant effects in different environments is derived from the same catalytic cycle and intermediates, whereby the catalyst environment determines the antioxidant/pro-oxidant outcome.[4-15] Knowledge of the mechanism and intermediates by which a complex catalyzes a redox reaction in a biological system is thus essential for developing its therapeutic applications.

We recently reported the **Ru1**-catalzyed reduction of $ABTS^{\bullet-}$ to $ABTS^{2-}$ in buffered aqueous solution with biologically relevant non-tertiary alcohols as terminal reductants (Scheme 3.1 A–B).[16] Although $ABTS^{\bullet-}$ is not found in biological systems, it is an ideal radical substrate because its oxidizing power ($ABTS^{\bullet-}/ABTS^{2-}$ $E_{1/2}$ = +0.68 V vs. NHE)[17] is comparable to radicals that are generated during biological oxidative stress

(e.g., $E°$ = 1.6 V for $RO^{\bullet}$, 1.0 V for $ROO^{\bullet}$, 0.92 V for $Cys–S^{\bullet}$, and so forth)[*,18] and its high absorptivity (1.5×10^4 M^{-1} cm^{-1})[19] permits quantification at lower concentrations than would be achievable with $O_2^{\bullet-}$ or H_2O_2.[†,20,21] No $ABTS^{\bullet-}$ reduction occurred with **Ru1** alone if either the O–H or C–H group of a CH–OH moiety was absent, or in pure H_2O solutions, which is consistent with alcohol oxidation by β-hydride elimination from a Ru–alkoxide. A similar process has been proposed for the aerobic oxidation of alcohols catalyzed by Ru-oxide/hydroxide materials, in which the resulting Ru–H intermediate reacts with O_2, the terminal oxidant, by 1,2–insertion (Scheme 3.1 C, top).[22]

If a Ru complex that can oxidize a biomolecule to yield a Ru–H species, and if that Ru–H species can then oxidized by O_2 to yield H_2O_2, then that Ru complex can exert catalytic pro-oxidant effects in biological systems, which has been shown to result in potent anticancer properties by Sadler et al.[23-25] Compounds such as *trans*-[$RuCl_4$(imidazole)(*S*-dmso)] (NAMI-A) and related coordination complexes that also possess anticancer properties, have similarly been shown to function by exertion of pro-oxidant effects.[26-28] Antioxidant effects have been observed with some Ru coordination complexes, but none exhibited catalytic antioxidant activity.[29,30] Inspired by the fact that 1) a single Mn porphyrin–based complex can produce either antioxidant or pro–oxidant effects in different environments through a conserved catalytic cycle and set of intermediates and, 2) a catalytic cycle involving a Ru–H intermediate can produce pro–oxidant effects, we hypothesized that a comparable catalytic cycle and Ru–H

[*] All redox potentials are reported relative to NHE unless specified otherwise.
[†] Achieving the same absorbance value as $ABTS^{\bullet-}$ requires a 7.9-fold higher concentration of $O_2^{\bullet-}$ (ε = 1.9 × 10^3 M^{-1} cm^{-1} at 250 nm) or a 344-fold higher concentration of H_2O_2 (ε = 43.6 M^{-1} cm^{-1} at 240 nm).

intermediate could also give rise to antioxidant effects. Herein, we present mechanistic evidence indicating that catalytic antioxidant effects by **Ru1** in the form of catalytic radical reduction (Scheme 3.1 C, bottom) are derived from a similar catalytic cycle and Ru–H intermediate previously shown to produce catalytic pro–oxidant effects.

RESULTS AND DISCUSSION

An organoruthenium–chloride complex and the corresponding aquo complex exit in H_2O solution that is determined by the relative ligand affinities and total Cl^- ion concentration, but ligand exchange is rapid for both the aquation and anation reactions.[31,32] Therefore, the Cl^- ligand in **Ru1** will be similarly labile toward substitution with other ligands in phosphate–buffered saline (PBS) solutions, such as $ABTS^{\bullet-}$, H_2O and EtOH. The chemical synthesis of $ABTS^{\bullet-}$ from $ABTS^{2-}$ does not reach 100% completion,[19] therefore an additional 100 μM of $ABTS^{2-}$ was included to control the variation in rates caused by unreacted $ABTS^{2-}$. Addition of 5 μM **Ru1** to an aqueous solution containing 100 μM of $ABTS^{2-}$ will result in rapid ligand exchange (relative to turnover) to afford $[L_nRu–A_{red}]^{1-}$ and begin the catalytic cycle (Scheme 3.2). Substitution of $ABTS^{2-}$ with H_2O will yield $[L_nRu–OH_2]^{1+}$ (step 1), which will undergo ligand exchange with EtOH to produce $[L_nRu–(EtOH)]^{1+}$ (step 2). Complexes similar to $[L_nRu–OH_2]^{1+}$ exhibit pK_a values > 9,[33,34] therefore $[L_nRu–OH_2]^{1+}$ is expected to be the predominant form at pH 7.4 rather than $[L_nRu–OH]$. Proton transfer from the EtOH ligand to the buffered solution will form $[L_nRu–OEt]$ (step 3). Subsequent β–hydride elimination from the ethoxide ligand (via **TS4**) and acetaldehyde dissociation will afford the catalytically-active $[L_nRu–H]$ intermediate (step 4). This Ru^{II}–hydride species will

then undergo $1e^-$ oxidation by $ABTS^{\bullet-}$ to yield a Ru^{III}–hydride cation (step 5). Deprotonation by buffer, oxidation by a second equivalent of $ABTS^{\bullet-}$, and subsequent coordination of $ABTS^{2-}$ to Ru will regenerate $[L_nRu–A_{red}]^{1-}$ and restart the cycle (dashed arrow, Scheme 3.2).

To elucidate the steps in the catalytic cycle, we conducted rate law studies by varying the initial concentration of $ABTS^{\bullet-}$, $ABTS^{2-}$, EtOH and **Ru1**, as well as solution pH and temperature.‡ The initial rate (v_0) increased linearly with $[ABTS^{\bullet-}]_0$ (Fig. 3.1A), consistent with a reaction that is first-order in $[ABTS^{\bullet-}]$ [Eq. (1)]. This result also suggests that the 2 equiv. of $ABTS^{\bullet-}$ per turnover were reduced in separate steps (that is, step 5 followed by the dashed arrow in Scheme 3.2). A linear relationship was apparent in the plot of k_{obs} versus $1/[ABTS^{2-}]_0$ (Fig. 3.1B), which suggested that $ABTS^{2-}$ dissociation from Ru is necessary for the reaction to proceed (consistent with step 1). An inverse relationship is observed between k_{obs} and $[H^+]$ (Fig. 3.1C), which is expected for H^+ transfer from the EtOH ligand to the (buffered) solution before or during the rate–determining step (consistent with step 3). In contrast, the values of k_{obs} increased as $[EtOH]_0$ increased (Fig. 3.1 D), which implied that ligand substitution of the Ru–aquo intermediate by EtOH is a necessary step in the catalytic cycle (consistent with step 2). The plot of k_{obs} vs. [**Ru1**] is also linear (Fig. 3.1E), which suggests that the predominant Ru–containing species in solution leading up to the rate–determining step is mononuclear. However, the possibility that multinuclear species were present in solution

‡ For experimental details and data plots, see synthetic procedures and figures. For equation derivations, see "Derivation of General Rate Law"

in minor amounts cannot be definitively excluded. Overall, the rate of $ABTS^{\bullet-}$ reduction is proportionally dependent on $[ABTS^{\bullet-}]_0$, $[EtOH]_0$, and $[\mathbf{Ru1}]_0$, but inversely dependent on $[ABTS^{2-}]_0$ and $[H^+]_0$ [Eq. (2)], which is similar to the rate laws derived by Sigman et al.[35,36] and Stahl et al.[37,38] for the Pd- and Cu-catalyzed aerobic oxidation of alcohols.

$$v_0 = -\frac{d[ABTS^{\bullet-}]}{dt} = k_{obs}[ABTS^{\bullet-}] \qquad (1)$$

$$-\frac{d[ABTS^{\bullet-}]}{dt} \propto \frac{[EtOH]_0 * [\mathbf{Ru1}]_0}{[ABTS^{2-}]_0 * [H^+]_0}[ABTS^{\bullet-}] \qquad (2)$$

Plotting $\ln(k_{obs}/T)$ versus $1/T$ (Fig. 3.1F) yields a positive $\Delta S^{\ddagger}$ value (28.9 ± 1.7 cal mol^{-1} K^{-1}), which reveals that disorder increases during the rate–determining step and could arise from ligand dissociation or fragmentation (consistent with step 4). Positive $\Delta S^{\ddagger}$ values were also observed for **Ru1**-catalyzed $ABTS^{\bullet-}$ reduction with *i*-PrOH (32.2 ± 2.3 cal mol^{-1} K^{-1}; Fig. 3.2 , MeOH (11.4 ± 2.9 cal mol^{-1} K^{-1}; Fig. 3.3), and ethylene glycol (32.8 ± 2.1 cal mol^{-1} K^{-1}; Fig. 3.4),[§] which suggests that these alcohols undergo β-hydride elimination (via a **TS4–**like transition state). The presence of acetone did not inhibit the rate of $ABTS^{\bullet-}$ reduction with *i*-PrOH, therefore we conclude that β-hydride elimination with concomitant dissociation of acetone to generate [L_nRu–H] (step 4) is irreversible. A negative $\Delta S^{\ddagger}$ value would be expected if step 5 (a bimolecular reaction) was rate-determining but v_0 would not vary with $[ABTS^{\bullet-}]_0$ if step 4 was rate–determining.[§] Therefore, neither step 4 nor 5 is the unique rate-determining step for the **Ru1**-catalyzed reduction of $ABTS^{\bullet-}$ into $ABTS^{2-}$. Instead, both steps are likely to exert a comparable influence on catalyst turnover. No $ABTS^{\bullet-}$ reduction occurred with *t*–BuOH,

[§] For experimental details and data plots, see synthetic procedures and figures. For equation derivations, see "Derivation of General Rate Law"

consistent with the inability of [L_nRu–O–*t*–Bu] to undergo β–hydride elimination (step 4 is blocked). This lack of reactivity with *t*–BuOH also suggests that $ABTS^{\bullet-}$ reduction does not occur by oxidation of [L_nRu–OR], because a *t*–BuO^- ligand would render the Ru center more electron–rich, and thus easier to oxidize, than either EtO^- or *i*–PrO^-. A similar lack of reactivity with 1,2–dimethoxyethane was unsurprising, given that no [L_nRu–OR] intermediate can be formed (step 3 is blocked).

To confirm that C–H and O–H bond breakage occurred before or during the rate-determining step, **Ru1**–catalyzed $ABTS^{\bullet-}$ reduction was performed with EtOH, EtOH–d_6, *i*–PrOH, and *i*–PrOH–d_8 in protio and deutero PBS.[**] Significantly greater kinetic isotope effects (KIEs) were observed for the C–H/D and O–H/D isotopic substitutions in protio versus deutero PBS, consistent with the role of H_2O in multiple steps of the proposed mechanism: displacement of $ABTS^{2-}$ by H_2O (step 1), ligand exchange with EtOH (step 2), and H^+ transfer from the EtOH ligand to the buffered solution (step 3). Substituting H_2O with D_2O can affect the equilibrium for each step, therefore it is unsurprising to observe a solvent KIE value for **Ru1**-catalayzed $ABTS^{\bullet-}$ reduction. The solvent KIE values calculated using EtOH and *i*–PrOH as terminal reductants (1.76 ± 0.39 and 1.72 ± 0.37, respectively) were consistent with base-catalyzed H^+ transfer (that is not rate-determining) and agreed with previously-reported values for catalytic redox reactions involving $ABTS^{\bullet-}$,[39] Ru-mediated alcohol oxidation,[40] and enzymes[41-43] in H_2O and D_2O solutions.

[**] For experimental details and data plots, see synthetic procedures and figures. For equation derivations, see "Derivation of General Rate Law"

The KIEs for the C–H/D and O–H/D isotopic substitutions in EtOH and *i*–PrOH were unambiguous for primary KIEs,[44] which demonstrated that O–H and C–H bond breakage both occurred before or during the rate–determining steps (consistent with step 3 and **TS4**). Notably, the C–H/D KIE values measured for **Ru1**–catalyzed $ABTS^{\bullet-}$ reduction with EtOH (2.88 ± 0.27) and *i*–PrOH (2.86 ± 0.31) were nearly identical to the corresponding C–H/D values reported by Bäckvall et al. (2.57 ± 0.26) and Casey et al. (2.86 ± 0.20) for respective H_2 transfer from 1-(4-fluorophenyl)ethanol and *i*–PrOH to other Ru complexes similar to **Ru1**.[45,46] In contrast, the O–H/D KIE values observed for **Ru1**–catalyzed $ABTS^{\bullet-}$ reduction with EtOH (2.92 ± 0.51) and *i*–PrOH (4.18 ± 0.60) were significantly greater than the corresponding values reported by Bäckvall et al. (1.87 ± 0.17) and Casey et al. (1.79 ± 0.07). One possible cause for this difference is that $[L_nRu–H]$ is formed by H^+ transfer from the O–H group in a separate step before β–hydride elimination (that is, step 3 followed by **TS4**), whereas the systems studied by Bäckvall et al. and Casey et al. involved H_2 transfer from the CH–OH moiety in a single, concerted step. The slightly smaller O–H/D KIE value measured for EtOH versus *i*–PrOH with **Ru1** could be due to the greater acidity of EtOH, which lowers the activation barrier to H^+ dissociation and renders ionic O–H bond breakage less sensitive to H/D isotopic substitution.

We propose that $[L_nRu–H]$ undergoes $1e^-$ oxidation by $ABTS^{\bullet-}$ to produce a cationic 17 e^- Ru^{III} complex, $[L_nRu–H]^{1+}$ (Scheme 3.3A). Deprotonation of $[L_nRu–H]^{1+}$ followed by coordination of an additional ligand L' from solution (for example, H_2O) generates $[L_nRu–L']$. This 19 e^- Ru^{I} complex is oxidized by a second equivalent of

$ABTS^{\bullet-}$ and subsequently combines with the resultant $ABTS^{2-}$ to produce $[L_nRu–A_{red}]^{1-}$ and complete the catalytic cycle. Direct observation of these subsequent steps was not possible because these reactions occurred after the rate-determining step. However, literature precedent (see below) suggests that the proposed $1e^-$ oxidation of $[L_nRu–H]$ and $[L_nRu–L']$ by $ABTS^{\bullet-}$, as well as deprotonation of $[L_nRu–H]^{1+}$ at pH 7.4, will be thermodynamically favorable.

Tilset and Norton et al. have shown that $\mathbf{M1_{red}}$ undergoes $1e^-$ oxidation at +0.060 V to form $\mathbf{M1_{ox}}$, which has a pK_a 20–25 log units lower than $\mathbf{M1_{red}}$ (Scheme 3.3B).[47,48] Oxidation of $\mathbf{M1_{red}}$ to $\mathbf{M1_{ox}}$ by $ABTS^{\bullet-}$ is expected to be thermodynamically feasible because the $ABTS^{\bullet-}/ABTS^{2-}$ redox couple occurs at +0.68 V.[17] Tilset and Norton et al. also noted that the deprotonation of $\mathbf{M1_{ox}}$ will occur even if it is thermodynamically unfavorable by 4 pK_a units, provided that the 19 e^- Ru^I conjugate base ($\mathbf{M2_{red}}$) is irreversibly oxidized. Even a weak oxidant, such as $[Co(\eta^5–C_5Me_5)_2]^{1+}$ ($E_{1/2}$ = –1.51 V),[49] could oxidize $\mathbf{M2_{red}}$ because the $1e^-$ reduction of $\mathbf{M2_{ox}}$ to $\mathbf{M2_{red}}$ occurs at –2.02 V (Scheme 3.3C),[47] Oxidation of the 19 e^- Ru^I intermediate $[L_nRu–L']$ (analogous to $\mathbf{M2_{red}}$) by $ABTS^{\bullet-}$ should be similarly favorable, and would likewise facilitate deprotonation of $[L_nRu–H]^{1+}$.

An anionic $\eta^5–C_5H_5$ ligand is more electron-donating than a neutral η^6-cymene, thus it is more relevant to compare the oxidation of $[L_nRu–H]$ to other Ru complexes with η^6–cymene ligands rather than $\mathbf{M1_{red}}$. Unsurprisingly, the oxidation of $\mathbf{M3_{red}}$ (+0.16 V; Scheme 3.3D) occurred at a higher potential than $\mathbf{M1_{red}}$,[50] but still well below the $ABTS^{\bullet-}/ABTS^{2-}$ redox couple. The difference in oxidation potentials between $[L_nRu–H]$

and **M3**$_{red}$ is expected to be smaller than that between **M3**$_{red}$ and **M1**$_{red}$, therefore ABTS$^{\bullet-}$ should be a sufficient strong oxidant to oxidize [L$_n$Ru–H] and [L$_n$Ru–L'].

The complex most similar to [L$_n$Ru–H]$^{1+}$ for which a pK_a value has been reported is **M4**$_{red}$ (pK_a = 22.5 ± 0.1 in CH_3CN; Scheme 3.3 E)[51] The pK_a for **M4**$_{red}$ in H_2O can be estimated as 15.9 using Morris' method to estimate acidity in different solvents.[52] However, **M4**$_{red}$ is an 18 e^- Ru^{II} species and [L$_n$Ru–H]$^{1+}$ is a 17 e^- Ru^{III} species, therefore a more relevant comparison would involve **M4**$_{ox}$, which has not been reported. Using the observations of Tilset and Norton et al. that 1e^- oxidation of an 18 e^- Ru^{II} complex typically lowers the pK_a by 20–25 log units,[47,48] the pK_a for **M4**$_{ox}$ in H_2O is estimated to be in the range of –4 to –9. Similarly dramatic decreases in pK_a have been observed following 1e^- oxidation of [RuH(η^5–C_5H_5)(CO)(PPh_3)] (from 27–28 to 4–5)[53] and [WH(η^5–C_5H_5)$(CO)_2$] (from 16 to –3).[54] Therefore, [L$_n$Ru–H]$^{1+}$ should be sufficiently acidic to undergo complete deprotonation in pH 7.4 aqueous solution.

Synthetic Procedures

General synthetic considerations. N-(*p*-tolyl)benzimidazole and ABTS$^{\bullet-}$ were prepared as previously described.[19,55] All other materials were of reagent quality and used as received. All solvents used were HPLC grade. ^{1}H and ^{13}C {^{1}H} NMR spectra were recorded using a Bruker 500 MHz spectrometer. Chemical shifts δ (in ppm) for ^{1}H and ^{13}C NMR are referenced to $SiMe_4$ using the residual protio-solvent as an internal standard. For ^{1}H NMR: $CDCl_3$, 7.26 ppm; DMSO-d_6, 2.50 ppm. For ^{13}C NMR: $CDCl_3$, 77.16 ppm; DMSO-d_6, 39.52 ppm.[56] Coupling constants (*J*) are expressed in hertz (Hz). Infrared spectra were recorded with 4 cm^{-1} resolution on a Shimadzu IRAffinity-1S

spectrometer equipped with a Pike Technologies MIRacle ATR (diamond) sampling accessory. Elemental analyses were performed at Atlantic Microlab, Inc. (Norcross, GA). All reactions were performed under an inert atmosphere under an N_2 atmosphere using standard Schlenk or glovebox techniques with the exclusion of light. All subsequent manipulations were performed under ambient conditions using standard benchtop techniques without the exclusion of light. When required, solvents were dried and deoxygenated using an Innovative Technologies solvent purification system, and then stored over molecular sieves (3 Å) in a drybox.

Synthesis of 2-(3-{*p*-tolyl}-benzimidazol-1-ium-1-yl)-acetate hydrobromide [1H$_2$][Br]. Bromoacetic acid (503 mg, 3.62 mmol) and N-(*p*-tolyl)benzimidazole (500 mg, 2.41 mmol) were dissolved with 20 mL of toluene in a vial equipped with a stir bar. The vial was then sealed with a Teflon-lined cap and the clear, dark orange-brown solution was heated to 120 °C. After 16 h, a white precipitate had formed, at which point the reaction mixture was allowed to cool to room temperature and the precipitate was collected by filtration. The resulting solid was washed with minimum toluene followed by CH_2Cl_2 and was then dried *in vacuo* to afford 514 mg (1.48 mmol, 80% yield) of the desired product as a white powder. ^{1}H NMR (500 MHz, DMSO-d_6): δ = 13.95 (s, 1H), 10.18 (s, 1H), 8.18 (d, J = 8.0, 1H), 7.85 (d, J = 8.0, 1H), 7.78–7.73 (m, 4H), 7.57 (d, J = 8.0, 2H), 5.58 (s, 2H), 2.47 (s, 3H). ^{13}C NMR (125 MHz, DMSO-d_6): δ 167.5, 143.3, 140.5, 131.5, 130.8, 130.6, 130.4, 127.4, 127.1, 124.8, 114.3, 113.4, 47.8, 20.7. FT-IR (KBr): 3421 (vw), 2953 (m), 2372 (m), 1718 (m), 1560, 1508 (m), 1381 (m), 1300 (m),

1225 (m), 822, 754, 742, 482 (vw) cm^{-1}. Anal. Calcd. for $C_{16}H_{16}BrN_2O_{2.5}$ ([**1**H_2][Br]•0.5H_2O): C, 53.95; H, 4.53; N, 7.86. Found: C, 54.01; H, 4.35; N, 7.79.

Synthesis of [Ag(1)]$_n$ (2). To a solution of [**1**H_2][Br] (500 mg, 144 μmol) in anhydrous CH_2Cl_2 (50 mL) under nitrogen was added Ag_2O (502 mg, 217 μmol), and the resulting white suspension was allowed to stir at room temperature in the absence of light. After 24 h, the reaction mixture was filtered and the resulting grey solid was washed with $CHCl_3$ (10 mL). The filtrate solvent was removed under reduced pressure and the resulting solids were then dried *in vacuo* to afford 452 mg (121 μmol, 84% yield) of the desired product as an off-white powder. ^{1}H NMR (500 MHz, DMSO-d_6): δ 7.71 (d, J = 8.5, 1H), 7.58 (d, J = 8.0, 2H), 7.44–7.38 (m, 5H), 5.09 (s, 2H), 2.39 (s, 3H). ^{13}C NMR (125 MHz, DMSO-d_6): δ 138.6, 135.2, 134.1, 133.4, 130.3, 125.6, 124.1, 112.7, 111.6, 99.5, 79.1, 52.1, 20.6. FT-IR (KBr): 3416 (w), 1608, 1516, 1475, 1439, 1385, 1308, 1250, 1207 (m), 1109 (m), 1094 (m), 1018 (m), 835, 814, 746, 715, 482 (w) cm^{-1}. Anal. Calcd. for $C_{16}H_{14}N_2O_{2.5}Ag$ (**2**•0.5H_2O): C, 50.36; H, 3.77; N, 7.49. Found: C, 50.23; H, 4.09; N, 7.05.

Synthesis of [RuCl(1)(η^6-cymene)] (Ru1). To a stirred solution of **2** (100 mg, 134 μmol) in anhydrous CH_2Cl_2 (10 mL) under nitrogen was added [RuCl(η^6-cymene)(μ-Cl)]$_2$ (82 mg, 134 μmol) dissolved in 10 mL of CH_2Cl_2. During the course of the addition, the mixture changed first to a clear red and then to a clear orange solution with concomitant formation of a white precipitate, and the reaction was allowed to stir at room temperature. After 24 h, the reaction mixture was filtered through a 0.2 μm PTFE filter (to remove AgCl) with the aid of CH_2Cl_2 (4 mL). The filtrate solvent was removed under

reduced pressure and the resulting solids were then dried *in vacuo* to afford 71.7 mg (134 μmol, 98%) of the desired product as a light red-orange powder. ^{1}H NMR (500 MHz, $CDCl_3$): δ 7.95 (d, *J* = 8.0, 1H), 7.49–7.44 (m, 2H), 7.41 (d, *J* = 10.0, 1H), 7.37–7.32 (m, 2H), 7.25–7.23 (m, 1H), 7.04 (d, *J* = 8.5, 1H), 5.43 (d, *J* = 6.0, 1H), 5.16 (d, *J* = 6.5, 1H), 5.04 (d, *J* = 5.5, 1H), 4.91 (d, *J* = 17.0, 1H), 4.71 (d, *J* = 17, 1H), 3.95 (d, *J* = 5.5, 1H), 2.60 (sep, 1H), 2.52 (s, 3H), 2.03 (s, 3H), 1.08 (d, *J* = 7.5, 6H). ^{13}C NMR (125 MHz, $CDCl_3$): δ 186.6, 169.2, 140.3, 136.8, 136.0, 134.0, 131.1, 131.0, 129.7, 127.4, 124.2, 124.1, 111.3, 110.2, 104.7, 103.2, 90.0, 89.4, 83.6, 80.3, 49.9, 30.9, 23.3, 22.0, 21.5, 19.0. FT-IR (KBr): 3429 (vw), 3055 (w), 2959 (m), 2872 (w), 2230 (w), 2100 (w), 1628 (vs), 1514, 1475, 1443, 1373 (w), 1356, 1300, 1244, 1207 (m), 1190 (m), 1014, 930, 862, 843 (m), 827 (m), 804, 748, 663 (m), 615, 555, 476 (m), 470, 424, 405 cm^{-1}. Anal. Calcd. for $C_{26}H_{27}ClN_2O_2Ru$: C, 58.26; H, 5.08; N, 5.23. Found: C, 57.98; H, 4.95; N, 5.17.

Spectroscopic and Kinetic Analysis Procedures

General spectroscopic considerations. UV–visible absorption spectra were acquired on a Varian Cary 50 Bio spectrometer equipped with a water-cooled Quantum Northwest TC-125 peltier temperature controller. All solution measurements were performed at 25.0 ± 0.1 °C in matched gas-tight quartz cuvettes (Precision Scientific) with 1 cm path lengths and 3.0 mL analyte solution volumes. Absorption spectra were acquired from 900 to 200 nm with a scanning speed of 300 nm min^{-1} and a resolution of 0.5 nm. Each kinetic analysis experiment (5 second intervals) was performed in quadruplicate on four different days. Stock solutions were prepared fresh daily and filtered (0.2 μm PTFE) immediately prior to use.

General procedure for kinetic analysis of $ABTS^{\bullet-}$ degradation by Ru1 in PBS. An aliquot of $ABTS^{2-}$ (30 μL from stock solution in H_2O) and an aliquot of $ABTS^{\bullet-}$ (35 μL from stock solution in H_2O) were added to PBS (pH 7.4) and this working solution was allowed to equilibrate at 25 °C for 10 min. The absorbance spectrum of this working solution was acquired to confirm $ABTS^{\bullet-}$ concentration and the single wavelength kinetics program was initiated. After 20 s, the cuvette was removed from the spectrometer without stopping the kinetics program, an aliquot of **Ru1** (30 μL from stock solution in CH_3CN) was added, the cuvette was covered and mixed via repeated inversion for 3 s, placed back in the spectrometer, and the kinetics program was allowed to continue. After 5 min, an aliquot of EtOH (30 μL from stock solution in H_2O) was added, the cuvette was covered and mixed via repeated inversion for 3 s, placed back in the spectrometer, and the kinetics program was allowed to continue. After the kinetics program had completed, the absorbance spectrum was acquired to confirm the formation of $ABTS^{2-}$ from the peak at 340 nm. Standard conditions (unless specified otherwise): 100 μM $ABTS^{2-}$, 50 μM $ABTS^{\bullet-}$, 5 μM **Ru1**, 50 mM EtOH, PBS (pH 7.4), 25 °C; absorbance measured at 734 nm.

Rate law experiments. The concentrations of $ABTS^{2-}$, $ABTS^{\bullet-}$, **Ru1** and EtOH employed in the rate law experiments (cf. Figure 1) were obtained using this general kinetic procedure by varying stock solution concentration and holding aliquot volume constant. The H^+ concentrations were obtained using PBS adjusted to different pH values before the addition of any aliquots. The temperatures were obtained by allowing the working solution to equilibrate at different temperatures before the addition of **Ru1**.

Kinetic isotope effect experiments. The general kinetic procedure and standard conditions were employed, with minor modifications. Experiments were performed in either protio PBS (pH 7.4) or deutero PBS (pD 7.4). Protio and deutero alcohol stock solutions were prepared in H_2O and D_2O (5.0 M) to obtain all 4 permutations of C–H and O–H isotopic substitution. For example, EtOH-d_6 stock solutions in H_2O and D_2O enabled comparison of k_{obs} with CD_3CD_2OH and CD_3CD_2OD.

Derivation of General Rate Law

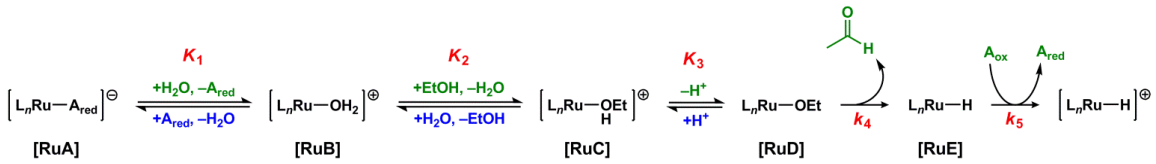

Proposed Mechanism: Adapted from Scheme 2 in manuscript. The intermediates $[L_nRu–Ared]1–$, $[L_nRu–OH_2]^{1+}$, $[L_nRu–(EtOH)]^{1+}$, $[L_nRu–OEt]$ and $[L_nRu–A_{red}]^{1–}$ have been abbreviated in the following equations as [**RuA**], [**RuB**], [**RuC**], [**RuD**] and [**RuE**], respectively, to enhance clarity.

(1) Based on the observation that the rate is directly proportional to the concentration of $ABTS^{\bullet-}$ (cf. Fig.3.1 A) the underlying reaction is the oxidation of $[L_nRu–H]$ by $ABTS^{\bullet-}$:

$$\text{rate} = -\frac{d[\mathbf{A_{ox}}]}{dt} = k_5[\mathbf{A_{ox}}][\mathbf{RuE}]$$

(2) The sum of the concentrations of the Ru-containing species leading up to the rate-determining step is equal to the total concentration of **Ru1** added at the beginning of the experiment:

$$[\mathbf{Ru1}]_0 = [\mathbf{RuA}] + [\mathbf{RuB}] + [\mathbf{RuC}] + [\mathbf{RuD}] + [\mathbf{RuE}]$$

(3) Assuming that steps 1-3 achieve equilibrium rapidly (with respect to turnover):

$$K_1 = \frac{[\mathbf{RuB}][\mathbf{A_{red}}]}{[\mathbf{RuA}]} \qquad K_2 = \frac{[\mathbf{RuC}]}{[\mathbf{RuB}][\mathrm{EtOH}]} \qquad K_3 = \frac{[\mathbf{RuD}][\mathrm{H^+}]}{[\mathbf{RuC}]}$$

(4) Assuming the system achieves steady-state rapidly (with respect to turnover):

$$\frac{d[\mathbf{RuE}]}{dt} = k_4[\mathbf{RuD}] - k_5[\mathbf{A_{ox}}][\mathbf{RuE}]$$

$$[\mathbf{RuD}] = \frac{k_5[\mathbf{A_{ox}}]}{k_4}[\mathbf{RuE}]$$

(5) Solving (2) for [**RuE**] using the relationships established in (3) and (4):

$$[\mathbf{Ru1}]_0 = \left(\frac{[\mathbf{A_{red}}]}{K_1} + 1\right)[\mathbf{RuB}] + [\mathbf{RuC}] + [\mathbf{RuD}] + [\mathbf{RuE}]$$

$$[\mathbf{Ru1}]_0 = \left(\frac{[\mathbf{A_{red}}]}{K_1K_2[\mathrm{EtOH}]} + \frac{1}{K_2[\mathrm{EtOH}]} + 1\right)[\mathbf{RuC}] + [\mathbf{RuD}] + [\mathbf{RuE}]$$

$$[\mathbf{Ru1}]_0 = \left(\frac{[\mathbf{A_{red}}][\mathrm{H^+}]}{K_1K_2K_3[\mathrm{EtOH}]} + \frac{[\mathrm{H^+}]}{K_2K_3[\mathrm{EtOH}]} + \frac{[\mathrm{H^+}]}{K_3} + 1\right)[\mathbf{RuD}] + [\mathbf{RuE}]$$

(6) For convenience, quotients are substituted with terms Q_1, Q_2 and Q_3:

$$Q_1 = \frac{K_1}{[\mathbf{A_{red}}]} \qquad Q_2 = K_2[\mathrm{EtOH}] \qquad Q_3 = \frac{K_3}{[\mathrm{H^+}]}$$

$$\frac{1}{Q_1} = \frac{[\mathbf{A_{red}}]}{K_1} \qquad \frac{1}{Q_2} = \frac{1}{K_2[\mathrm{EtOH}]} \qquad \frac{1}{Q_3} = \frac{[\mathrm{H^+}]}{K_3}$$

(7) Continuing from (5):

$$[\mathbf{Ru1}]_0 = \left(\frac{1}{Q_1Q_2Q_3} + \frac{1}{Q_2Q_3} + \frac{1}{Q_3} + 1\right)[\mathbf{RuD}] + [\mathbf{RuE}]$$

$$[\mathbf{Ru1}]_0 = \left(\frac{1 + Q_1 + Q_1Q_2 + Q_1Q_2Q_3}{Q_1Q_2Q_3}\right)\left(\frac{k_5[\mathbf{A_{ox}}]}{k_4}\right)[\mathbf{RuE}] + [\mathbf{RuE}]$$

$$[\mathbf{Ru1}]_0 = \left\{\frac{(1 + Q_1 + Q_1Q_2)(k_5[\mathbf{A_{ox}}]) + (k_5[\mathbf{A_{ox}}] + k_4)(Q_1Q_2Q_3)}{k_4Q_1Q_2Q_3}\right\}[\mathbf{RuE}]$$

$$[\mathbf{RuE}] = \left\{\frac{k_4 Q_1 Q_2 Q_3}{(1 + Q_1\{1 + Q_2\})(k_5[\mathbf{A_{ox}}]) + (k_5[\mathbf{A_{ox}}] + k_4)(Q_1 Q_2 Q_3)}\right\}[\mathbf{Ru1}]_0$$

(8) Plugging this result into (1) gives the general rate law:

$$\text{rate} = \frac{k_4 k_5 Q_1 Q_2 Q_3 [\mathbf{Ru1}]_0 [\mathbf{A_{ox}}]}{(1 + Q_1\{1 + Q_2\})(k_5[\mathbf{A_{ox}}]) + (k_5[\mathbf{A_{ox}}] + k_4)(Q_1 Q_2 Q_3)}$$

CONCLUSIONS

In summary, mechanistic data for the catalytic reduction of $ABTS^{\bullet-}$ into $ABTS^{2-}$ by **Ru1**, with EtOH as the terminal reductant, suggests that β–hydride elimination from a Ru-alkoxide species generates the catalytically active Ru–H intermediate. In light of previous reports indicating that, 1) Ru–H intermediates can achieve anticancer properties by exerting catalytic pro–oxidant effects,[23-25] and 2) some Mn porphyrin–based complexes can produce catalytic antioxidant or pro–oxidant effects in different environments with distinct therapeutic uses, [4-15] we believe that new therapeutic strategies and applications can potentially be developed that utilize the catalytic radical reducing ability we have demonstrated for complexes that form Ru–hydride intermediates.

Acknowledgements

This work was supported by the National Science Foundation (DMR-1555224). We thank Dr. A. Mangalum for prior work with **Ru1** and helpful discussions.

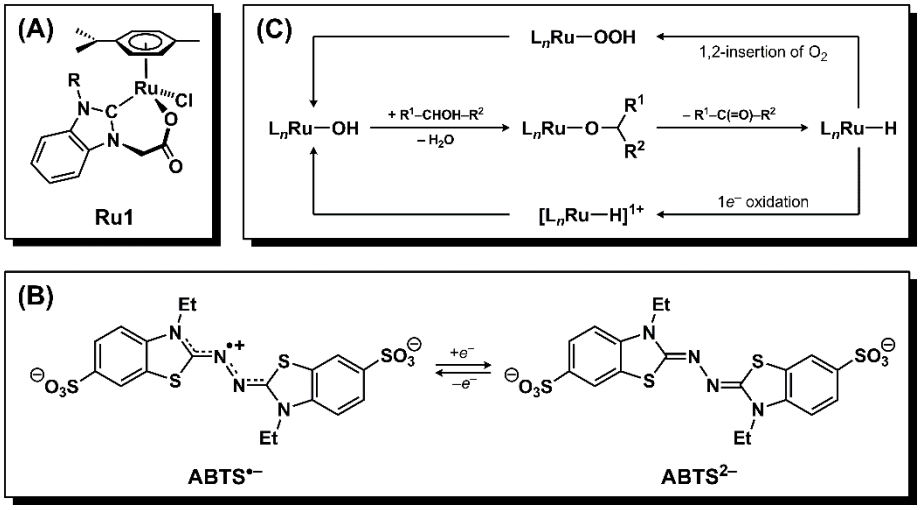

Scheme 3.1. (**A**) Structure of **Ru1**. (**B**) 1 e^- interconversion between $ABTS^{\bullet-}$ and $ABTS^{2-}$. (**C**) Formation of Ru–hydride in catalytic aerobic alcohol oxidation (top) and $ABTS^{\bullet-}$ reduction (bottom).

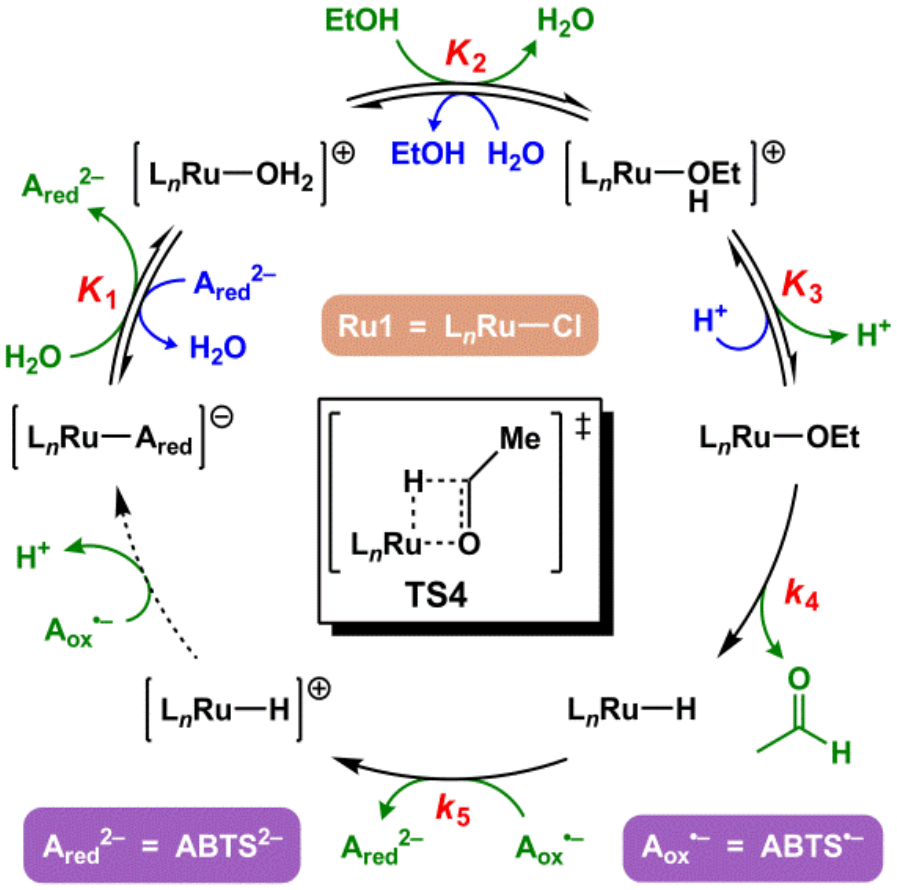

Scheme 3.2. Proposed mechanism for **Ru1**-catalyzed reduction of $ABTS^{\bullet-}$ to $ABTS^{2-}$, with EtOH as the terminal reductant. Forward reactions (clockwise green), reverse reactions (counter-clockwise, blue). Each K_n or k_n corresponds to the equilibrium or rate constant, respectively, for the forward reaction in step "n" (step 1 has equilibrium constant K_1, and so forth). The transition-state structure for step 4 is shown as **TS4** in the center. The dashed arrow includes multiple transformations that occur after the rate-determining steps. The spectator ligand set "L_n" comprises the η^6-cymene and κ^2-(C,O)-benzimidazolylidene-carboxylate ligands, but their hapticity/denticity may decrease to accommodate additional ligands.

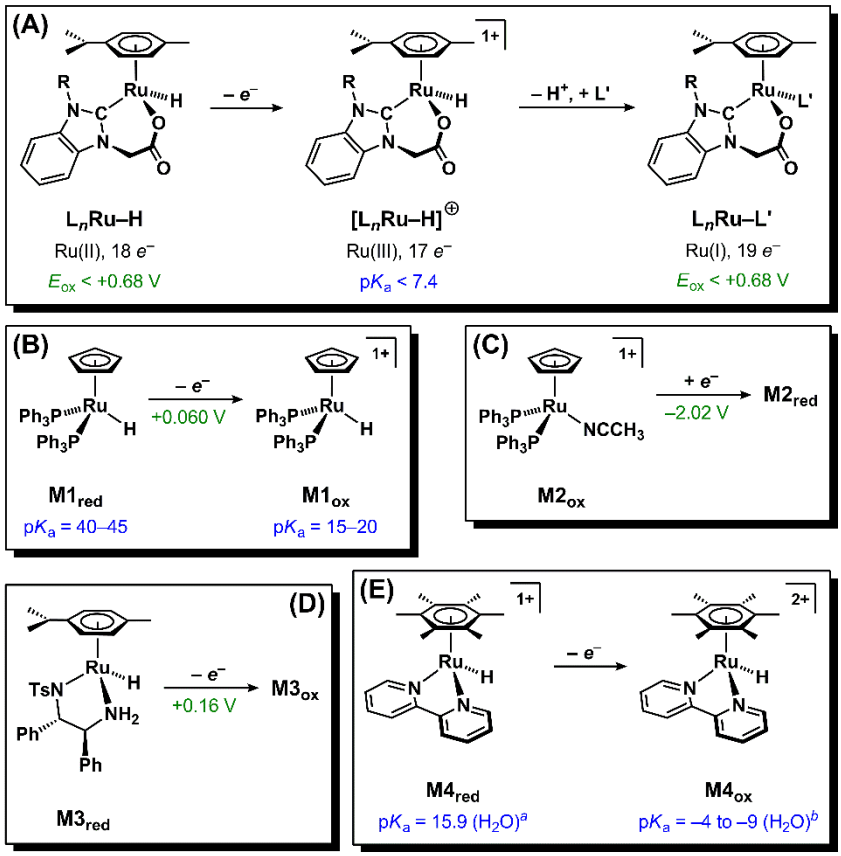

Scheme 3.3. A) Proposed completion of the catalytic cycle starting from [L_nRu-H], and B–E) literature precedent. Unless specified otherwise, pK_a values and redox potentials were measured in CH_3CN solutions. [a] pK_a value for **M4$_{red}$** in H_2O estimated using ref 52.[b] pK_a value for **M4$_{ox}$** estimated using ref. 47, 48.

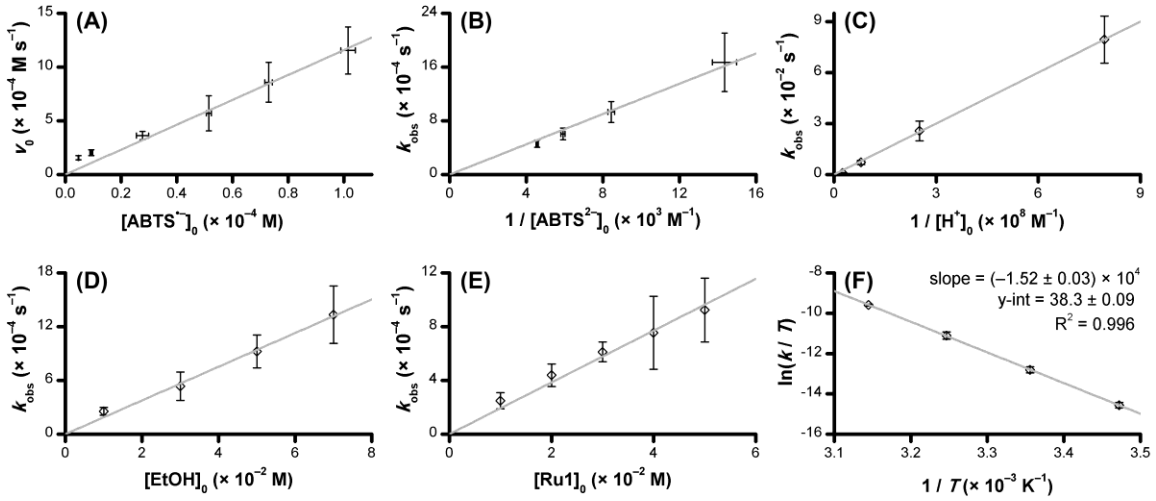

Fig. 3.1. (**A**) Dependence of initial rate (v_0) of **Ru1**-catalyzed $ABTS^{\bullet-}$ reduction on [$ABTS^{\bullet-}$]$_0$ = 5, 10, 25, 50, 75 or 100 μM. Dependence of observed rate constant (k_{obs}) for **Ru1**-catalyzed $ABTS^{\bullet-}$ reduction on: (**B**) [$ABTS^{2-}$]$_0$ = 50, 100, 150 or 200 μM; (**C**) pH = 7.4, 7.9, 8.4 or 8.9; (**D**) [EtOH]$_0$ = 10, 30, 50 or 70 mM; (**E**) [**Ru1**]$_0$ = 1, 2, 3, 4 or 5 μM; (**F**) T = 15, 25, 35 or 45 °C. Each data point (◊) is the average of 4 experiments. Conditions: [**Ru1**]$_0$ = 5 μM, [$ABTS^{\bullet-}$]$_0$ = 50 μM, [$ABTS^{2-}$]$_0$ = 100 μM, [EtOH]$_0$ = 50 mM, PBS (pH 7.4), 25 °C; absorbance measured at 734 nm.

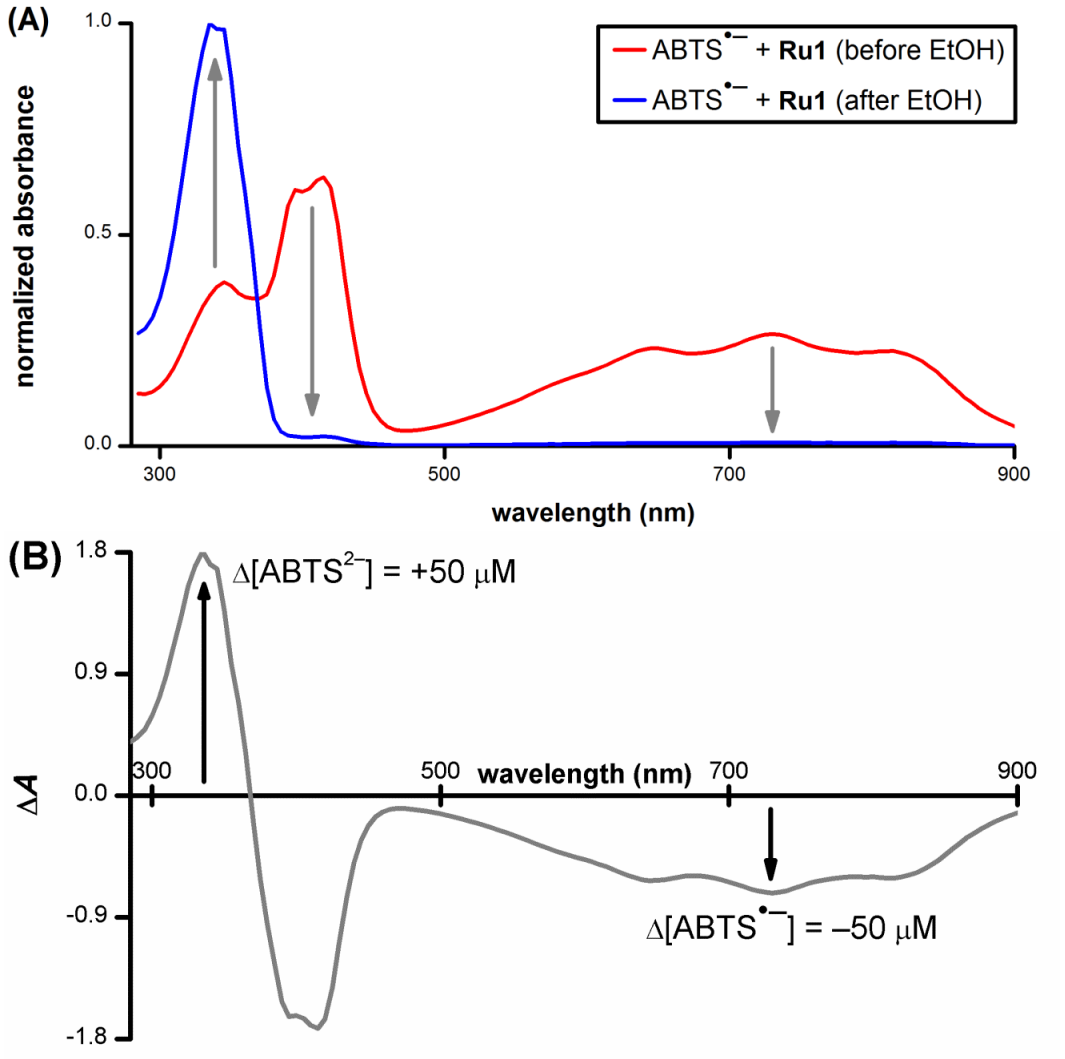

Fig. 3.2. (**A**) Normalized absorption spectrum of 50 μM $ABTS^{\bullet-}$ and 5 μM **Ru1** in PBS (red) and after 50 mM EtOH was added and 30 minutes had elapsed (blue). (**B**) Difference spectrum obtained by subtracting red trace from blue trace, which showed that the 50 μM decrease in $ABTS^{\bullet-}$ concentration was accompanied by a 50 μM increase in $ABTS^{2-}$ concentration. Conditions: $[\mathbf{Ru1}]_0$ = 5 μM, $[ABTS^{\bullet-}]_0$ = 50 μM, $[ABTS^{2-}]_0$ = 100 μM, $[EtOH]_0$ = 50 mM, PBS (pH 7.4), 25 °C; absorbance measured from 285–900 nm

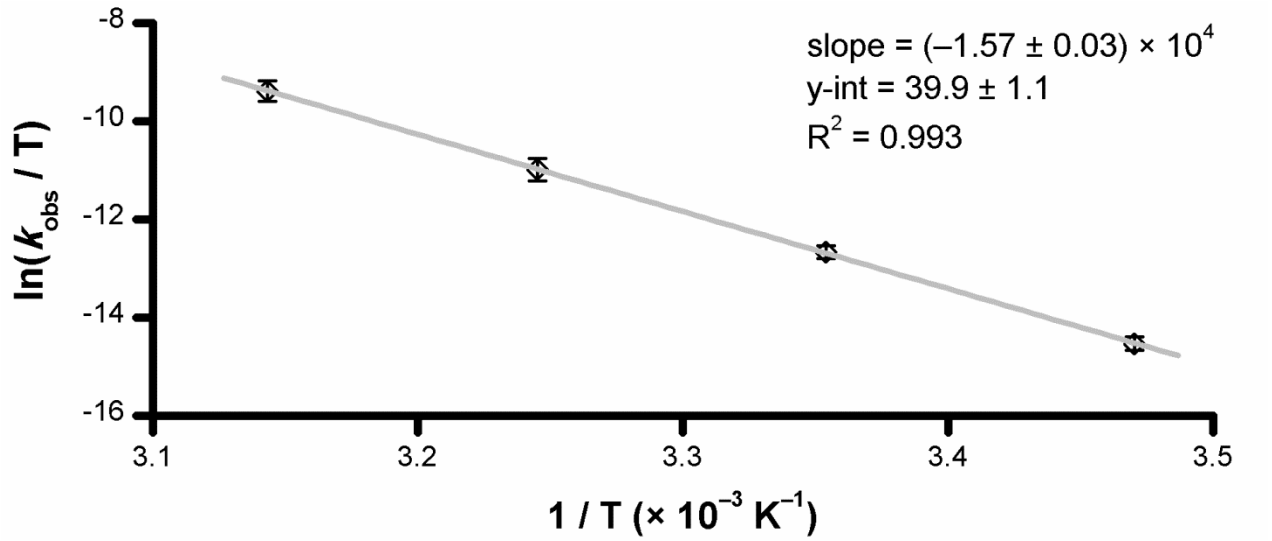

Fig. 3.3. Eyring plot for **Ru1**-catalyzed $ABTS^{\bullet-}$ reduction with *i*-PrOH (T = 15, 25, 35 or 45 °C). Each data point (◊) is the average of 4 experiments. Conditions: $[\mathbf{Ru1}]_0$ = 5 μM, $[ABTS^{\bullet-}]_0$ = 50 μM, $[ABTS^{2-}]_0$ = 100 μM, [*i*-PrOH]$_0$ = 50 mM, PBS (pH 7.4); absorbance measured at 734 nm.

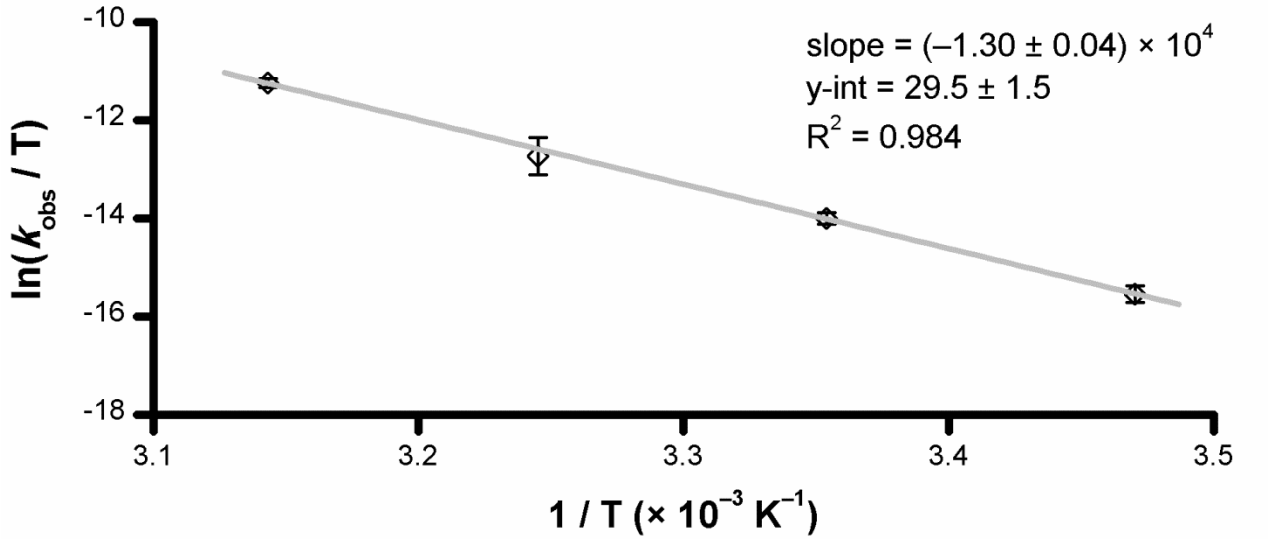

Fig. 3.4. Eyring plot for **Ru1**-catalyzed $ABTS^{\bullet-}$ reduction with MeOH (T = 15, 25, 35 or 45 °C). Each data point (◊) is the average of 4 experiments. Conditions: $[\mathbf{Ru1}]_0$ = 5 μM, $[ABTS^{\bullet-}]_0$ = 50 μM, $[ABTS^{2-}]_0$ = 100 μM, $[MeOH]_0$ = 50 mM, PBS (pH 7.4); absorbance measured at 734 nm.

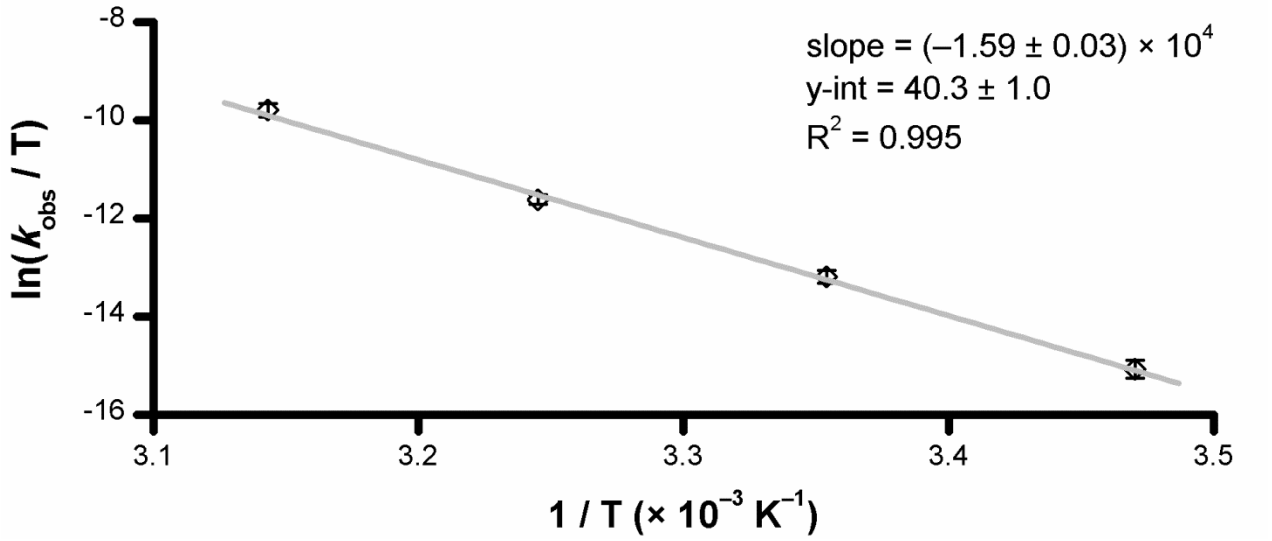

Fig. 3.5. Eyring plot for **Ru1**-catalyzed $ABTS^{\bullet-}$ reduction with ethylene glycol (EG) (T = 15, 25, 35 or 45 °C). Each data point (◊) is the average of 4 experiments. Conditions: $[\mathbf{Ru1}]_0$ = 5 μM, $[ABTS^{\bullet-}]_0$ = 50 μM, $[ABTS^{2-}]_0$ = 100 μM, $[EG]_0$ = 50 mM, PBS (pH 7.4); absorbance measured at 734 nm.

Table 3.1. Ratio of observed rate constants (k_{obs}) for **Ru1**-catalyzed $ABTS^{\bullet-}$ reduction with protio and deutero EtOH and *i*-PrOH measured in PBS-buffered H_2O and D_2O solutions

	X = H	X = D
CH_3CH_2OX / CD_3CD_2OX (C–H/C–D for EtOH)	5.05 ± 1.02 [a]	2.88 ± 0.27 [b]
$(CH_3)_2CHOX$ /$(CD_3)_2CDOX$ (C–H/C–D for *i*-PrOH)	4.93 ± 0.93 [a]	2.86 ± 0.31 [b]
CX_3CX_2OH / CX_3CX_2OD (O–H/O–D for EtOH)	5.13 ± 0.71 [c]	2.92 ± 0.51 [d]
$(CX_3)_2CXOH$ /$(CX_3)_2CXOD$ (O–H/O–D for *i*-PrOH)	7.21 ± 1.18 [c]	4.18 ± 0.60 [d]

[a] Ratio of k_{obs} measured for protio alcohol ÷ deutero alcohol in protio PBS (O–H groups conserved). [b] Ratio of k_{obs} measured for protio alcohol ÷ deutero alcohol in deutero PBS (O–D groups conserved). [c] Ratio of k_{obs} measured for protio alcohol in protio PBS ÷ protio alcohol in deutero PBS. [d] Ratio of k_{obs} measured for deutero alcohol in protio PBS ÷ deutero alcohol in deutero PBS. Values reported as the average ± standard deviation of 4 independent experiments performed on 4 different days. Alcohols were added from 5.0 M stock solutions in H_2O or D_2O (e.g., CH_3CH_2OD was added from 5.0 M EtOH stock solution in D_2O). Conditions: [**Ru1**]$_0$ = 5 μM, [$ABTS^{\bullet-}$]$_0$ = 50 μM, [$ABTS^{2-}$]$_0$ = 100 μM, [alcohol]$_0$ = 50 mM, PBS in H_2O (pH 7.4) or PBS in D_2O (pD 7.4), T = 25 °C.

REFERENCES

(1) Murphy, M. J. "How mitochondria produce reactive oxygen species." *Biochem. J.* **2009**, *417*, 1-13.

(2) Valko, M.; Leibfritz, D.; Moncol, J.; Cronin, M. T.; Mazur, M.; Telser, J. "Free radicals and antioxidants in normal physiological functions and human disease." *Int J Biochem Cell Biol* **2007**, *39*, 44-84.

(3) Nordberg, J.; Arner, E. S. "Reactive oxygen species, antioxidants, and the mammalian thioredoxin system." *Free Radic Biol Med* **2001**, *31*, 1287-312.

(4) Batinic-Haberle, I.; Tovmasyan, A.; Spasojevic, I. "An educational overview of the chemistry, biochemistry and therapeutic aspects of Mn porphyrins--From superoxide dismutation to H2O2-driven pathways." *Redox Biol* **2015**, *5*, 43-65.

(5) Evans, M. K.; Tovmasyan, A.; Batinic-Haberle, I.; Devi, G. R. "Mn porphyrin in combination with ascorbate acts as a pro-oxidant and mediates caspase-independent cancer cell death." *Free Radic Biol Med* **2014**, *68*, 302-14.

(6) Miriyala, S.; Spasojevic, I.; Tovmasyan, A.; Salvemini, D.; Vujaskovic, Z.; St Clair, D.; Batinic-Haberle, I. "Manganese superoxide dismutase, MnSOD and its mimics." *Biochim Biophys Acta* **2012**, *1822*, 794-814.

(7) Batinic-Haberle, I.; Rajic, Z.; Tovmasyan, A.; Reboucas, J. S.; Ye, X.; Leong, K. W.; Dewhirst, M. W.; Vujaskovic, Z.; Benov, L.; Spasojevic, I. "Diverse functions of cationic Mn(III) N-substituted pyridylporphyrins, recognized as SOD mimics." *Free Radic Biol Med* **2011**, *51*, 1035-53.

(8) Batinic-Haberle, I.; Reboucas, J. S.; Spasojevic, I. "Superoxide dismutase mimics: chemistry, pharmacology, and therapeutic potential." *Antioxid Redox Signal* **2010**, *13*, 877-918.

(9) Doctrow, S. R.; Huffman, K.; Marcus, C. B.; Tocco, G.; Malfroy, E.; Adinolfi, C. A.; Kruk, H.; Baker, K.; Lazarowych, N.; Mascarenhas, J.; Malfroy, B. "Salen-manganese complexes as catalytic scavengers of hydrogen peroxide and cytoprotective agents: structure-activity relationship studies." *J Med Chem* **2002**, *45*, 4549-58.

(10) Tovmasyan, A.; Sampaio, R. S.; Boss, M. K.; Bueno-Janice, J. C.; Bader, B. H.; Thomas, M.; Reboucas, J. S.; Orr, M.; Chandler, J. D.; Go, Y. M.; Jones, D. P.; Venkatraman, T. N.; Haberle, S.; Kyui, N.; Lascola, C. D.; Dewhirst, M. W.; Spasojevic, I.; Benov, L.; Batinic-Haberle, I. "Anticancer therapeutic potential of Mn porphyrin/ascorbate system." *Free Radic Biol Med* **2015**, *89*, 1231-47.

(11) Do Amaral, S.; Esposito, B. P. "Fluorimetric study of the pro-oxidant activity of EUK8 in the presence of hydrogen peroxide." *Biometals* **2008**, *21*, 425-32.

(12) Kubota, R.; Imamura, S.; Shimizu, T.; Asayama, S.; Kawakami, H. "Synthesis of water-soluble dinuclear mn-porphyrin with multiple antioxidative activities." *ACS Med Chem Lett* **2014**, *5*, 639-643.

(13) Sharpe, M. A.; Ollosson, R.; Stewart, V. C.; Clark, J. B. "Oxidation of nitric oxide by oxomanganese-salen complexes: a new mechanism for cellular protection by superoxide dismutase/catalase mimetics." *Biochem J* **2002**, *366*, 97-107.

(14) Itoh, M.; Motoda, K.-i.; Shindo, K.; Kamiusuki, T.; Sakiyama, H.; Matsumoto, N.; Okawa, H. *J. Chem. Soc. Dalton Trans.* **1995**, 3635-3641.

(15) Naruta, Y.; Maruyama, K. *J. Am. Chem. Soc.* **1991**, *113*, 3595-3596.

(16) Htet, Y.; Tennyson, A. G. "Catalytic radical reduction in aqueous solution via oxidation of biologically-relevant alcohols." *Chem. Sci.* **2016**, *7*, 4052-4058.

(17) Scott, S. L.; Chen, W. J.; Bakac, A.; Espenson, J. H. "Spectroscopic parameters, electrode potentials, acid ionization constants, and electron exchange rates of the 2,2'-azinobis(3-ethylbenzothiazoline-6-sulfonate) radicals and ions." *The Journal of Physical Chemistry* **1993**, *97*, 6710-6714.

(18) Jungwirth, U.; Kowol, C. R.; Keppler, B. K.; Hartinger, C. G.; Berger, W.; Heffeter, P. "Anticancer activity of metal complexes: involvement of redox processes." *Antioxid Redox Signal* **2011**, *15*, 1085-127.

(19) Re, R.; Pellegrini, N.; Proteggente, A.; Pannala, A.; Yang, M.; Rice-Evans, C. "Antioxidant activity applying an improved ABTS radical cation decolorization assay." *Free Radical Biology and Medicine* **1999**, *26*, 1231-1237.

(20) Bielski, B. H. J.; Allen, A. O. "Mechanism of the disproportionation of superoxide radicals." *The Journal of Physical Chemistry* **1977**, *81*, 1048-1050.

(21) Yusa, K.; Shikama, K. "Oxidation of oxymyoglobin to metmyoglobin with hydrogen peroxide: involvement of ferryl intermediate." *Biochemistry* **1987**, *26*, 6684-6688.

(22) Nikaidou, F.; Ushiyama, H.; Yamaguchi, K.; Yamashita, K.; Mizuno, N. "Theoretical and Experimental Studies on Reaction Mechanism for Aerobic Alcohol Oxidation by Supported Ruthenium Hydroxide Catalysts." *The Journal of Physical Chemistry C* **2010**, *114*, 10873-10880.

(23) Soldevila-Barreda, J. J.; Romero-Canelón, I.; Habtemariam, A.; Sadler, P. J. "Transfer hydrogenation catalysis in cells as a new approach to anticancer drug design." *Nat. Commun.* **2015**, *6*, 6582.

(24) Fu, Y.; Romero, M. J.; Habtemariam, A.; Snowden, M. E.; Song, L.; Clarkson, G. J.; Qamar, B.; Pizarro, A. M.; Unwin, P. R.; Sadler, P. J. "The contrasting chemical reactivity of potent isoelectronic iminopyridine and azopyridine osmium(II) arene anticancer complexes." *Chem. Sci.* **2012**, *3*, 2485–2494.

(25) Dougan, S. J.; Habtemariam, A.; McHale, S. E.; Parsons, S.; Sadler, P. J. "Catalytic organometallic anticancer complexes." *Proc. Natl. Acad. Sci. USA* **2008**, *105*, 11628–11633.

(26) Vadori, M.; Florio, C.; Groppo, B.; Cocchietto, M.; Pacor, S.; Zorzet, S.; Candussio, L.; Sava, G. *J. Biol. Inorg. Chem.* **2015**, *20*, 831-840.

(27) Hu, H.; You, Y.; He, L.; Chen, T. *J. Mater. Chem. B* **2015**, *3*, 6338-6346.

(28) Fischer, B.; Heffeter, P.; Kryeziu, K.; Gille, L.; Meier, S. M.; Berger, W.; Kowol, C. R.; Keppler, B. K. *Dalton Trans.* **2014**, *43*, 1096-1104.

(29) Cameron, B. R.; Darkes, M. C.; Yee, H.; Olsen, M.; Fricker, S. P.; Skerlj, R. T.; Bridger, G. J.; Davies, N. A.; Wilson, M. T.; Rose, D. J.; Zubieta, J. *Inorg. Chem.* **2003**, *42*, 1868-1876.

(30) Fricker, S. P.; Slade, E.; Powell, N. A.; Vaughan, O. J.; Henderson, G. R.; Murrer, B. A.; Megson, I. L.; Bisland, S. K.; Flitney, F. W. *Br. J. Pharmacol.* **1997**, *122*, 1441-1449.

(31) Chen, H.; Parkinson, J. A.; Morris, R. E.; Sadler, P. J. "Highly selective binding of organometallic ruthenium ethylenediamine complexes to nucleic acids: novel recognition mechanisms." *J Am Chem Soc* **2003**, *125*, 173-86.

(32) Dadci, L.; Elias, H.; Frey, U.; Hoernig, A.; Koelle, U.; Merbach, A. E.; Paulus, H.; Schneider, J. S. ".pi.-Arene Aqua Complexes of Cobalt, Rhodium, Iridium, and Ruthenium: Preparation, Structure, and Kinetics of Water Exchange and Water Substitution." *Inorganic Chemistry* **1995**, *34*, 306-315.

(33) Peacock, A. F. A.; Melchart, M.; Deeth, R. J.; Habtemariam, A.; Parsons, S.; Sadler, P. J. *Chem. Eur. J.* **2007**, *13*, 2601-2613.

(34) Fernandez, R.; Melchart, M.; Habtemariam, A.; Parsons, S.; Sadler, P. J. *Chem. Eur. J.* **2004**, *10*, 5173-5179.

(35) Mueller, J. A.; Cowell, A.; Chandler, B. D.; Sigman, M. S. *J. Am. Chem. Soc.* **2005**, *127*, 14817-14824.

(36) Schultz, M. J.; Adler, R. S.; Zierkiewicz, W.; Privalov, T.; Sigman, M. S. *J. Am. Chem. Soc.* **2005**, *127*, 8499-8507.

(37) McCann, S. D.; Stahl, S. S. *J. Am. Chem. Soc.* **2016**, *138*, 199-206.

(38) Hoover, J. M.; Ryland, B. L.; Stahl, S. S. *J. Am. Chem. Soc.* **2013**, *135*.

(39) Panicucci, R.; Bruice, T. C. "Dynamics of the reaction of hydrogen peroxide with a water soluble non .mu.-oxo dimer forming iron(III) tetraphenylporphyrin. 2. The reaction of hydrogen peroxide with 5,10,15,20-tetrakis(2,6-dichloro-3-sulfonatophenyl)porphinato iron(III) in aqueous solution." *Journal of the American Chemical Society* **1990**, *112*, 6063-6071.

(40) Kelson, E. P.; Phengsy, P. P. "Kinetic study of 2-propanol and benzyl alcohol oxidation by alkaline hexacyanoferrate(III) catalyzed by a terpyridyl ruthenium complex." *International Journal of Chemical Kinetics* **1999**, *32*, 760-770.

(41) Nicoll, A. J.; Allemann, R. K. "Nucleophilic and general acid catalysis at physiological pH by a designed miniature esterase." *Org Biomol Chem* **2004**, *2*, 2175-80.

(42) Kim, J. H.; Ryan, M. G.; Knaut, H.; Hille, R. "The reductive half-reaction of xanthine oxidase. The involvement of prototropic equilibria in the course of the catalytic sequence." *J Biol Chem* **1996**, *271*, 6771-80.

(43) Bishop, G. R.; Davidson, V. L. "Intermolecular electron transfer from substrate-reduced methylamine dehydrogenase to amicyanin is linked to proton transfer." *Biochemistry* **1995**, *34*, 12082-6.

(44) Gomez-Gallego, M.; Sierra, M. A. "Kinetic isotope effects in the study of organometallic reaction mechanisms." *Chem Rev* **2011**, *111*, 4857-963.

(45) Johnson, J. B.; Backvall, J. E. "Mechanism of ruthenium-catalyzed hydrogen transfer reactions. Concerted transfer of OH and CH hydrogens from an alcohol to a (Cyclopentadienone)ruthenium complex." *J Org Chem* **2003**, *68*, 7681-4.

(46) Casey, C. P.; Johnson, J. B. "Kinetic isotope effect evidence for a concerted hydrogen transfer mechanism in transfer hydrogenations catalyzed by [p-(Me2CH)C6H4Me]Ru- (NHCHPhCHPhNSO2C6H4-p-CH3)." *J Org Chem* **2003**, *68*, 1998-2001.

(47) Smith, K.-T.; Tilset, M.; Kristjansdottir, S. S.; Norton, J. R. "Kinetic Isotope Effects on Metal to Nitrogen Proton Transfers." *Inorganic Chemistry* **1995**, *34*, 6497-6504.

(48) Smith, K. T.; Roemming, C.; Tilset, M. "Unexpected disproportionation mechanism for proton-transfer reactions between 17-electron metal hydride cation radicals and neutral 18-electron metal hydrides." *Journal of the American Chemical Society* **1993**, *115*, 8681-8689.

(49) Connelly, N. G.; Geiger, W. E. "Chemical Redox Agents for Organometallic Chemistry." *Chem Rev* **1996**, *96*, 877-910.

(50) Brownell, K. R.; McCrory, C. C.; Chidsey, C. E.; Perry, R. H.; Zare, R. N.; Waymouth, R. M. "Electrooxidation of alcohols catalyzed by amino alcohol ligated ruthenium complexes." *J Am Chem Soc* **2013**, *135*, 14299-305.

(51) Matsubara, Y.; Fujita, E.; Doherty, M. D.; Muckerman, J. T.; Creutz, C. "Thermodynamic and kinetic hydricity of ruthenium(II) hydride complexes." *J Am Chem Soc* **2012**, *134*, 15743-57.

(52) Morris, R. H. "Estimating the acidity of transition metal hydride and dihydrogen complexes by adding ligand acidity constants." *J Am Chem Soc* **2014**, *136*, 1948-59.

(53) Ryan, O. B.; Tilset, M.; Parker, V. D. "Oxidation of the ruthenium hydride complex (.eta.5-C5H5)Ru(CO)(PPh3)H: generation of a dihydrogen complex by oxidatively induced intermolecular proton transfer." *Organometallics* **1991**, *10*, 298-304.

(54) Ryan, O. B.; Tilset, M.; Parker, V. D. "Chemical and electrochemical oxidation of group 6 cyclopentadienylmetal hydrides. First estimates of 17-electron metal-hydride cation-radical thermodynamic acidities and their decomposition of 17-electron neutral radicals." *Journal of the American Chemical Society* **1990**, *112*, 2618-2626.

(55) Hanan, E. J.; Chan, B. K.; Estrada, A. A.; Shore, D. G.; Lyssikatos, J. P. "Mild and General One-Pot Reduction and Cyclization of Aromatic and Heteroaromatic 2-Nitroamines to Bicyclic 2H-Imidazoles." *Synlett* **2010**, 2759-2764.

(56) Fulmer, G. R.; Miller, A. J. M.; Sherden, N. H.; Gottlieb, H. E.; Nudelman, A.; Stoltz, B. M.; Bercaw, J. E.; Goldberg, K. I. "NMR Chemical Shifts of Trace Impurities: Common Laboratory Solvents, Organics, and Gases in Deuterated Solvents Relevant to the Organometallic Chemist." *Organometallics* **2010**, *29*, 2176–2179.

CHAPTER FOUR

NAD^+ AS A HYDRIDE DONOR AND REDUCTANT

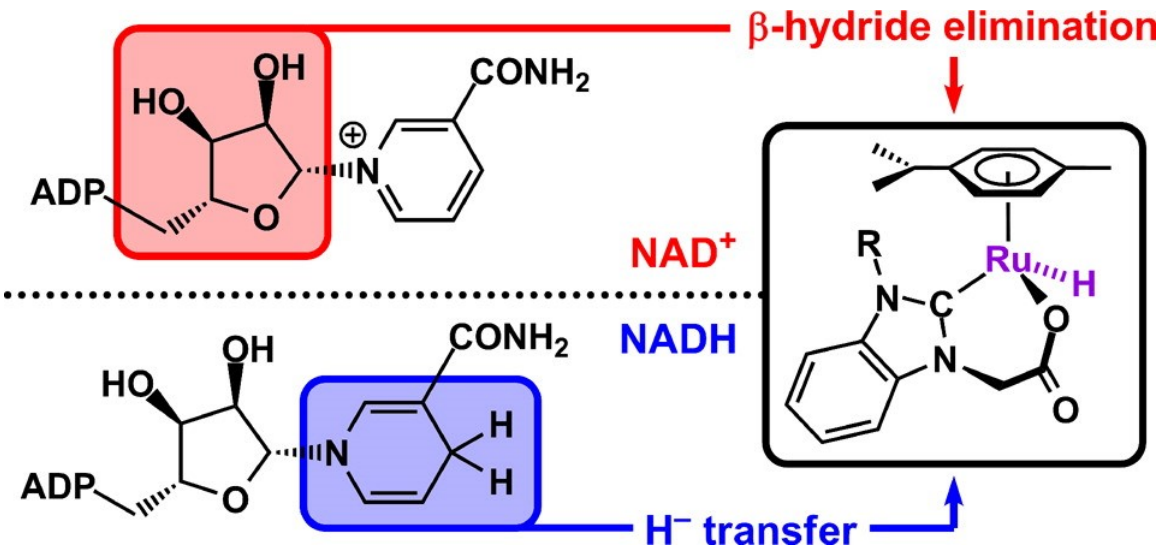

Figure 4. An organoruthenium complex reduced radicals catalytically using NAD^+ , a nature's oxidizing agent, as a hydride donor.

Reprinted with permission from Htet, Y.; Tennyson, A. G. "NAD as a Hydride Donor and Reductant" *J. Am. Chem. Soc.* **2016**, *138*, 15833−15836. DOI: 10.1021/jacs.6b10451 Copyright 2016 American Chemical Society."

ABSTRACT

Reduced nicotinamide adenine dinucleotide (NADH) can generate a ruthenium−hydride intermediate that catalyzes the reduction of O_2 to H_2O_2, which endows it with potent anticancer properties. A catalyst that could access a Ru−H intermediate using oxidized nicotinamide adenine dinucleotide (NAD^+) as the H^- source, however, could draw upon a supply of reducing equivalents 1000-fold more abundant than NADH, which would enable significantly greater H_2O_2 production. Herein, it is demonstrated, using the reduction of $ABTS^{\bullet-}$ to $ABTS^{2-}$, that NAD^+ can function as a reductant. Mechanistic evidence is presented that suggests a Ru−H intermediate is formed via β-hydride elimination from a ribose subunit in NAD^+. The insight gained from the heretofore unknown ability of NAD^+ to function as a reductant and H^- donor may lead to undiscovered biological carbohydrate oxidation pathways and new chemotherapeutic strategies.

INTRODUCTION

Redox reactions provide the chemical motive force essential for all forms of life.[1,2] Reduced nicotinamide adenine dinucleotide (NADH) supplies two e^- to mitochondrial electron transport by donating H^- from its hydropyridine moiety (Scheme 4.1, blue box) to flavin mononucleotide.[3,4] Conversely, oxidized nicotinamide adenine dinucleotide (NAD^+) accepts two e^- from glyceraldehyde-3-phosphate or lactate dehydrogenase by accepting H^- into its pyridinium moiety (Scheme 4.1, purple box).[5,6] The H^- donating ability of NADH has been harnessed for catalytic applications ranging from the reduction of O_2 to cytotoxic H_2O_2 in cancer cells[7-9] to petroleum-free H_2 production[10] to alcohol deracemization.[11]

Free NAD^+ is 640−1100 times more abundant in cells than free NADH;[12-15] therefore, a catalyst that could utilize NAD^+ would have access to a significantly greater H^-/e^- supply than NADH. Because catalytic carbohydrate oxidation can be performed by enzymatic[16] and transition metal-based systems,[17,18] we reasoned that oxidation of a ribose subunit (Scheme 4.1, red boxes) could enable NAD^+ to function as a reductant. Catalytic oxidation of ribose has been achieved by a Ru complex to afford ribonolactone with concomitant H_2 transfer to an alkene.[19] We therefore hypothesized that (1) a ribose subunit in NAD^+ could similarly undergo oxidation by a Ru complex via H^- transfer to the metal center and (2) the resulting Ru−H species would exhibit catalytic reduction activity. Herein, we report the first instance of H^- donation via β-hydride elimination from a ribose subunit of NAD^+, which enables NAD^+ to function as a reductant.

RESULTS AND DISCUSSION

To probe for Ru−H formation, the conversion of 2,2′-azino-bis(3-ethylbenzothiazoline-6-sulfonate) radical monoanion ($ABTS^{\bullet-}$, Scheme 4.2.A) to $ABTS^{2-}$ was selected as a spectroscopically more convenient reduction reaction than the conversion of O_2 to H_2O_2, given that $ABTS^{\bullet-}$ consumption can be quantified at significantly lower concentrations and longer wavelengths than H_2O_2 production.[††,‡‡] [20,21] Furthermore, the reduction of $ABTS^{\bullet-}$ to $ABTS^{2-}$ (0.68 V vs NHE)[22] occurs at nearly the same potential as the reduction of O_2 to H_2O_2 (0.70 V vs NHE).[23] Therefore, from a thermodynamic perspective, the reactivity of Ru−H with $ABTS^{\bullet-}$ can provide insight into its reactivity with O_2.

We recently reported the catalytic reduction of $ABTS^{\bullet-}$ to $ABTS^{2-}$ in aqueous solution using biologically relevant alcohols as terminal reductants, including arabinose, a diastereomer of ribose (Scheme 4.2.B).[24] Subsequent kinetic studies elucidated the mechanism: in aqueous solution, **Ru1** converts to Ru−aquocomplex $\mathbf{I}_A$, followed by ligand exchange with a nontertiary alcohol (R^1−CHOH−R^2) and deprotonation to afford Ru−alkoxide species $\mathbf{I}_B$, which then undergoes β-hydride elimination ($\mathbf{TS}_{B/C}$) to generate the catalytically active Ru−H intermediate $\mathbf{I}_C$ that reduces $ABTS^{\bullet-}$.[25] We reasoned that a ribose subunit of NAD^+ could likewise undergo β-hydride elimination to produce $\mathbf{I}_C$, whose presence could be inferred from the reduction of $ABTS^{\bullet-}$ to $ABTS^{2-}$.

[††] A 3.3 μM decrease in [$ABTS^{\bullet-}$] would produce a measurable change in absorbance (0.050), but a comparable absorbance change would require a 1.1 mM increase in [H_2O_2]. If a catalyst concentration of 5 μM is used, it would be possible to observe the reduction of less than 1 equiv of $ABTS^{\bullet-}$, but O_2 reduction would not be observable until more than 200 equiv of H_2O_2 had been produced.

[‡‡] In aqueous buffer, ε = 15,000 M^{-1} cm^{-1} at λ = 734 nm for $ABTS^{\bullet-}$ vs ε = 43.6 M^{-1} cm^{-1} at λ = 240 nm for H_2O_2

Addition of 5 μM **Ru1** to 50 μM $ABTS^{\bullet-}$ in phosphate buffered saline (PBS, pH 7.4) followed by the addition of 25 mM NAD^+ produced an 87% decrease in radical absorbance within 30 min (Fig. 4.1A, red line) that was 100% complete within 45 min. The UV/vis spectrum after 45 min confirmed a 1:1 correlation between $ABTS^{\bullet-}$ consumed and $ABTS^{2-}$ produced (Fig. 4.2). Attempts to characterize the NAD^+ oxidation product were unsuccessful, due to the low concentration constraints of the $ABTS^{\bullet-}$ reduction reaction, but calorimetric and computational studies by others suggest that dehydrogenation of the −CHOH− moiety at the ribose 2′-position would be thermodynamically the most favorable.[26,27] No radical reduction occurred in the presence of 5 μM **Ru1** alone (Fig. 4.1A, green line), which revealed that **Ru1** by itself could not reduce $ABTS^{\bullet-}$. Similarly, no $ABTS^{\bullet-}$ reduction was observed in the absence of **Ru1**, even with NAD^+ concentrations as high as 50 mM, which demonstrated that NAD^+ by itself could not reduce $ABTS^{\bullet-}$. However, addition of 5 μM NADH produced a rapid (within mixing time) 18% decrease in radical absorbance (Fig. 4. 1A, blue line), consistent with NADH functioning as a two e^- reductant. After the initial decrease, no additional $ABTS^{\bullet-}$ reduction was observed beyond normal thermal decay.

To determine if **Ru1** remained catalytically active after the reduction of 10 equiv of $ABTS^{\bullet-}$, two subsequent aliquots of 50 μM $ABTS^{\bullet-}$ were added (*) and [$ABTS^{\bullet-}$] decreased to zero each time (Fig. 4.1B). The time necessary for complete $ABTS^{\bullet-}$ reduction increased with each successive aliquot due to the fact that $ABTS^{2-}$ inhibits **Ru1**-catalyzed $ABTS^{\bullet-}$ reduction.[25] After the initial decrease produced by NADH, however, addition of 10 μM $ABTS^{\bullet-}$ aliquots (*) only increased absorbance proportional

to the [$ABTS^{\bullet-}$] in each aliquot (Fig. 4.1C), which indicated that the reducing ability of NADH had been exhausted. Treatment of this solution containing 70 μM $ABTS^{\bullet-}$ with 5 μM **Ru1** and 25 mM NAD^+ (§), produced complete $ABTS^{\bullet-}$ reduction within 1 h.

The ability of **Ru1** to catalyze $ABTS^{\bullet-}$ reduction was assayed with the individual components of NAD^+: nicotinamide, adenine, and ribose. No $ABTS^{\bullet-}$ reduction occurred upon treatment of 50 μM $ABTS^{\bullet-}$ and 5 μM **Ru1** with either 25 mM nicotinamide or 1.0 mM adenine, which indicated that neither component afforded NAD^+ its terminal reductant ability. In contrast, the addition of 25 mM D-ribose or 1.0 mM D-ribose phosphate produced complete $ABTS^{\bullet-}$ reduction within 20 min (Figs. 4.3−4.4). The faster reactivity with D-ribose phosphate is consistent with the higher affinity of cationic $\mathbf{I}_A$ for anionic D-ribose phosphate than neutral D-ribose. Collectively, these results demonstrated that the terminal reductant function of NAD^+ is derived from its ribose subunits.

The kinetics of **Ru1**-catalyzed $ABTS^{\bullet-}$ reduction with NAD^+ were analyzed for consistency with the mechanism in Scheme 4.2. Increasing the solution pH led to faster $ABTS^{\bullet-}$ reduction, with no reduction observed in pure H_2O (Fig. 4.5), which indicated that H^+ dissociation was necessary and was consistent with the conversion of $\mathbf{I}_A$ to $\mathbf{I}_B$. Varying the reaction temperature revealed $\Delta S^{\ddagger} = 17.1 \pm 4.9$ cal mol^{-1} K^{-1} (Fig. 4.6), which demonstrated that disorder was increasing during the rate-determining step and suggested ligand fragmentation and dissociation (i.e., $\mathbf{TS}_{B/C}$ and $R^1{-}C(=O){-}R^2$ elimination, respectively) was occurring. The $\Delta S^{\ddagger}$ value observed with NAD^+ also fell within the range of values measured for **Ru1**-catalyzed $ABTS^{\bullet-}$ reduction with other non-

tertiary alcohols ($\Delta S^{\ddagger}$ = 11.4−32.8 cal mol^{-1} K^{-1}).[25] Collectively, these results were consistent with the formation of $\mathbf{I}_C$ via β-hydride elimination from a ribose subunit coordinated to Ru and dissociation of the oxidized NAD^+.

The observed rate constant (k_{obs}) for **Ru1**-catalyzed $ABTS^{\bullet-}$ reduction with NAD^+ was 2.53-fold lower in deutero PBS (pD 7.4) than in proteo PBS. This $ABTS^{\bullet-}$ reduction reaction exhibits a solvent kinetic isotope effect (KIE) of 1.74, which reflects the role of H_2O as an H+ acceptor in the conversion of $\mathbf{I}_A$ to $\mathbf{I}_B$ and $\mathbf{I}_C$ back to $\mathbf{I}_A$.[25] Dividing the proteo/deutero k_{obs} ratio of 2.53 by 1.74 yielded the O−H/D KIE value of 1.45 for NAD^+. Breakage of an O−H bond in a ribose subunit of NAD^+ is essential for the formation of $\mathbf{I}_B$, whereby H/D substitution causes the activation barrier to increase and the k_{obs} for $ABTS^{\bullet-}$ reduction to decrease. In our previous mechanistic study, the smaller O−H/D KIE value for EtOH (2.92) compared to *i*-PrOH (4.18) reflected the lower pK_a of EtOH (15.9 vs 16.5 for *i*-PrOH).[25] Increasing the acidity of the O−H group will increase the $O^{\delta-}$−$H^{\delta+}$ bond polarization, which will lower the activation barrier to H^+ dissociation and thus render the O−H bond less sensitive to H/D isotopic substitution. The substantially lower O−H/D KIE value for NAD^+ compared to EtOH and *i*-PrOH was thus consistent with the substantially greater acidity of ribose (pK_a = 11.8).[28]

We next sought to demonstrate that NAD^+ could serve as a reductant under conditions in which the biological supply of NADH had been exhausted. Treatment of a 50 μM $ABTS^{\bullet-}$ solution (Fig. 4.7, *i*) with 18 μM NADH caused a rapid (within mixing time) decrease in radical absorbance corresponding to the reduction of 34 μM $ABTS^{\bullet-}$ (Fig. 4.7, *ii*). This $ABTS^{\bullet-}$/NADH reaction stoichiometry of 1.9 was consistent with

NADH functioning as a two e^- reductant. Importantly, 16 μM $ABTS^{\bullet-}$ was not reduced, and no further decreases in [$ABTS^{\bullet-}$] occurred. Subsequent addition of 5 μM **Ru1** and 12.5 mM NAD^+ caused the radical absorbance to decrease to zero within 22 min, signifying complete reduction of the remaining $ABTS^{\bullet-}$ (Fig. 4.7, *iii*). The ratio of NAD^+/NADH used in this experiment (694:1) was consistent with the ratio found in cells,[12-15] which demonstrates that, under conditions that exhausted the free cellular NADH supply, **Ru1** could utilize the substantially more abundant cellular stores of free NAD^+ to alleviate or prevent oxidative stress.

In the presence of horseradish peroxidase (HRP), addition of H_2O_2 to $ABTS^{2-}$ in PBS results in $ABTS^{\bullet-}$ formation, and the kinetics of this reaction can be used to evaluate the ability of an antioxidant to prevent or mitigate the onset of oxidative stress.[29] Inclusion of 5 μM **Ru1** and 25 mM NAD^+ significantly inhibited $ABTS^{\bullet-}$ formation, which never exceeded 4.8 μM (Fig. 4.8A, red line). After 15 min, the radical absorbance began to decrease, and complete $ABTS^{\bullet-}$ reduction was observed 6.6 min later. In contrast, 5 μM NADH completely inhibited $ABTS^{\bullet-}$ formation for 3.3 min, whereupon the absorbance gradually increased to a maximum of 11 μM (Fig. 4.8A, blue line). This concentration was 7 μM lower than the maximum observed in the control experiment and was consistent with NADH functioning as a two e^- reductant. The subsequent gradual decrease was due to normal $ABTS^{\bullet-}$ thermal decay.

After complete $ABTS^{\bullet-}$ reduction was observed following the first H2O2 aliquot, two additional 10 μM H_2O_2 aliquots ($^{\#}$) were introduced and [$ABTS^{\bullet-}$] peaked at 6.4 μM before being reduced completely each time (Fig. 4.8B), demonstrating that the catalyst

and terminal reductant were both still present and active. Different behavior was observed with NADH after [$ABTS^{\bullet-}$] peaked. Adding a second H_2O_2 aliquot ($^{\#}$) caused [$ABTS^{\bullet-}$] to increase to 17 μM (Fig. 4.8C), corresponding to 94% $ABTS^{2-}$ oxidation (complete oxidation = 18 μM).[24] No change in absorbance was produced by the third H_2O_2 aliquot ($^{\#}$), consistent with all of the $ABTS^{2-}$ having been completely oxidized by the previous H_2O_2 aliquots. Subsequent treatment of this solution with 5 μM **Ru1** and 25 mM NAD^+ (§) resulted in complete $ABTS^{\bullet-}$ reduction within 45 min.

To demonstrate that the reactivity exhibited by **Ru1** and NAD^+ in Fig. 4.8 derived specifically from $ABTS^{\bullet-}$ reduction, two 10 μM aliquots of chemically synthesized $ABTS^{\bullet-}$ (*) were added after the initial reaction with H_2O_2 was complete (Fig. 4.9, red line). The [$ABTS^{\bullet-}$] immediately increased by 8.8 μM each time, then decreased to zero 19 and 29 min after addition of the first and second $ABTS^{\bullet-}$ aliquots, respectively. We had previously shown that $ABTS^{2-}$ is an inhibitor for **Ru1**-catalyzed $ABTS^{\bullet-}$ reduction with nontertiary alcohols,[25] and given that the concentration of $ABTS^{2-}$ increased as each successive $ABTS^{\bullet-}$ aliquot was reduced, it was unsurprising that the time required for complete $ABTS^{\bullet-}$ reduction likewise increased. With the NADH experiment, however, the first and second $ABTS^{\bullet-}$ aliquots produced 9.4 and 9.3 μM increases in [$ABTS^{\bullet-}$], respectively, that were stable over time (Fig. 4.9, blue line). Subsequent addition of 5 μM Ru1 and 25 mM NAD^+ (§) then achieved quantitative $ABTS^{\bullet-}$ reduction in less than 39 min.

Synthetic Procedures

General synthetic considerations. The complex **Ru1**[24,25] and $ABTS^{\bullet-}$ were prepared as previously described.[20] All other materials were of reagent quality and used as received. All solvents used were HPLC grade. All manipulations were performed under ambient conditions using standard benchtop techniques.

General spectroscopic considerations. UV–visible absorption spectra were acquired on a Varian Cary 50 Bio spectrometer equipped with a water-cooled Quantum Northwest TC-125 peltier temperature controller. All solution measurements were performed at 25.0 ± 0.1 °C in matched gas-tight quartz cuvettes (Precision Scientific) with 1 cm path lengths and 3.0 mL analyte solution volumes. Absorption spectra were acquired from 900 to 200 nm with a scanning speed of 300 nm min^{-1} and a resolution of 0.5 nm. Each kinetic analysis experiment (5 second intervals) was performed in quadruplicate on four different days. Stock solutions were prepared fresh daily and filtered (0.2 μm PTFE) immediately prior to use.

Kinetic analysis of Ru1-catalyzed $ABTS^{\bullet-}$ reduction with NAD^+. An aliquot of $ABTS^{\bullet-}$ (40 μL from a 3.75 mM stock solution in H_2O) was added to PBS to afford the $ABTS^{\bullet-}$ working solution and the absorbance spectrum was acquired to confirm $ABTS^{\bullet-}$ concentration. The single wavelength kinetics program was initiated and, after 20 s, an aliquot of **Ru1** (30 μL from 0.5 mM stock solution in CH_3CN) was added, followed by an aliquot of NAD^+ (30 μL from 2.5 M stock solution in H_2O) 5 min later, and the kinetics program was allowed to continue. After the kinetics program had completed, the

absorbance spectrum was acquired to confirm formation of $ABTS^{2-}$ from the peak at 340 nm.

Inhibition of $ABTS^{\bullet-}$ formation by HRP in PBS. Derived from a literature procedure.[29] Aliquots of $ABTS^{2-}$ (30 μL from a 2.0 mM stock solution in H_2O), HRP (30 μL from a 1.0 μM stock solution in H_2O), and **Ru1**, NAD^+ or NADH were added to PBS (pH 7.4) to afford the $ABTS^{2-}$/**Ru1** (or NADH)/HRP working solution in PBS. The absorbance spectrum of this working solution was acquired to confirm no $ABTS^{\bullet-}$ had formed. An aliquot of H_2O_2 (30 μL from 1.0 mM stock solution in H_2O) was added and the single wavelength kinetics program was initiated.

CONCLUSIONS

In summary, NAD^+ is able to function as a terminal reductant for the **Ru1**-catalyzed reduction of $ABTS^{\bullet-}$ to $ABTS^{2-}$ in aerobic, aqueous solution. Because NAD^+ typically plays the role of H^- acceptor in biological systems, the classical expectation would be that it could not function as an H^- donor. However, the $ABTS^{\bullet-}$ reduction reactivity observed with NAD^+ and **Ru1** were highly conserved with our previous studies using other nontertiary alcohols as terminal reductants,[24,25] which suggested that the same mechanism was operative with NAD^+. The key intermediate responsible for $ABTS^{\bullet-}$ reduction with NAD^+ and **Ru1** was therefore inferred to be a Ru−H intermediate formed via β-hydride elimination from a ribose subunit coordinated to Ru, whereby this ability of NAD^+ to function as an H^- donor would give rise to its observed ability to function as a reductant. Previous studies by others have revealed that transition metal−hydride complexes formed via H^- transfer from NADH can react with atmospheric O_2 to generate

H_2O_2,[30,31] which in turn can produce cytotoxic effects against cancer cells.[7-9,32-34] Given that free NAD^+ is 640−1100 times more abundant in cells than free NADH,[12-15] we believe that a catalyst that can utilize NAD^+ as an H^- source will be able to generate significantly higher H_2O_2 levels and thus exhibit substantially greater anticancer potency. The biological applications of **Ru1** will be detailed in subsequent reports.

Acknowledgments

This work was supported by the National Science Foundation (DMR-1555224). We thank Dr. A. Mangalum for prior work with **Ru1** and helpful discussions.

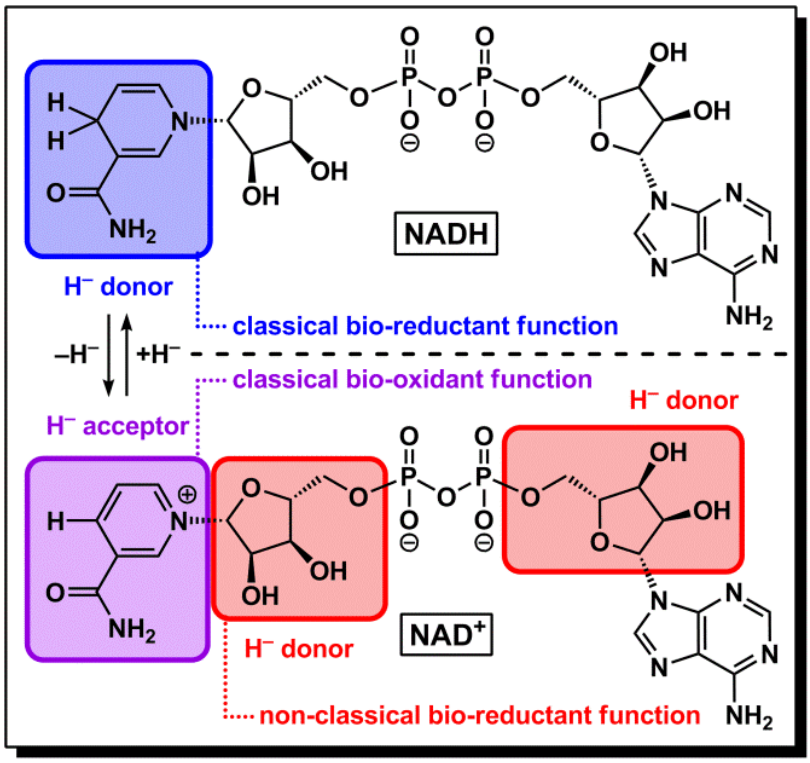

Scheme 4.1. Hydride Transfer with NADH and NAD^+

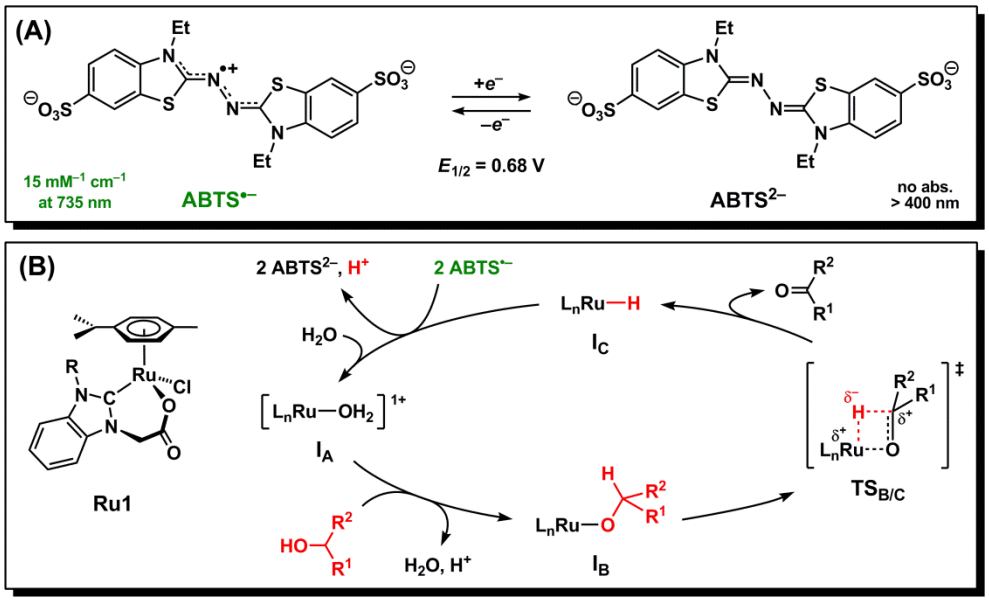

Scheme 4.2. **Ru1**-Catalyzed ABTS$^{\bullet-}$ Reduction with Alcohols

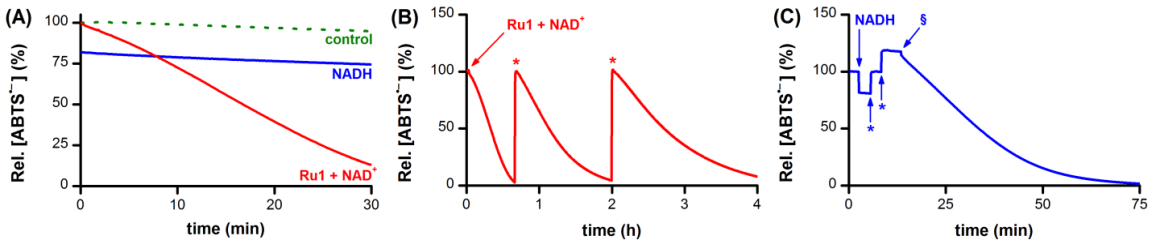

Fig. 4.1. Plot of relative [$ABTS^{\bullet-}$] vs time, which shows the reduction of $ABTS^{\bullet-}$ to $ABTS^{2-}$ following (A) the addition of **Ru1** and NAD^+ (red line), NADH (blue line), or **Ru1** without NAD^+ as a control (dotted green line), (B) two additional 50 μM $ABTS^{\bullet-}$ aliquots (*) after the initial reduction by **Ru1** and NAD^+, or (C) two additional 10 μM $ABTS^{\bullet-}$ aliquots (*) after the initial reduction by NADH, followed by **Ru1** and NAD^+ (§). Conditions: [**Ru1**]$_0$ or [NADH]$_0$ = 5 μM, [$ABTS^{\bullet-}$]$_0$ = 50 μM, [NAD^+]$_0$ = 25 mM, PBS (pH 7.4), 25 °C.

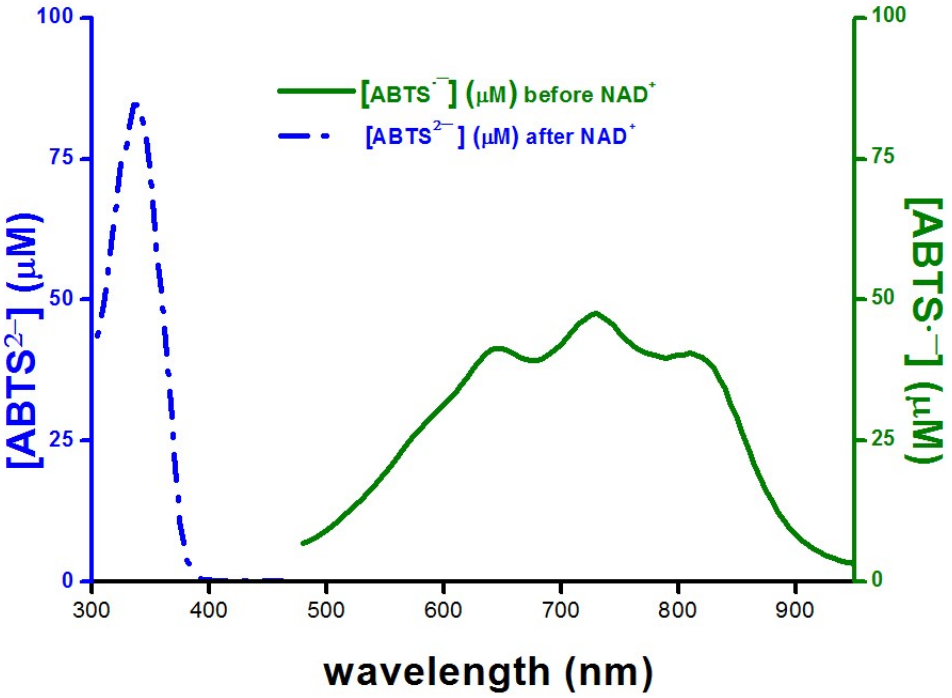

Fig. 4.2. UV/vis of $ABTS^{2-}$ formed from $ABTS^{\bullet-}$ reduction catalyzed by **Ru1** with NAD^+ as terminal reductant. Green line shows the spectra obtained at t = 0 before the addition of NAD^+, representing the amount of $ABTS^{\bullet-}$ and blue dash line shows the spectra obtained at t = 40 min, representing the amount of the additional $ABTS^{2-}$ produced as well as the $ABTS^{2-}$ from the original stock solution (30 μM). $ABTS^{\bullet-}$ has maximum absorption at 734 nm and $ABTS^{2-}$ has the maximum absorbance at 340 nm (blue dash line). Conditions: $[\mathbf{Ru1}]_0$ = 5 μM, $[ABTS^{\bullet-}]_0$ = 50 μM, $[NAD^+]_0$ = 25 mM; PBS, pH 7.4, 25 °C, absorbance measured from 300–950 nm.

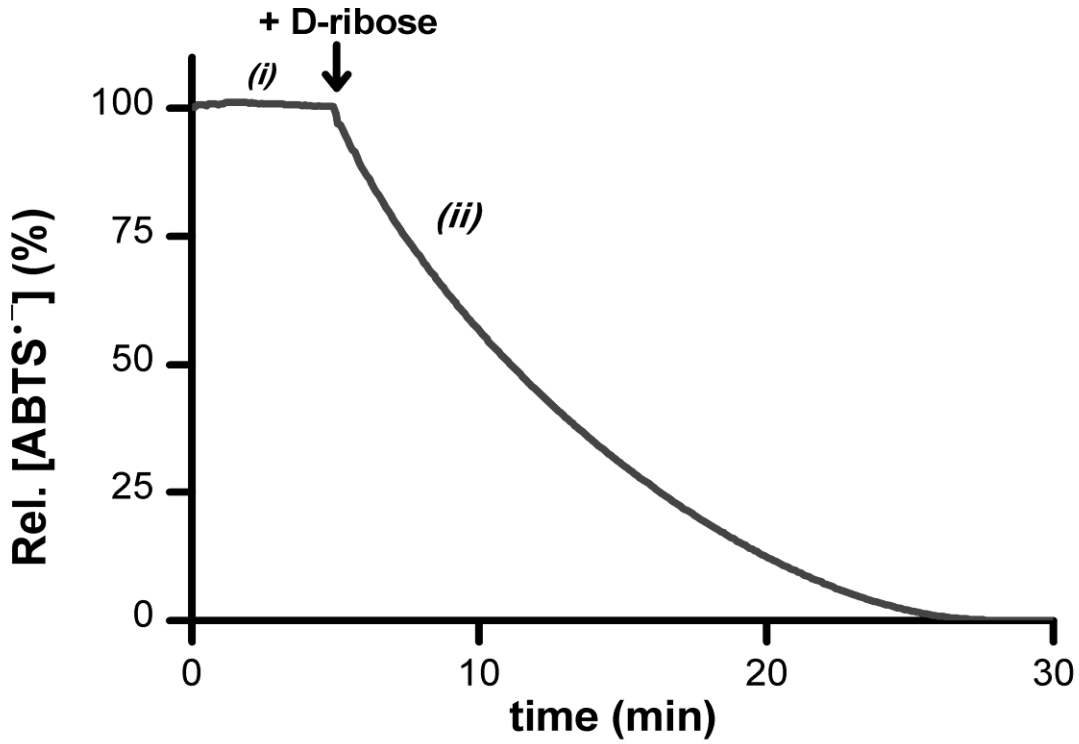

Fig. 4.3. D-Ribose caused complete reduction of $ABTS^{\bullet-}$ in the presence of **Ru1** catalyst. *(i)* In PBS solution containing only **Ru1**, no reduction of $ABTS^{\bullet-}$ was observed, but *(ii)* the absorbance decreased gradually after the addition of D-ribose. Conditions: $[ABTS^{\bullet-}]_0$ = 50 μM, $[\mathbf{Ru1}]_0$ = 5 μM, $[\text{D-ribose}]_0$ = 25 mM; PBS, pH 7.4, 25 °C, absorbance measured at 734 nm.

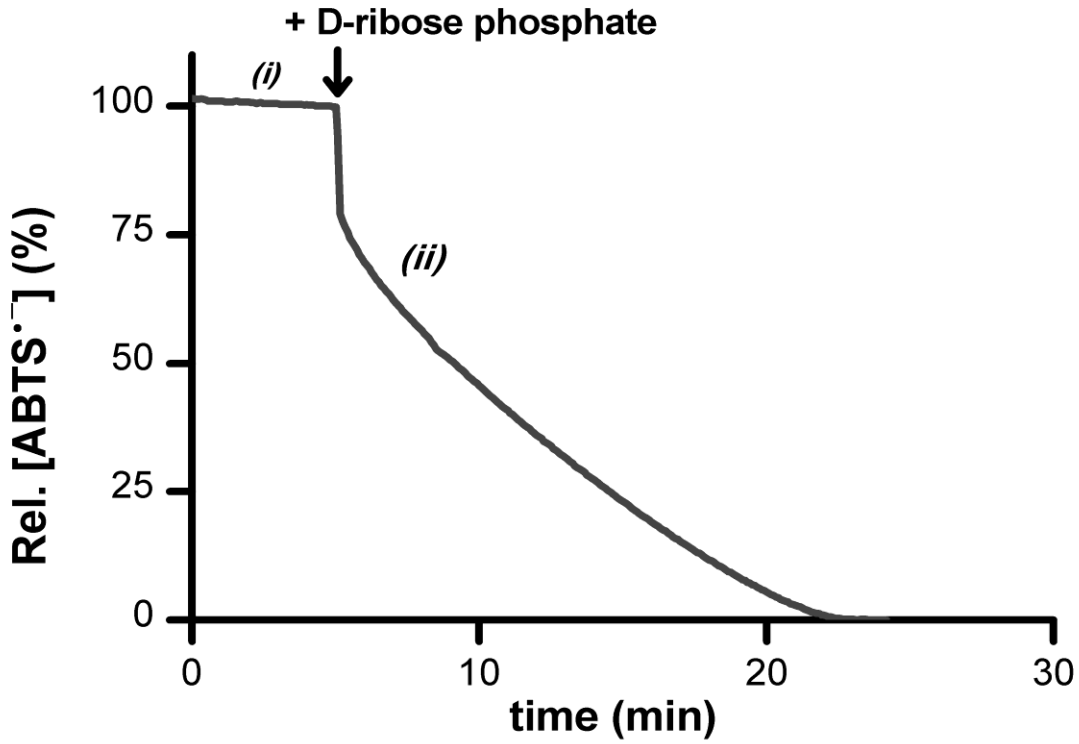

Fig. 4.4. D-Ribose phosphate caused complete reduction of $ABTS^{\bullet-}$ in the presence of **Ru1** catalyst. *(i)* In PBS solution containing only **Ru1**, no reduction of $ABTS^{\bullet-}$ was observed, but *(ii)* the absorbance decreased rapidly after the addition of ribose phosphate. Conditions: $[ABTS^{\bullet-}]_0$ = 50 μM, $[\mathbf{Ru1}]_0$ = 5 μM, $[\text{D-ribose phosphate}]_0$ = 1 mM; PBS, pH 7.4, 25 °C, absorbance measured at 734 nm.

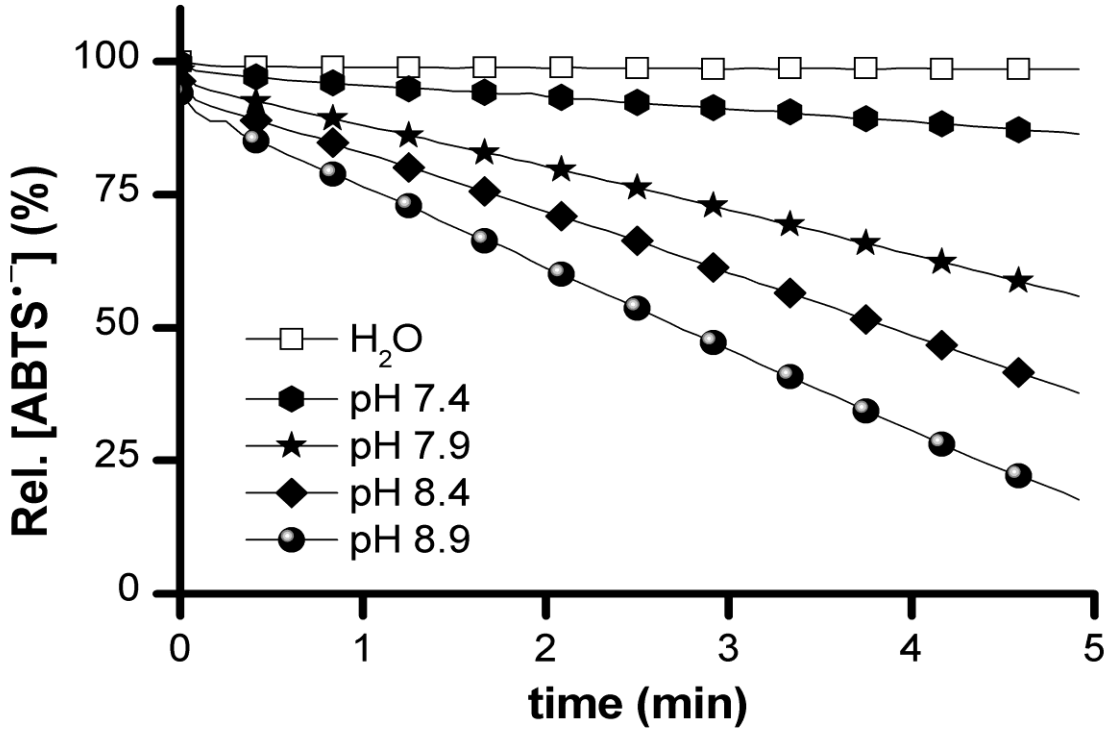

Fig. 4.5. In pure water, NAD^+ caused no reduction of $ABTS^{\bullet-}$ in the presence of **Ru1** catalyst whereas faster rates of reduction by NAD^+ were observed in PBS solutions with increasing pH. Conditions: $[ABTS^{\bullet-}]_0$ = 50 μM, [**Ru1**]$_0$ = 5 μM, $[NAD^+]_0$ = 25 mM, pH = 7.4, 7.9, 8.4 or 8.9; PBS or H_2O, 25 °C, absorbance measured at 734 nm.

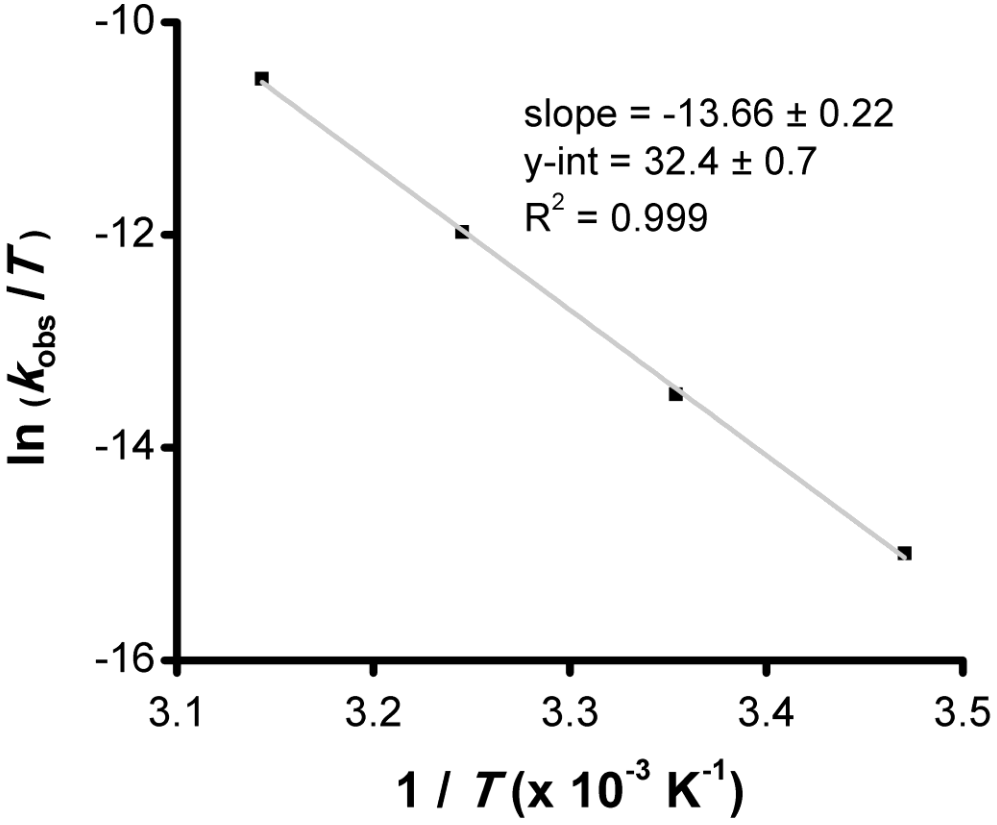

Fig. 4.6. Eyring plot for $ABTS^{\bullet-}$ reduction catalyzed by **Ru1** with NAD^+ as terminal reductant. Conditions: $[\mathbf{Ru1}]_0$ = 5 μM, $[ABTS^{\bullet-}]_0$ = 50 μM, $[ABTS^{2-}]_0$ = 100 μM, $[NAD^+]_0$ = 25 mM, T = 15, 25, 35 or 45 °C; PBS, pH 7.4, absorbance measured at 734 nm.

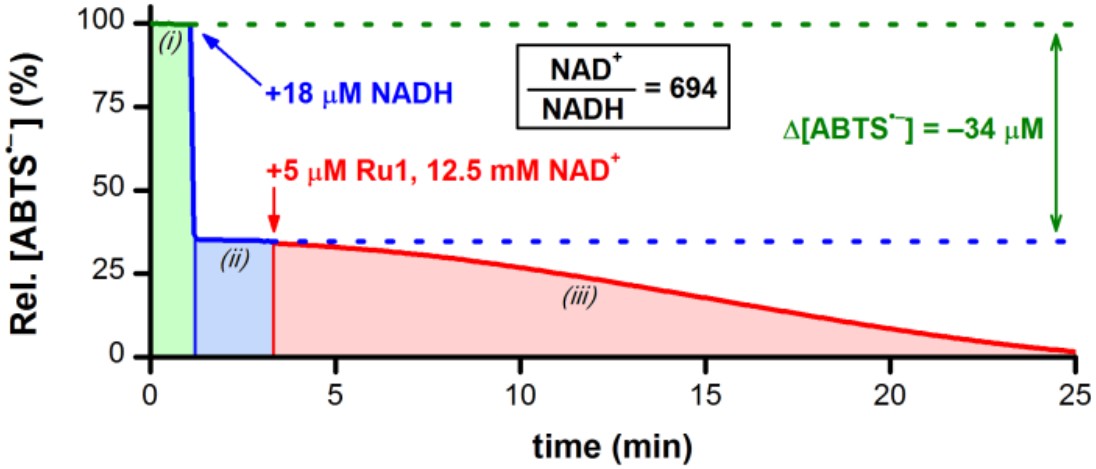

Fig. 4.7. Plot of relative [$ABTS^{\bullet-}$] vs time (i), which shows the 2:1 stoichiometric reduction of $ABTS^{\bullet-}$ by NADH (ii), followed by the catalytic reduction of $ABTS^{\bullet-}$ by **Ru1** and NAD^+ (iii). Conditions: [**Ru1**]$_0$ = 5 μM, or [NADH]$_0$ = 18 μM, [$ABTS^{\bullet-}$]$_0$ = 50 μM, [NAD^+]$_0$ =12.5 mM, PBS (pH 7.4), 25 °C.

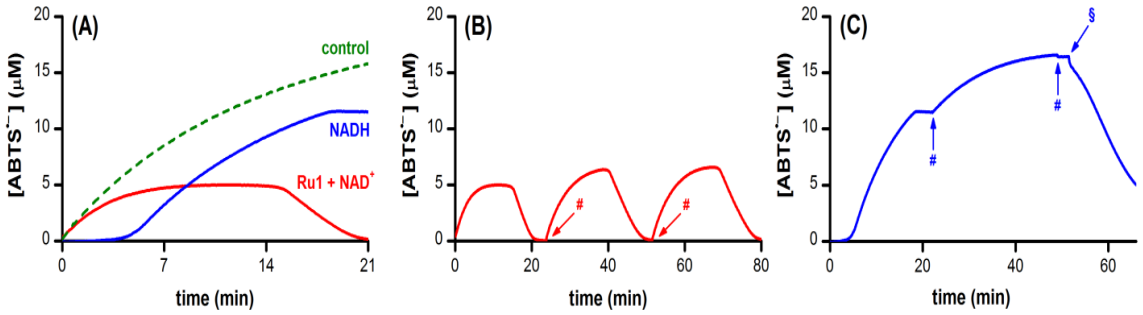

Fig. 4.8. (A) Plot of [ABTS$^{\bullet-}$] vs time, which shows the oxidation of ABTS^{2-} to ABTS$^{\bullet-}$ *in situ* by HRP and H_2O_2 in the presence of **Ru1** and NAD^+ (red line), NADH (blue line), or **Ru1** without NAD^+ as a control (dotted green line). Plot of [ABTS$^{\bullet-}$] vs time, which shows ABTS$^{\bullet-}$ formation following two additional aliquots of 10 μM H_2O_2 ($^{\#}$) in the presence of (B) **Ru1** and NAD^+ or (C) NADH. For the NADH experiment shown in (C), **Ru1** and NAD^+ were added (§) after the final aliquot of 10 μM H_2O_2. Conditions: $[HRP]_0$ = 10 nM, $[\mathbf{Ru1}]_0$ or $[NADH]_0$ = 5 μM, $[H_2O_2]_0$ = 10 μM, $[ABTS^{2-}]_0$ = 20 μM, $[NAD^+]_0$ = 25 mM, PBS (pH 7.4) at 25 °C.

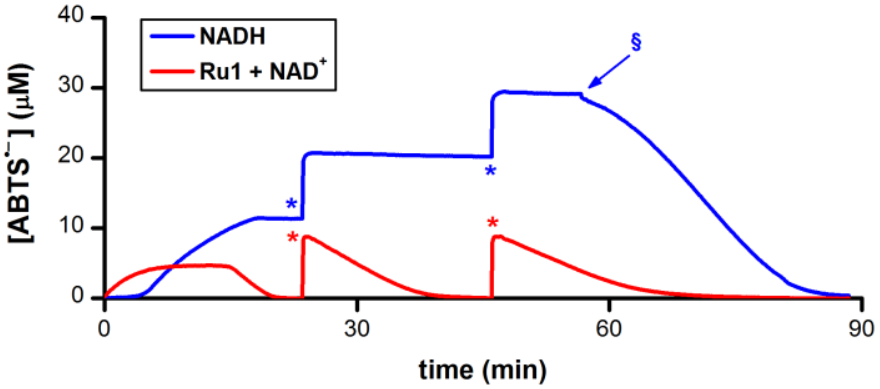

Fig. 4.9. Plot of [ABTS$^{\bullet-}$] vs time, which shows the oxidation of ABTS^{2-} to ABTS$^{\bullet-}$ *in situ* by HRP and H_2O_2 followed by subsequent ABTS$^{\bullet-}$ reactivity in the presence of **Ru1** and NAD^+ (red line) or NADH (blue line). After the initial reaction of **Ru1** and NAD^+ or NADH had completed, two additional aliquots of 10 μM ABTS$^{\bullet-}$ (*) were introduced. For the NADH experiment (blue line), 5 μM **Ru1** and 25 mM NAD^+ were added (§) after the final aliquot of 10 μM ABTS$^{\bullet-}$. Conditions: $[HRP]_0$ = 10 nM, $[\mathbf{Ru1}]_0$ or $[NADH]_0$ = 5 μM, $[H_2O_2]_0$ = 10 μM, $[ABTS^{2-}]_0$ = 20 μM, $[NAD^+]_0$ = 25 mM, PBS (pH 7.4) at 25 °C.

REFERENCES

(1) Borch, T.; Kretzschmar, R.; Kappler, A.; Cappellen, P. V.; Ginder-Vogel, M.; Voegelin, A.; Campbell, K. "Biogeochemical redox processes and their impact on contaminant dynamics." *Environ. Sci. Technol.* **2010**, *44*, 15-23.

(2) Falkowski, P. G.; Fenchel, T.; Delong, E. F. "The microbial engines that drive Earth's biogeochemical cycles." *Science* **2008**, *320*, 1034-1039.

(3) Hirst, J. "Mitochondrial complex I." *Annu. Rev. Biochem.* **2013**, *82*, 551-575.

(4) Nissen, M. S.; Youn, B.; Knowles, B. D.; Ballinger, J. W.; Jun, S. Y.; Belchik, S. M.; Xun, L.; Kang, C. "Crystal structures of NADH:FMN oxidoreductase (EmoB) at different stages of catalysis." *J. Biol. Chem.* **2008**, *283*, 28710-28720.

(5) Talfournier, F.; Colloc'h, N.; Mornon, J. P.; Branlant, G. "Comparative study of the catalytic domain of phosphorylating glyceraldehyde-3-phosphate dehydrogenases from bacteria and archaea via essential cysteine probes and site-directed mutagenesis." *Eur. J. Biochem.* **1998**, *252*, 447-457.

(6) Deng, H.; Zheng, J.; Clarke, A.; Holbrook, J. J.; Callender, R.; Burgner, J. W., 2nd "Source of catalysis in the lactate dehydrogenase system. Ground-state interactions in the enzyme-substrate complex." *Biochemistry* **1994**, *33*, 2297-2305.

(7) Soldevila-Barreda, J. J.; Romero-Canelon, I.; Habtemariam, A.; Sadler, P. J. "Transfer hydrogenation catalysis in cells as a new approach to anticancer drug design." *Nat. Commun.* **2015**, *6*, 6582.

(8) Ritacco, I.; Russo, N.; Sicilia, E. "DFT Investigation of the Mechanism of Action of Organoiridium(III) Complexes As Anticancer Agents." *Inorg. Chem.* **2015**, *54*, 10801-10810.

(9) Liu, Z.; Sadler, P. J. "Organoiridium complexes: anticancer agents and catalysts." *Acc. Chem. Res.* **2014**, *47*, 1174-1185.

(10) Fukuzumi, S.; Suenobu, T. "Hydrogen storage and evolution catalysed by metal hydride complexes." *Dalton. Trans.* **2013**, *42*, 18-28.

(11) Voss, C. V.; Gruber, C. C.; Faber, K.; Knaus, T.; Macheroux, P.; Kroutil, W. "Orchestration of concurrent oxidation and reduction cycles for stereoinversion and deracemisation of sec-alcohols." *J. Am. Chem. Soc.* **2008**, *130*, 13969-13972.

(12) Zhang, Q.; Piston, D. W.; Goodman, R. H. "Regulation of corepressor function by nuclear NADH." *Science* **2002**, *295*, 1895-1897.
(13) Hedeskov, C. J.; Capito, K.; Thams, P. "Cytosolic ratios of free [NADPH]/[NADP+] and [NADH]/[NAD+] in mouse pancreatic islets, and nutrient-induced insulin secretion." *Biochem. J.* **1987**, *241*, 161-167.

(14) Veech, R. L.; Guynn, R.; Veloso, D. "The time-course of the effects of ethanol on the redox and phosphorylation states of rat liver." *Biochem. J.* **1972**, *127*, 387-397.

(15) Williamson, D. H.; Lund, P.; Krebs, H. A. "The redox state of free nicotinamide-adenine dinucleotide in the cytoplasm and mitochondria of rat liver." *Biochem. J.* **1967**, *103*, 514-527.

(16) Kruger, N. J.; von Schaewen, A. "The oxidative pentose phosphate pathway: structure and organisation." *Curr. Opin. Plant Biol.* **2003**, *6*, 236-246.

(17) Besson, M. G., P. "Selective oxidation of alcohols and aldehydes on metal catalysts." *Catal. Today* **2000**, *57*, 127-141.

(18) Arts, S. J. H. F. M., E. J. M.; van Bekkum, H.; Sheldon, R. A. "Hydrogen peroxide and oxygen in catalytic oxidation of carbohydrates and related compounds." *Synthesis* **1997**, *6*, 597-613.

(19) Saburi, M. I., Y.; Kaji, N.; Aoi, T.; Sasaki, I.; Yoshikawa, S.; Uchida, Y. "Highly Selective Synthesis of Aldonolactones from Protected Alditols by Ruthenium Complex-Catalyzed Dehydrogenation. A Method of Converting Aldopentoses to Their Stereoisomers." *Chem. Lett.* **1989**, *18*, 563-566.

(20) Re, R.; Pellegrini, N.; Proteggente, A.; Pannala, A.; Yang, M.; Rice-Evans, C. "Antioxidant activity applying an improved ABTS radical cation decolorization assay." *Free Radic. Biol. Med.* **1999**, *26*, 1231-1237.

(21) Yusa, K.; Shikama, K. "Oxidation of oxymyoglobin to metmyoglobin with hydrogen peroxide: involvement of ferryl intermediate." *Biochemistry* **1987**, *26*, 6684-6688.

(22) Scott, S. L. C., W.-J.; Bakac, A.; Espenson, J. H. "Spectroscopic parameters, electrode potentials, acid ionization constants, and electron exchange rates of the 2,2'-azinobis(3-ethylbenzothiazoline-6-sulfonate) radicals and ions." *J. Phys. Chem.* **1993**, *97*, 6710-6714.

(23) Jungwirth, U.; Kowol, C. R.; Keppler, B. K.; Hartinger, C. G.; Berger, W.; Heffeter, P. "Anticancer activity of metal complexes: involvement of redox processes." *Antioxid. Redox Signaling* **2011**, *15*, 1085-1127.

(24) Htet, Y. T., A. G. "Catalytic radical reduction in aqueous solution via oxidation of biologically-relevant alcohols." *Chem. Sci.* **2016**, *7*, 4052-4058.

(25) Htet, Y.; Tennyson, A. G. "Catalytic Radical Reduction in Aqueous Solution by a Ruthenium Hydride Intermediate." *Angew. Chem., Int. Ed.* **2016**, *55*, 8556-8560.

(26) Achrainer, F.; Emel'yanenko, V. N.; Tantawy, W.; Verevkin, S. P.; Zipse, H. "Transfer hydrogenation as a redox process in nucleotides." *J. Phys. Chem. B* **2014**, *118*, 10426-10429.

(27) Achrainer, F.; Zipse, H. "Transfer hydrogenation in open-shell nucleotides - a theoretical survey." *Molecules* **2014**, *19*, 21489-21505.

(28) Sen, S.; Pal, U.; Maiti, N. C. "pKa determination of D-ribose by Raman spectroscopy." *J. Phys. Chem. B* **2014**, *118*, 909-914.

(29) Pitulice, L. P., I.; Vilaseca, E.; Madurga, S.; Isvoran, A.; Cascante, M.; Mas, F. "Influence of Macromolecular Crowding on the Oxidation of $ABTS^{\bullet-}$ by Hydrogen Peroxide Catalyzed by HRP." *J. Biocatal. Biotransformation* **2013**, *2*.

(30) Suenobu, T.; Shibata, S.; Fukuzumi, S. "Catalytic Formation of Hydrogen Peroxide from Coenzyme NADH and Dioxygen with a Water-Soluble Iridium Complex and a Ubiquinone Coenzyme Analogue." *Inorg. Chem.* **2016**, *55*, 7747-7754.

(31) Maid, H.; Bohm, P.; Huber, S. M.; Bauer, W.; Hummel, W.; Jux, N.; Groger, H. "Iron catalysis for in situ regeneration of oxidized cofactors by activation and reduction of molecular oxygen: a synthetic metalloporphyrin as a biomimetic NAD(P)H oxidase." *Angew. Chem., Int. Ed.* **2011**, *50*, 2397-2400.

(32) Liu, Z.; Romero-Canelon, I.; Qamar, B.; Hearn, J. M.; Habtemariam, A.; Barry, N. P.; Pizarro, A. M.; Clarkson, G. J.; Sadler, P. J. "The potent oxidant anticancer activity of organoiridium catalysts." *Angew. Chem., Int. Ed.* **2014**, *53*, 3941-3946.

(33) Fu, Y. R., M. J.; Habtemariam, A.; Snowden, M. E.; Song, L.; Clarkson, G. J.; Qamar, B.; Pizarro, A. M.; Unwin, P. R.; Sadler, P. J. "The contrasting catalytic efficiency and cancer cell antiproliferative activity of stereoselective organoruthenium transfer hydrogenation catalysts." *Chem. Sci.* **2012**, *3*.

(34) Dougan, S. J.; Habtemariam, A.; McHale, S. E.; Parsons, S.; Sadler, P. J. "Catalytic organometallic anticancer complexes." *Proc. Natl. Acad. Sci. U. S. A.* **2008**, *105*, 11628-11633.